LABORATORI NAZIONALI DI FRASCATI
SIS – Pubblicazioni

LNF–03/012 (P)
11 Luglio 2003

Papers presented at PAC 2003

Accelerator Division

Presented at the
2003 Particle Accelerator Conference (PAC 2003)
Portland, Oregon, May 12-16, 2003

CONTENTS

Invited Oral

Contributed Oral

Contributed Posters

FUTURE PLANS FOR e^+e^- FACTORIES

C.Biscari, LNF-INFN, Frascati, Italy

Abstract

In the last decade luminosities of lepton colliders have greatly risen. There are several ingredients of the success: the progress in the handling of high currents and multibunch regimes, in the beam-beam interaction limits understanding, in particle dynamics simulation codes, in the diagnostic systems to control beam sizes and orbits, in the background shielding.

Now is time to go further in the high luminosity frontiers: experiments are asking for more precision measurements, and the accelerator community is facing projects where the increase of luminosity by orders of magnitude is conceivable. New ideas, main upgrades and plans in the factories presently in operation around the world are the subject of this paper.

INTRODUCTION

The frontier of high luminosity does not coincide with the high energy one. Non-search colliders dedicated to precision physics have in last decade advanced the luminosity by one order of magnitude. The great success of B-factories which in few years have reached their design goals has demonstrated to the physics community the possibility of reaching in their experiments unprecedented precisions approaching theory limits.

For sake of discussion, the diagram of the luminosity, L, versus energies, E, can be divided in three zones (see Fig.1): in the first zone the energy increase is privileged for new particles production, reaching the maximum with LEP; the corresponding luminosity is continuously improved, both for its dependence on energy and for the advances in technologies and collision physics. Beyond LEP linear colliders will supplant circular ones; VLLC should double LEP energy but at the price of one order of magnitude in ring size. In the second zone there are the present factories, with luminosities one order of magnitude larger than the previous ones at the same intermediate energies. The third zone represents the future, in which upgrades by a factor 10 seem reachable with present technologies, while higher upgrades are subjected to R&D progress.

The physics community asks for higher fluxes of particles at the intermediate energies[1-4]. The annihilation production cross section in e^+e^- collisions is proportional to the inverse square of the energy, and the necessary integrated luminosity scales accordingly:

$$\int L \propto \frac{1}{\sigma} \propto E^2 \qquad (1)$$

Table I shows the approximate integrated luminosities already collected by all experiments in the energy range between the Φ and the B, and the luminosities requested for competitive experiments in the LHC era. There is a long path before reaching the wanted specifications. A review of the plans of e^+e^- factories according to their energy is described in the paper.

Table 1 - Collected and requested integrated luminosities

	E_{cm} (GeV)	logged ∫L	requested ∫L
Beauty	10.6	~ 300fb^{-1}	10 ab^{-1}
τ-charm	3.9	< 1 fb^{-1}	>100 fb^{-1}
light quarks	1-2	< 100pb^{-1}	500 pb^{-1}
Φ	1	< 1 fb^{-1}	100 fb^{-1}

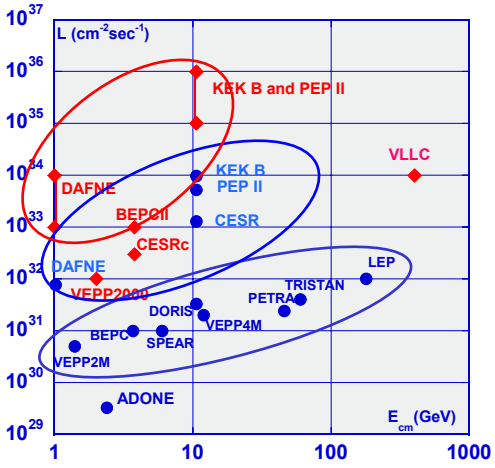

Figure 1: Luminosity versus energy in lepton circular colliders. Past and present results (blue dots), future projects and designs (red diamonds)

LUMINOSITY CONSIDERATIONS

Storing high currents in closely spaced bunches and squeezing as much as possible beam sizes translates in luminosity increase, according to:

$$L = \frac{f_{coll}}{4\pi} \frac{N^+ N^-}{\sigma_x^* \sigma_y^*} \qquad (2)$$

The collision frequency, f_{coll}, the bunch populations, $N^{+,-}$, the transverse beam sizes, $\sigma_{x,y}^*$, apparently independent, are strongly related by the beam-beam interaction and by collective effects. According to the collider regime, L can be written in terms of the characteristic beam-beam tune shift parameters, $\xi_{x,y}$, the emittances, $\varepsilon_{x,y}$, the betatron functions at the IP, $\beta_{x,y}^*$: when the reachable $\xi_{x,y}$ is the most severe luminosity limitation, L for flat beams is usually expressed as:

$$L = \frac{\pi f_{coll}}{r_o^2} \frac{\gamma^2 \varepsilon_x}{\beta_y^*} \xi_x \xi_y \qquad (3)$$

which compared with eq.1 shows the same dependence with the energy.

High currents

All high current issues have been addressed by the collider physicists together with the synchrotron radiation community. The understanding and control of machine impedances has increased the threshold instabilities in all high brilliance rings. The present generation of bunch by bunch feedbacks for multibunch operation, first tested in synchrotron light sources[5], is operational in all factories and is also a powerful diagnostic tool.

Ion trapping in electron rings, already known when first generation factories were designed, is controlled by gaps in bunch trains and/or ion clearing electrodes. Electron cloud instability (ECI) in e^+ rings, which was first observed at the KEK Photon Factory in 1995, is one of the main limiting effects in increasing the currents in B-factories. The photoemission and multipacting creates additional loads to vacuum and cryogenic systems, and the emittance blow-up constitutes a serious limitation to luminosity. Solenoidal windings are the present cure of the instability; new vacuum chamber designs are being developed, in collaboration with the hadron collider community, also threatened by the ECI.

Besides instabilities induced by collective effects, high currents are responsible for intense photon fluxes on the vacuum chambers and high loads on rf system; vacuum, cooling and rf technology developments are always correlated with every achievement in the luminosity scale[6].

Beam-beam

Beam-beam effect limits the single bunch luminosity. All present factories, but VEPP2000, are based on the multibunch regime. Crossing angle is now better understood. The Piwinski factor relating the crossing angle θ with the characteristic dimensions of the bunch:

$$\phi = \theta \frac{\sigma_L}{\sigma_x} \qquad (4)$$

has reached values that 10 years ago were considered dangerous source of synchrobetatron resonances.

Small values of β_y* are obtained thanks to magnet technology, which has developed small dimension - high gradient quadrupoles to be placed near IPs.

Careful tuning of single ring working point, dynamic aperture optimisation, possibility of coupling corrections up to very small values (coupling of the order of 0.1% have been obtained), are all dowels of the puzzle for obtaining high beam-beam tune shifts.

Background

Background rejection from experiments is one of the key points of any collider. Continuous optimization of background is done routinely at all present factories, and adding masks, collimators, and cooling is envisaged in next future in all of them. In the lower energy factories, where background is dominated by Touschek losses, the lattice configuration of the whole ring is optimized for minimisation of losses in the detector areas.

Lifetime and injection

Average to peak luminosities ratios depend on lifetime and injection rates. Lifetimes decrease as currents are raised due to beam-gas scattering and Touschek effect, this last becoming predominant in low-energy rings. At extremely high luminosity the annihilation process becomes the predominant particle loss effect. Presently the beam lifetimes are of the order of hours, but will be shortened to few minutes in the super-factories regime. Only continuous injection will allow the operation of the colliders, and background at injection becomes one the key-point to be solved.

BEAUTY FACTORIES

The two B-factories, KEK-B and PEP II, on the opposite sides of the Pacific Ocean, have reached their design values in a very short time, compared to the scale of accelerator history, despite these values were considered challenging when in the 90's the projects were conceived. During the preparation of this manuscript I have corrected the luminosity records several times.

CESR has also operated in this range of energy; this collider has shown along the years an increase in performances able to compete with the newer collider generations, and is now going towards lower energies. It kept for some time the record of luminosity and it can cover all the physics from the J/Ψ to the Beauty.

Both KEKB and PEPII plan upgrades for next two-three years, optimizing the existing systems to reach luminosities of few 10^{34}cm^{-2}sec^{-1}. Further steps on luminosity are being planned in a time scale of 10 years. Table 2 shows some of the main parameters for the future upgrades [7-8].

Table 2 - B factories from 10^{34} to 10^{36} cm^{-2}sec^{-1}

Collider	KEK-B		PEP-II		
	super	hyper	next	super	hyper
E + (GeV)	3.5	3.5	3.1	3.5	3.5
E - (GeV)	8.0	8.0	9.0	8.0	8.0
C (m)	3016	3016	2199	2199	2199
L 10^{34}cm^{-2}s^{-1}	10	40-100	2.5 - 4	20	100
IPs	1	1	1	1	1
β^* (m) (h)	0.30	0.15	0.5	0.3	0.15
β^* (m) (v)	0.003	0.003	0.0065	0.0037	0.0015
ε (n rad) (h)	33	33	44	44	44
ε (n rad) (v)	2	0.33	0.44	0.44	0.44
θ (mrad)	±15	0	0 -± 4	±10	±15
ξ (h)	0.068	0.1	0.08	0.10	0.10
ξ (v)	0.05	0.2	0.08	0.10	0.10
N bunches	5018	5018	1700	3400	7000
I+ (A)	9.4	17.2	4.5	11.0	10.3
I - (A)	4.1	7.8	2.0	4.8	2.35
f_{RF} (MHz)	509	509	476	476	952

PEP-II upgrades

The goal of reaching L of the order of 10^{34} $cm^{-2}sec^{-1}$ by 2005 is based on adding rf stations in order to increase currents and number of bunches. Shorter bunches, and therefore smaller β_y^* will be possible. An upgrade of the longitudinal feedback system with new electronics and DAFNE-like kicker[9] will increase the effectiveness of the system. Higher injection rate, correlated with added collimators to shield injection background will pay on the integrated luminosity. Solenoidal windings for ECI together with increased cooling should help in the current increase.

The same philosophy is foreseen up to 2008, but pushing parameters to more limiting values: β_y^* will be decreased by 50% by moving quadrupoles closer to IP, a small crossing angle in the new IR will be introduced, higher currents will be based on the feedback system upgrade to go to 2-bucket spacing. All these actions should push luminosities up to 2-4 10^{34} $cm^{-2}sec^{-1}$. $\xi_{x,y}$ of 0.08 are considered achievable.

Higher luminosity considerations will be of course related to the achievements obtained at that point; with the today know-how, the idea is to increase the collision frequency by filling all buckets, without increasing bunch currents, together with a larger crossing angle and smaller betas at IP. The total current will be doubled and to save wall power the energy asymmetry will be diminished. Tune shifts will be 0.1 and L of the order of $10^{35}cm^{-2}sec^{-1}$.

The main upgrade for a further increase is again doubling the number of bunches by changing f_{rf} to 950 MHz, and still increasing the crossing angle. With the same b-b tune shift and slighly lower currents per bunch the total L could reach values of 10^{36} $cm^{-2}sec^{-1}$. R&D on the rf cavity and related systems is already in progress.

KEK-B upgrades

The Japanese B-factory has recently exceeded the 10^{34} $cm^{-2}sec^{-1}$ goal, the maximum luminosity ever reached. The upgrades for a factor 10 are based on an increase of the bunch number by a factor 4, together with an increase of the bunch current, lowering β_y^* by a factor 2 and increasing the crossing angle. An increase of the emittance keeps the b-b tune shifts equal to the present ones. The main challenge are the high current effects; the rf system will be upgraded and SC rf cavities will be added. A beam-energy switch is envisaged, so that e^+ are stored in the HER with lower currents to weaken the ECI effect. An upgrade of the injector is thus being studied to accelerate positrons up to 8 GeV. Intensive R&D on vacuum chamber design, with antichambers and special rf shields is in progress, and prototypes are being constructed to be installed soon in the collider for first tests.

Crab crossing and head-on collisions are the key point to reach 10^{36} $cm^{-2}sec^{-1}$: higher b-b tune shifts by doubling the current per bunch and no reduction factor due to crossing angle are predicted by simulations. The very high ξ_y is obtained also by lowering the coupling.

TAU-CHARM FACTORIES

BEPCII, CESRc

CESR is moving toward lower energies. Wigglers are added to increase radiation damping, and this is the main feature for the new configuration. The first wiggler has just been installed and commissioned. Other 12-14 wigglers will be installed in one year and CESR will run until 2008 at three energies between 3.1 and 4.1 GeV.

In China BEPC will be upgraded to become the first completely dedicated tau-charm factory, still mantaining the synchotron radiation production. Its design is based on the double ring scheme, with energies ranging between 1.5 and 2.5GeV per beam, optimized at 1.89 GeV. An inner ring will be installed inside the old one, so that each beam will travel in half outer ring and half inner one. Superconducting cavities fitting the bunch length requirements will be installed. The production began in 2002 and commissioning is foreseen for 2006.

Table 3 shows the design values of the Chinese τ-charm factory[10] together with the CESR-c[11] parameters at the same energy.

Table 3 - Tau charm factories

Collider	CESRc	BEPC II
status	operating	in construction
E (GeV)	1.88	1.89
C (m)	768	237.5
L (10^{32} $cm^{-2}s^{-1}$)	3	10
IPs	1	1
β* (m) (h / v)	0.7/ 0.011	1 / .015
ε (μ rad) (h / v)	0.22	0.17 / 0.002
θ (mrad)	± 2.8	± 11
ϕ (rad)	0.07	0.4
σ_z (cm)	1.0	1.5
N_b (10^{10})	6.4	4.8
ξ (h / v)	0.03 / 0.03	0.04 / 0.04
N bunches	45	93
I (A)	.18	0.91
f_{RF} (MHz)	500.0	499.8
V (MV)	10	1.5

.

LIGHT QUARKS FACTORIES

Physics at energies between the ϕ and τ have been covered during last years by VEPP-2M (shut down in 2000) and BEPC colliders. The interest for this energy range had produced the proposal for PEP-N[12]. Now a collider, innovative in its design and concepts, is in construction: VEPP2000. At this energy range the interesting physics needs moderate integrated luminosities, as shown in Table 1.

VEPP2000

A 2 GeV collider (from there the 2000 in the name), whose design is based on the concept of round colliding beams, is being constructed in Novosibirsk[13], after the shutdown of VEPP-2M three years ago. This is a very important step in the beam-beam interaction understanding. The expected b-b tune shift is twice smaller than the corresponding flat-beam one with the same particle density, thus predicting a single bunch luminosity of $10^{32}cm^{-2}sec^{-1}$[14].

The collider can be operated also with flat beams and at energies ranging from 500 Mev to 1 GeV per beam. Its compact design is based on very high field normal conducting dipoles (2.4T) and houses two experiments in the two simmetric Interaction Regions. Focusing in the two interaction regions is performed by SC solenoids, which also rotate by $\pi/2$ the planes of betatron oscillations, thus creating emittance in both transverse modes. Dynamic aperture is challenging due to the high chromaticity and beam sizes on both planes.

Dipoles are bein installed, solenoids are in the construction phase and first beam is foreseen in one year from now.

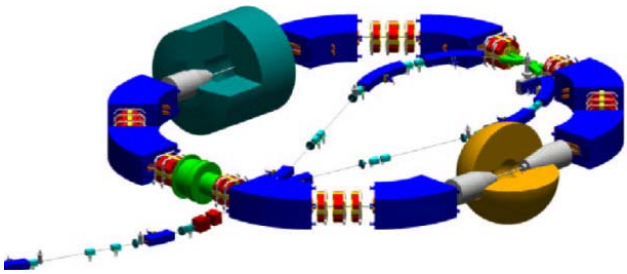

Fig. 2 - View of the VEPP-2000 collider

Table 4 - Light quarks factories

Collider	VEPP2000	DAFNE 2
status	in construction	design study
E (GeV)	1.	1.
C (m)	24	97
L (10^{32} $cm^{-2}s^{-1}$)	1	1
IPs	2	1
β^* (m) (h / v)	0.1 / 0.1	1.5 / 0.025
ε (μrad) (h / v)	0.136 / 0.136	0.5 / 0.0025
θ (mrad)	0	±15
ϕ (rad)(Piw)	0	0.26
σ_z (cm)	3	1.1
N_b (10^{10})	10	3
ξ (h / v)	0.1 / 0.1	0.014 / 0.024
N bunches	1	30
I (A)	0.20	0.45
f_{RF} (MHz)	172	368.3
V (MV)	0.12	0.25

DAFNE2

DAΦNE has been constructed to operate at the Φ resonance. Some of the systems are dimensioned to operate also at higher energies. It is presently under discussion which will be the future of the collider. One of the possibilities is to increase the energy by a factor of two [15]. The project is named DAFNE2, where "F" stands for Frascati and "2" for the E_{cm}. No crucial issues from the accelerator physics point of view are envisaged. The main hardware modifications concern dipoles, splitter magnets, and low-beta quadrupoles, while rf and vacuum systems are already dimensioned for the high energy, with a lower beam current. The main parameters are given in table 4 together with those of VEPP2000 for comparison.

Φ-FACTORIES

DAΦNE is the only Φ-Factory presently in operation. VEPP2000 can be operated also at the Φ resonance, with of course a lower luminosity than the optimum one.

DAΦNE

By the end of 2005 all the current physics programs are expected to be almost completed, with an overall delivered integrated luminosity in excess of $3fb^{-1}$ and luminosities higher than $10^{32}cm^{-2}sec^{-1}$. Operation is done in time sharing between the two experiments, since simultaneous collisions at both IPs are critical. After the DEAR completion [16], during the 2003 shutdown the third experiment, FINUDA, is being installed, and will share the collider with KLOE during the next few years. Crossing angle will be increased with respect to design values, by changing the low beta configuration from FDF to DF. Both β_x^* and β_y^* will be lowered. Sextupole components are being added to a family of quadrupoles for dynamic aperture optimization. Damaged ion clearing electrodes are being replaced.

The interest for values of the luminosity larger by a factor 10[4] than the design ones has lead to the study of possible new designs of the factory.

Experience has shown that powerful radiation damping is needed; presently in DAΦNE natural damping is increased by a factor two by the wigglers, which on one hand increase achievable b-b tune shifts, but on the other one limit the dynamic aperture. Simulations [17] show that roughly a factor 10 on τ_d would allow an increase of the b-b tune shifts by a factor of two. A preliminary design of a ϕ-factory is being studied. The parameters are shown in Table 4, together with those which are foreseen for next future in the present configuration. The preliminary design, named DAΦNE-w[18], is based on cells where positive and negative normal conducting bendings alternate, with a net positive bending angle and an increase in radiation damping. The layout and the vacuum chamber design are different from the present one. Special care is dedicated to optimise the dynamic aperture, and is mainly dominated by the non linear terms arising from the wiggling bendings. Increase of the average luminosity is expected from continuous injection scheme, based on the separation of the now shared e^+ and e- injection transfer lines.

Table 4 - ϕ factories

Collider	DAΦNE	DAΦNE w
status	until 2005	design study
E (GeV)	.51	.51
C (m)	97	80
L (10^{32} cm^{-2}s^{-1})	> 1	> 10
IPs	1	1
β* (m) (h / v)	1 / 0.025	0.5 / 0.01
ε (μ rad) (h / v)	0.6 / 0.006	0.2 / 0.001
θ (mrad)	± 16	± 15
ϕ (rad)	0.39	0.57
σ_z (cm)	2	1.2
N_b (10^{10})	3.6	3.5
ξ (h / v)	0.027 / 0.043	.079 / 0.070
N bunches	100	95
I (A)	1.8	2.0
f_{RF} (MHz)	368.3	369
V (MV)	0.2	0. 5

NEW IDEAS

New, original, sometimes daring ideas for increasing the particle production are arising. I will mention some of them.

Collision with four-beam scheme, which was tested in DORIS and DCI, with neutralization of the charge between e+ and e$^-$, and no b-b linear tune shift, has been revisited by the KEKB group[7] .

Collide beams of higher energies with large crossing angles, so that E_{cm} corresponds to the Φ, is being investigated for DAΦNE: two 1.5 GeV rings colliding at 140° (meaning that beams travel in the same direction), will produce Φ's with a boost such that K_s decays in length of 1m, while K_L can be detected at distances up to 10 m, simplifying the problem of detector background shielding. The main advantage is the less critical behaviour of a higher energy ring from the point of view of beam lifetime and radiation damping. Luminosity and ξ behaviour with large crossing angle have been investigated[19]. The main disadvantage is the need of very short bunch. Introduction of a "longitudinal low beta" at the IP, so that the beam changes its length along the ring and is minimum at the IP, by tuning the R_{56} term along the ring, is being investigated.

Collide ring against linac is another idea being taken into consideration.

CONCLUSIONS

The next steps of the lepton factories are straightforward and consist in optimizing all the techniques developed during last ten years, expecting in all cases an increase in peak and integrated luminosity by about a factor 10. New ideas to push the luminosity values by another order of magnitude are being investigated. Round beam collisions will soon be tested at VEPP2000, answering to the question whether b-b tune shift limits can be raised. Fig.3 summarizes the foreseen timetable for the present factories in next future.

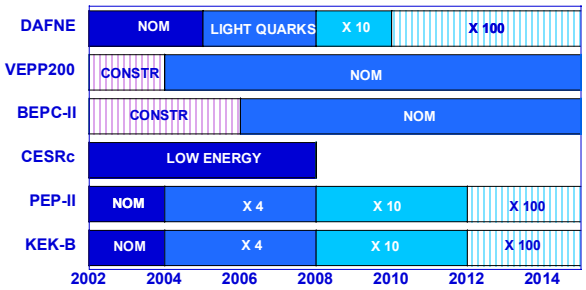

Fig. 3 - Timetable of foreseen factories future

ACKNOWLEDGMENTS

Colleagues from all the mentioned colliders have kindly provided informations about their projects. Without mentioning everybody, I thank them all, sure that the fruitful collaboration between laboratories will continue in the pursue for higher luminosities.

REFERENCES

[1] S. Olsen, "Search for New Physics at Super-B Factories", Report to the ICFA Seminar, CERN October 2002
[2] P.Roudeau, "Tau and Charm Physics Highlights", Proc. of Lepton-Photon 01,Rome, Italy, p.119,2001
[3] "e+e- Physics at Intermediate Energies Workshop, SLAC, 30April-2May 2001
[4] F.Bossi, G.Colangelo, G.Isidori, "Searching for KL-> πο ν ν at a Φ-factory", Eur.Phys.Jour. C6 (1999), 109-119
[5] D. Teytelman et al., "Operation and Performance of the PEPII Prototype Longitudinal Damping System at the ALS", IEEE PAC 1995:2420-2422 (QCD183:P3:1995)
[6] K.Akai, "High Intensity Issues for Super B-Factories", these proceedings (2003)
[7] Y. Ohnishi, private communication
[8] J.Seeman, private communication
[9] P. McIntosh et al. "An Over-damped Cavity Longitudinal Kicker for the PEP-II LER" these proceedings (2003)
[10] Zhang, Chuang, private communication
[11] D. Rice., for the CESR-c Working Group CESR-C*, "A Frontier Machine For QCD and Weak Decay Physics in the Charm Region", Proc. of EPAC02 Conference, Paris,2002
[12] Y.Cai et al. "PEP-N: a 0.8GeV x 3.1 GeV Collider at SLAC", Proc. of PAC2001, Chicago, p.3564
[13] Y.Shatunov et al. "Project of a New e-e+ Collider VEPP2000", Proc. of EPAC02 Conference, Paris,2002.
[14] A. Valishev, E. Perevedentsev , K. Ohmi, "Strong-Strong Simulation of Beam-Beam Interaction for Round Beams", these proceedings (2003).
[15] G. Benedetti et al., " Feasibility study of a 2 GeV lepton collider at DAFNE", these proceedings (2003).
[16] C. Curceanu, "Kaonic nitrogen and hydrogen", Proc.of "XLI International Winter Meeting on Nuclear Physics" Bormio, Italy, 2003
[17] M. Zobov, private communication
[18] Dafne team, "DAFNE-w design", LNF Technical Note, in preparation
[19] P.Raimondi, M.Zobov, "Tune Shift in b-b Collisions with a Crossing Angle", DAFNE Tech. Note, G58 April 2003

100 BUNCHES DAΦNE OPERATION

A. Drago, D. Alesini, G. Benedetti, M. Biagini, C. Biscari, R. Boni, M. Boscolo, A. Clozza, G.Delle Monache, G. Di Pirro, A. Gallo, A. Ghigo, S. Guiducci, F. Marcellini, G. Mazzitelli, C. Milardi, L.Pellegrino, M. Preger, P. Raimondi, R. Ricci, C. Sanelli, M. Serio, F. Sgamma, A. Stecchi, A.Stella, C. Vaccarezza, M. Vescovi, M. Zobov, I.N.F.N.- L.N.F., Frascati, Italy.

Abstract

The DAΦNE collider has been operating by filling 100 consecutive buckets out of the available 120 with a gap to avoid ion trapping in the electron beam. To reduce the effect of the parasitic crossings the crossing angle has been increased up to 29 mrad and the horizontal beta function at the interaction point lowered down to 1.7 m. Moreover both transverse and longitudinal feedbacks have been optimized for this more demanding mode of operation. Comparison between 100 and 50 bunches operation in 2002 runs is presented.

INTRODUCTION

DAΦNE is a e^+/e^- collider, with center of mass energy 1.02 GeV (Φ-Factory). It has two symmetric main rings and two IP's: KLOE detector is in IP1, DEAR detector is in IP2. The harmonic number is 120 and this is the maximum number of storable bunches. The minimum bunch distance is 2.7 nsec, corresponding to ~80 cm, and the maximum single bunch design current is 44 mA (achieved > 200 mA).

The peak luminosity can be expressed as function of number of bunches (n_b) and single bunch currents (I^+ and I^-)

$$L = \frac{n_b I^+ I^-}{4\pi f_{rev} e^2 \sigma_x \sigma_y} \qquad (1)$$

where f_{rev} is the revolution frequency, e is the electron charge, σ_x and σ_y are the horizontal and vertical r.m.s. sizes of the bunch.

The peak luminosity is proportional to the number of colliding bunches and to the product of the single bunch currents. We want to increase the luminosity and this can be done also increasing the number of colliding bunches and the single bunch currents.

Since the tune shift (ξ) is proportional to the bunch current (I) and tends to saturate when the current increases (up to now $\xi < 0.03$), it is not effective to inject the single bunch current over a threshold, so we have increased the number of colliding bunches.

An ion clearing gap is necessary for the e^- beam: it can be between 15% and 25% of the ring. Usually a uniform train of bunches followed by one gap is stored: every bunch of the train can be separated from the following one by N empty buckets (N=0,1,2,…).

Different bunch patterns have been used for collision in the past. In the year 1999 the collision bunch pattern was composed by a train of 23 bunches separated by 3 empty buckets and followed by ¼ ring gap.

During the year 2000 the collision bunch pattern was 30 bunches separated by 2 empty buckets and followed by ¼ ring gap.

In the year 2001 and 2002 the collision bunch pattern was 50 bunches separated by 1 empty bucket and followed by 1/6 ring gap.

In the last 2 months of the year 2002, in the IP2, for DEAR detector, the bunch pattern used for collision was 100 contiguous bunches followed by 1/6 ring gap. In Fig.1 a sketch of the colliding pattern in the years 1999-2002 is presented.

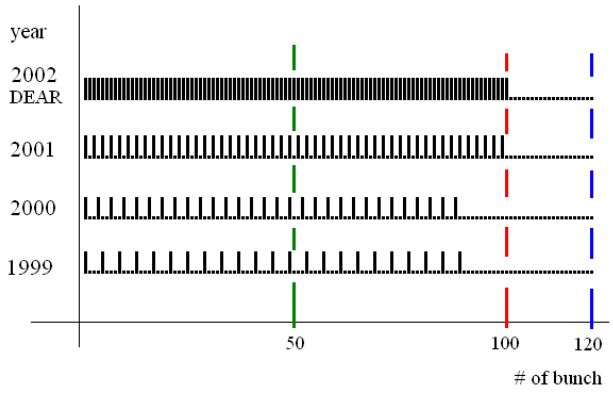

Fig. 1 – Colliding bunch patterns, years 1999-2002.

OPTICS DEVELOPMENTS

With the aim to bring into collision 100 contiguous bunches, some modifications to the optic layout have been implemented to minimize the effects of the parasitic crossings:

1) a lower horizontal beta in the Interaction Region (see Fig. 2);
2) a larger Crossing Angle at the IP, from 12.5*2 mrad to 14.5*2 mrad;
3) a smaller horizontal emittance.

With these modifications the first parasitic crossing horizontal separation (@40 cm from IP) has increased from 5 σ_x to 12 σ_x.

Minimizing of the horizontal size (see points 1 and 3 listed above) gave also a single bunch luminosity increase.

In order to reduce the non-linearities, three octupole magnets have been installed in each ring. Tuning correctly the machine non-linearities, it has been possible to reach better lifetimes, dynamic apertures and improve beam-beam performance. A machine model has been developed to study the linear and non-linear behaviour [1].

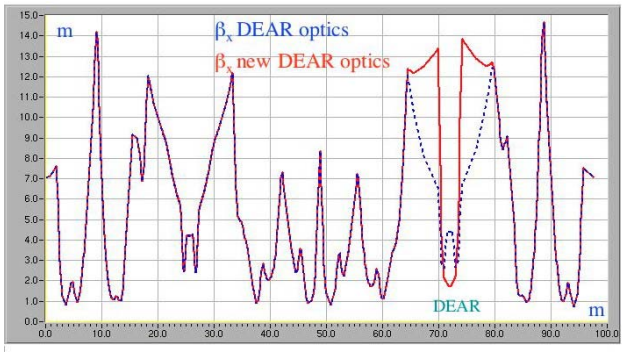

Figure 2: The horizontal beta at IP2 has been lowered: 4.4m at December 2001(blue), 1.7m after April 2002 (red).

The Piwinski's angle is evaluated as a "badness factor". It is given by the formula

$$\theta = \frac{\sigma_z \phi}{\sigma_x} < 1 \qquad (2)$$

where σ_z and σ_x are the longitudinal and horizontal r.m.s. sizes of the bunch and ϕ is the crossing angle.

Table 1: Piwinski's angle θ for different DAΦNE setup.

	σ_z cm	βx, m	β_y, m	ε_x, 10^{-6}	σ_x mm	σ_y μ	ϕ mrad	θ
Design	3	4.5	.045	1	2.12	20	12.5	.18
KLOE	2.5	2.7	.026	.74	1.41	20	11.5	.20
DEAR, Decemb. 2002	2	2.54	.040	.78	1.13	20	13.5	.24
DEAR, After April 2002	2	1.7	.030	.62	1.03	20	14.5	.28

In Table 1 are reported several machine parameters applied to four different machine setup: design, collision for Kloe, collision for DEAR before and after April 2002. β_x and β_y are the horizontal and vertical betatron functions, ε_x is the horizontal emittance, ϕ is the crossing angle at the IP, and θ is the Piwinski's angle.

As it can be seen, in order to bring into collision 100 bunches, the crossing angle and, as consequence, Piwinski's angle have been increased. However, this practically does not affect the single bunch luminosity.

BEAM DYNAMICS

The DAΦNE longitudinal dynamics is affected by strong coupled bunch synchrotron dipole oscillations well damped by the feedback developed with SLAC/LBL.

Besides in both rings, at high currents, harmful longitudinal quadrupole instabilities need to be cured.

In Fig. 3 a positron beam power spectrum measured by a powerful real time FFT analyzer HP3587s is shown. The beam spectrum, recorded with 100 bunches, 900mA, in collision, shows a large longitudinal quadrupole instability on the mode #76.

The Longitudinal feedback, built to damp the synchrotron dipole oscillations, is able, using a special setup, to damp the quadrupole motion [2].

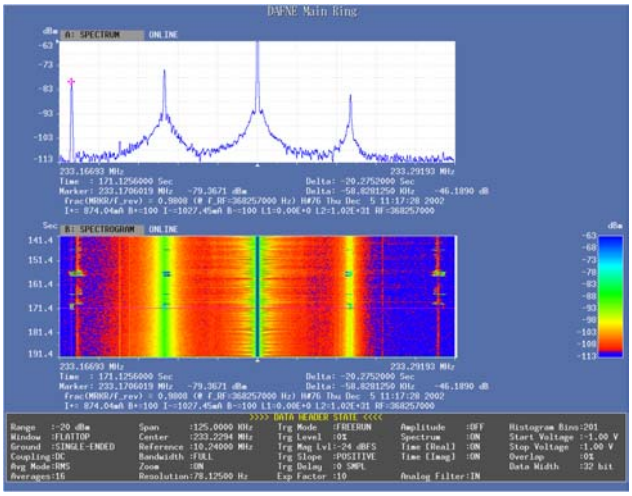

Fig.3 - e^+ beam power spectrum measured by a real time FFT analyzer HP3587. The beam spectrum, (100 bunches, 900mA, in collision) shows a large longitudinal quadrupole instability.

Vertical and horizontal instabilities require powerful feedback systems.

In the year 1999 the collision bunch pattern was 23 bunches each separated by 3 empty buckets. Only the longitudinal feedback was installed at full power (3x250W), without any transverse feedbacks.

During the year 2000 the collision bunch pattern was 30 bunches each separated by 2 empty buckets. The vertical feedbacks were added with reduced power (2x100W). In the year 2001 the collision bunch pattern was 50 bunches separated by 1 empty bucket. The vertical feedbacks were working at full power (2x250W) and the horizontal ones with reduced power (2x100W).

In the last 2 months of the year 2002 the bunch pattern was 100 contiguous bunches colliding in IP2 (DEAR) and the complete control of longitudinal quadrupole in both rings was successfully achieved.

With the new layout, it has been possible to store more than 1.8A with stable e^- beam in 90 contiguous bunches (single beam not colliding, >20mA per bunch), while in 50 bunches separated by 1 empty bucket, the maximum current achieved was smaller (~1.250A).

To achieve this, it has been necessary a very accurate transverse and longitudinal feedback setup and a complete separation of the signal of contiguous bunches in the feedbacks.

RESULTS

In this section we present the results obtained in the October–December 2002 shifts with 100 bunches colliding. In Fig.4 signals coming from two longitudinal pickups and showing the e^+ and e^- bunch train during collision, are monitored by an oscilloscope.

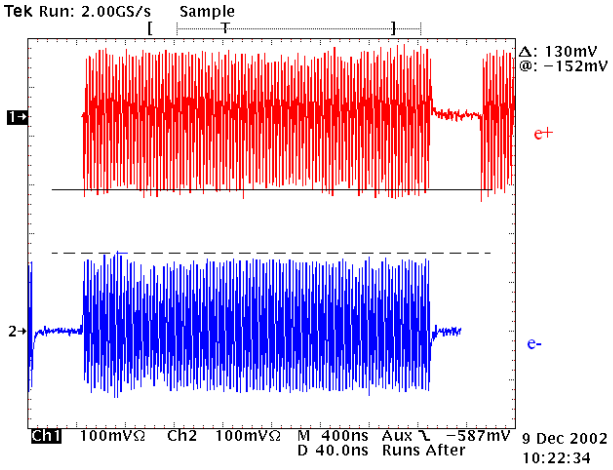

Fig.4 - Signals from two longitudinal pickups show the e^+ and e^- bunch train during collision monitored by an oscilloscope.

During the collision shifts more than 2 Ampere have been usually stored in two beams with acceptable background and lifetime.

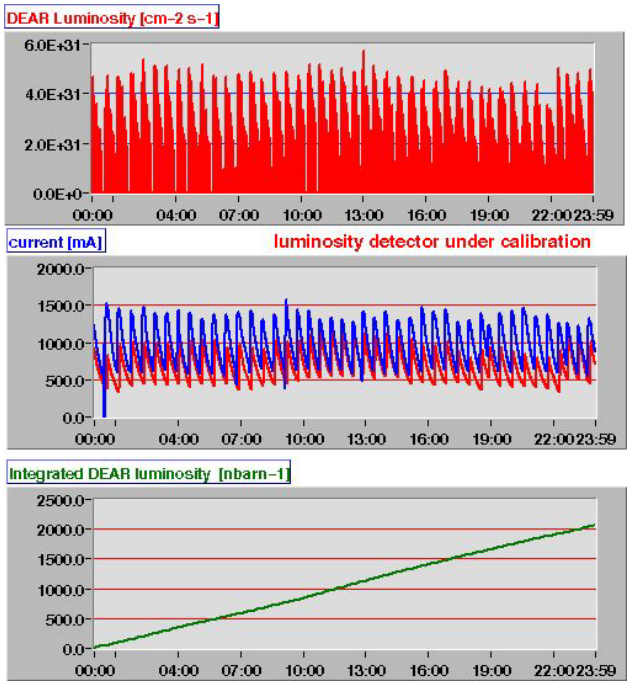

Fig.5 – Peak and integrated luminosity in 24h (12/8/02).

The collider has shown a very good reliability: in Fig. 5 the peak luminosity, currents and integrated luminosity are presented for one of the best 24 hours of data taking (12/8/2002, IP2). With 100 bunches a DEAR peak luminosity of $7*10^{31}$ cm-2 s-1 has been achieved while with 50 bunch it was $4.5*10^{31}$ cm-2 s-1. With 100 bunches a DEAR integrated luminosity of 2 $pbarn^{-1}$ per day has been reached while with 50 bunches the maximum value was 1.1 $pbarn^{-1}$. This has allowed completing the physics program for the DEAR experiment.

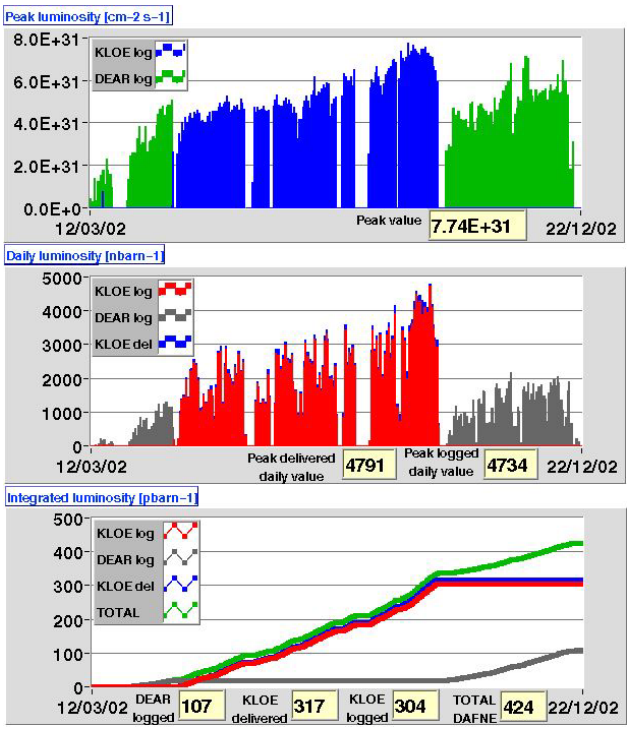

Fig. 6 – Year 2002 peak and integrated luminosity.

CONCLUSION

During 2002 it has been possible to collide with 100 contiguous bunches (out of 120) by implementing a new machine setup, lowering the horizontal beta at the IP, increasing the crossing angle and decreasing the horizontal emittance.

Storing high current in 100 bunches has become possible using powerful active feedback systems necessary to damp longitudinal dipole oscillations, longitudinal quadrupole, horizontal and vertical instabilities.

As result both peak and integrated luminosity have grown and there is still margin for further improvements increasing the currents up to 20mA per bunch; these results have been obtained in only two months.

With these shifts, DEAR experiment has completed the data taking. New IR's for KLOE and FINUDA detectors have been designed taking in mind this approach and are ready for the next shifts.

REFERENCES

[1] Milardi et al. "Developments in Linear and Non-Linear DAΦNE Lattice", RPAG025, these proceedings.

[2] A. Drago et al. "Longitudinal quadrupole instability and control in the Frascati DAΦNE electron ring", Phys. Rev. ST-AB, Vol.6, I5, 052801 (2003).

COLD- AND BEAM TEST OF THE FIRST PROTOTYPES OF THE SUPERSTRUCTURE FOR THE TESLA COLLIDER

J. Sekutowicz, C. Albrecht, V. Ayvazyan, R. Bandelmann, T. Büttner, P. Castro, S. Choroba, J. Eschke, B. Faatz, A. Gössel, K. Honkavaara, B. Horst, J. Iversen, K. Jensch, H. Kaiser, R. Kammering, G. Kreps, D. Kostin, R. Lange, J. Lorkiewicz, A. Matheisen, W.-D. Möller, H.-B. Peters, D. Proch, K. Rehlich, D. Reschke, H. Schlarb, S. Schreiber, S. Simrock, W. Singer, X. Singer, K. Twarowski, G. Weichert, M. Wendt, G. Wojtkiewicz, K. Zapfe,
DESY, 22603 Hamburg, FRG
M. Liepe, Cornell University, Ithaca, NY 14853, USA
M. Huening, FNAL, Batavia, IL 60510, USA
M. Ferrario, INFN, 00044 Frascati, Italy
E. Pławski, INS, 05400 Otwock, Poland
C. Pagani, INFN, Milano, 20090 Segrate, Italy
N. Baboi, SLAC, Menlo Park, CA 94025, USA
H. Chen, H. Wenhui, C. Tang, S. Zheng, Tsinghua University, 100084 Beijing, China

Abstract

After three years of preparation, two superstructures, each made of two superconducting 7-cell weakly coupled subunits, have been installed in the TESLA Test Facility linac (TTF) for the cold- and beam test. The energy stability, the HOMs damping, the frequency and the field adjustment methods were tested. The measured results confirmed expectation on the superstructure performance and proved that alternative layout for the 800 GeV upgrade of the TESLA collider, as it was proposed in TDR [1], is feasible. We report on the test and give here an overview of its results which are commented in more detail elsewhere in these Proceedings.

INTRODUCTION

The superstructures (SSTs), chains of superconducting multi-cell cavities (subunits) connected by λ/2 long tube(s) have been proposed as an alternative layout for the TESLA main accelerator. This concept is discussed in more detail in [2, 3]. We re-call here two main advantages of the layout in comparison to the standard one, based on 9-cell cavities. The first economical advantage is that structures made of more cells will reduce the number of the Fundamental Power Couplers (FPC) in the linac. Consequently, the number of all auxiliaries needed to distribute the RF power, like: waveguides, bends, circulators, 3-stub transformers, loads etc., can be reduced too. In addition, the layout reduces the amount of electronics controlling phase and amplitude of cavities in the linac and simplifies the design of cryomodules due to less openings for the FPCs. The second advantage is the increased filling of the linac tunnel with accelerating structures, since the distance between subunits is λ/2 only. The space saving can be significant and in the case of here discussed versions of SSTs it amounts to ~1.8 km. The first superstructure (SST-I), as it has been proposed in [2], was meant to be made of four 7-cell cavities. We have built a Cu model of this version and six Nb 7-cell subunits.Meanwhile, a 2x9-cell version (SST-II) was studied and was found to be more attractive for the TESLA collider. This version keeps the same fill factor of the tunnel as the first one. SST-II is shorter and its production, cleaning and handling will be easier. Savings in the investment cost are of the same order for both superstructures. The RF parameters of both versions are listed in Table 1.

Table 1. RF parameters of both superstructures.

Parameter		SST-I	SST-II
Number of cells in subunit		7	9
Number of subunits		4	2
(R/Q) per subunit	[Ω]	732	985
E_{peak} / E_{acc}		2	2
B_{peak} / E_{acc}	[mT/(MV/m)]	4.2	4.2
L_{active}	[m]	3.23	2.08

PREPARATION OF THE TEST

2x7-cell prototype

We have "split" the 4x7-cell prototype in two 2x7-cell prototypes. The main argument to split the prototype of SST-I was similarity in the RF-properties of the 2x7-cell and the favorable 2x9-cell versions. The computed bunch-to-bunch energy variation for all bunches in the TESLA macro-pulse (HOMDYN [4]) was very similar, $\pm 5 \cdot 10^{-5}$ for 2x9-cell and $\pm 3 \cdot 10^{-5}$ for 2x7-cell version. The scheme of the Higher Order Modes (HOM) suppression in both versions is very similar also and is based on the HOM couplers of the same type as those used for standard 9-cell TTF cavities. The conclusion was that the beam test of already existing 7-cells subunits assembled in two 2x7-cell prototypes will tell us more about the favorable SST-II superstructure, will benchmark our computation and will give finally twice as much statistics for the measured results.

TTF Linac

Both 2x7cell superstructures were assembled into a spare cryomodule and installed in the TTF linac next to the injector. The bunch-to-bunch energy measurement at the end of the linac, which was the main purpose of the experiment, was performed by means of the spectrometer dipole with two BPMs at its front and one BPM behind it. The highest estimated energy measurement accuracy was better than $2 \cdot 10^{-4}$. Due to a very intense experimental program at the TTF linac in the year 2002, a second cryomodule, housing eight 9-cell cavities, has been installed for a long-term performance test simultaneously with the superstructures. The presence of this cryomodule had consequences for the test as discussed below.

THE TEST

Balance of the stored energy in subunits

The field profiles of the accelerating mode of both superstructures have been measured with the help of the bead-pull (perturbation) technique before the final chemical treatment and the final high pressure water rinsing. Both prototypes (P1, P2) had a good field flatness, better than 92 % and 94 %, respectively. As usual, after final preparation and cool-down there is no more possibility to use a bead for the field measurement. Still, one can apply the perturbation method to balance the mean gradient in both subunits using the cold tuners instead of a bead to perturb the e-m fields. For this, the cold tuner of each subunit was moved by 1000, 2000 and 5000 steps and for each position the frequency change of the π-0 mode was measured. Then, the final positions of the tuners were chosen to maintain exactly f = 1.3 GHz of the π-0 mode and simultaneously to ensure that the change of frequency is the same, when the tuners are moved by the same number of steps. The final status of the prototypes was cross-checked in the following way. We compared, for each cold prototype, the fundamental passband frequencies with the frequencies measured at room temperature when the bead-pull method showed the best achievable field profile. The deviation from an ideal linear shift of frequencies is a very good indicator of any change in the profile. The measured deviation for both prototypes was very small, below $8 \cdot 10^{-6}$ and we concluded that profiles remained unchanged after the final preparation and after the cool-down.

Energy gain stability

This experiment was the “proof of principle” test. Our main concern was the energy flow via very weak coupling between subunits. The stability of the energy gain for all bunches in the train means that the cells’ stored energy is refilled in time between two consecutive bunches. The test was performed in two parts. In the first one, we subjected the prototypes to a slow decay of the stored energy during the acceleration. In the second part we measured directly bunch-to-bunch energy modulation at the end of the linac. In this test both prototypes were operated very reliably at 15 MV/m. The operation of the injector, with the smallest charge fluctuation of 2.8 % within the macro-pulse, was possible, when the bunch charge did not exceeded 4 nC. We chose the bunch spacing of t_b = 1 µs to meet the highest sampling rate of the implemented BPMs’ electronics. The rise time of e-m fields resulting from the matched Q_{load} value was 790 µs and the longest beam on time was limited to 530 µs by the klystron pulse length. Each prototype has been equipped with four field probes, placed one near each end-cell. They were used to monitor the field strength during the acceleration. An example of measured signals is shown in Fig. 1. Without the energy re-filling the beam would take almost 70% of the energy stored in the cells and the voltage would drop by 45 %. No such phenomenon was observed. All signals had noisy fluctuations. The strongest oscillation was at 250 kHz. It was caused by down-converters of the low level RF-system controlling the phase and the amplitude of accelerating fields. We found, in the second part of the experiment, six more oscillations caused by the feedback loops. The Fourier transformation of three signals (from the BPM behind the dipole), measured for three different gains in the feedback loop, is shown in Fig. 2. One can see in total 15 oscillations. Peaks No. 1, 2, 12 and 13 increased when the loop gain increased. Peaks No. 14 and 15 decreased vs. the gain. All other peaks remained unchanged. Seven peaks were due to the feedback loops, eight (No. 3÷10) were caused by the second cryomodule. All eight cavities of this cryomodule have been detuned from 1.3 GHz by roughly 200 kHz and no power was delivered to them during the entire energy gain test. Still, the beam induced voltage in these cavities has modulated the energy of bunches. Finally, the conclusion from the energy stability test was that, no slow gradient decay and

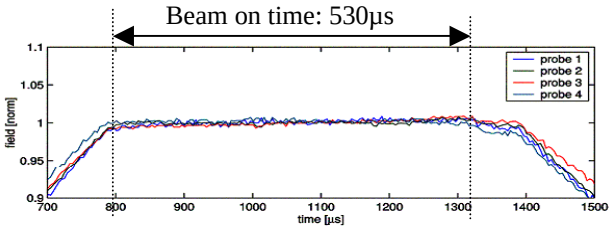

Figure 1: Signals from field probes of P2 measured during the acceleration of 530 bunches, q = 4 nC, t_b = 1 µs.

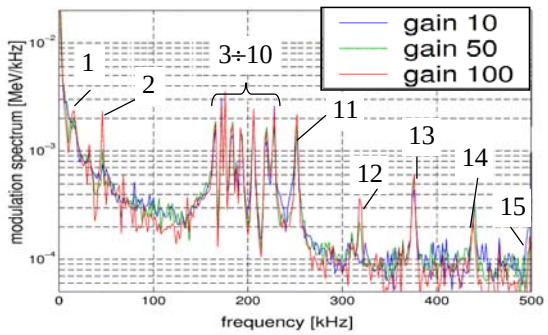

Figure 2: Spectrum of the energy modulation as measured at the end of the linac.

no modulation caused by superstructure prototypes was seen within the accuracy limit in the measurement [5]. This result proves that superstructures fulfill the TDR specification for the energy variation, which must be below $5 \cdot 10^{-4}$.

HOM damping

Each prototype had three HOM couplers, which had been attached to the end beam tubes and to the interconnection. The SST-II version will have four cells more and we plan to attach two HOM couplers at the interconnection to compensate for that. We will report on the results we measured for the transversal modes, since these modes are relevant for the quality of the TESLA beam. Three methods were applied to measure frequency and impedance, $Z = (R/Q) \cdot Q_{ext,}$ of HOMs. At first, we measured the modes' frequency and Q_{ext} with a network analyzer. We measured modes up to 3.2 GHz. The method gives the mode impedance when one assumes that the actual (R/Q) is equal to its computed value. The method is limited to well "isolated" modes. The error in frequency measurement increases when Q_{ext} of a mode gets lower and when neighboring modes overlap.

The second method we applied was the active mode excitation [6]. Modes with high impedance were excited via one of the HOM couplers by means of a cw amplifier. By controlling the power coupled out by two other HOM couplers we estimated transversal kick (Z) and deflection of the on axis injected beam. It was compared to the value measured in the BPM, 15 m downstream from the cryomodule. The method can give all actual parameters of an excited mode: Z and the polarization if deflection is measured in x and y direction. It is sensitive to the setting of the beam line optics between cryomodule and the BPM. One can apply this method to modes, which couple well to HOM couplers. Forty-seven modes were measured with this method. The third method, applied to measure Z, was based on the HOM excitation by the accelerated beam when it passes the cavity off axis. The results are reported in [7]. All three methods verified a very good damping of HOMs. The suppression of dipoles with $(R/Q) > 1\ \Omega/cm^2$ is shown in Fig. 3. All modes relevant

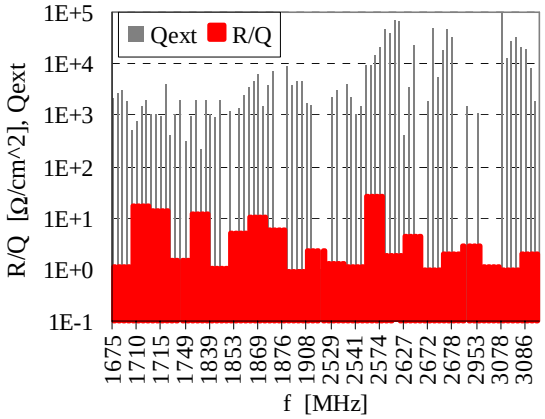

Figure 3: Damping of dipoles with $(R/Q) \geq 1\ \Omega/cm^2$.

for the TESLA collider, up to 2.58 GHz, were damped by a factor 5 to 100 better than the specification ($Q_{ext} \leq 10^5$). We have found a few modes only (in 5th passband, ~3.08 GHz), among 420 measured modes, with $Q_{ext}=10^7 \div 2 \cdot 10^8$. Their (R/Q)s are almost zero and thus they cannot degrade the quality of the TESLA beam.

FINAL REMARKS

The cold- and beam test of both prototypes has confirmed that one can use weakly coupled structures for the acceleration. Neither beam energy modulation, slow gradient decay nor insufficient HOM's damping resulting from the coupling of two subunits have been observed. The stability of the bunch-to-bunch energy gain was measured within the limit of the beam diagnostics in the TTF linac. Although, the accuracy of the energy gain measurement has not reached the level of the theoretical estimation, which was one order of magnitude smaller, the experiment showed that the TESLA specification already has been fulfilled. We have demonstrated two methods to balance the gradient in the weakly coupled subunits. The agreement of both methods was good and both confirmed that final chemical cleaning may be performed without additional degradation in the field flatness.

The experiment showed that the electronics for phase and amplitude control, used routinely to operate standard 9-cell cavities in the TTF linac, can be applied to operate the superstructures. Further improvement of the control system seems to be possible to provide better suppression of the modulations coming from the control system itself.

ACKNOWLEDGMENTS

We would like to express our gratitude to the TESLA collaboration group for many helpful discussions and to all operators of the TTF linac for their help.

REFERENCES

[1] R. Brinkmann et al., "TESLA Technical Design Report, Part II: The Accelerator", DESY 2001-01, Hamburg, March 2001.

[2] J. Sekutowicz et al., "Superconducting Superstructure", LC'97, Zvenigorod, October 1997.

[3] J. Sekutowicz et al., "Superconducting Superstructure for the TESLA Collider; A Concept", PR-ST AB, 1999.

[4] M. Ferrario et al., "Multi-Bunch Energy Spread Induced by Beam Loading in a Standing Wave Structure", Particle Accelerators, Vol. 52, 1996.

[5] H. Schlarb et al., "Bunch-to-Bunch Energy Stability Test of the Nb Prototypes of the TESLA Superstructure", PAC03, Portland, May 2003.

[6] J. Sekutowicz et al., "Active HOMs Excitation in the First Prototype of Superstructure", PAC03, Portland, May 2003.

[7] P. Castro et al., "Analysis of the HOM Damping with Modulated Beam in the First Prototype Superstructure", PAC03, Portland, May 2003.

Bunch Frequency Multiplication in the CLIC Test Facility CTF3

F. Tecker*, R. Corsini, L. Rinolfi, CERN, Geneva, Switzerland
C. Biscari, A. Ghigo, M. Preger, LNF-INFN, Frascati, Italy
P. Royer, Institut de Physique des Hautes Energies, Université de Lausanne, Switzerland
A. Ferrari†, Department of Radiation Sciences, Uppsala University, Sweden

Abstract

The aim of the CLIC Test Facility CTF3 at CERN is to prove the feasibility of key issues of the two-beam based Compact Linear Collider (CLIC) study. In particular, it addresses the generation of a drive beam with the appropriate time structure to produce high power RF pulses at a frequency of 30 GHz.

The first major goal of CTF3 was to demonstrate, at low charge, the combination of successive bunch trains by RF deflectors in an isochronous ring. This bunch frequency multiplication has been successfully performed for various combination factors up to five and will be presented.

INTRODUCTION

The Compact Linear Collider (CLIC) study [1] aims at a multi-TeV ($0.5-5$ TeV centre-of-mass), high-luminosity ($8 \cdot 10^{34}\,\mathrm{cm}^{-2}\,\mathrm{s}^{-1}$) electron-positron collider for particle physics. The CLIC scheme is based on the Two-Beam Acceleration concept where a low-energy, high-intensity drive beam powers the main beam of a high-frequency (30 GHz) linear accelerator with a gradient of 150 MV/m.

One main challenge of this scheme is to generate the drive beam in a low-frequency accelerator and to obtain the required high-frequency bunch structure needed for 30 GHz RF production. This bunch structure is obtained by sending the beam through an isochronous combiner ring using RF deflectors to inject and combine electron bunches, thus increasing the bunch repetition frequency.

The aim of the CLIC Test Facility 3 (CTF3) project is to demonstrate the technical feasibility of the key concepts of CLIC. In a first stage (CTF3 Preliminary Phase) [2], a low current test of the bunch train combination was performed, where the injection into the ring by RF deflectors and the multiplication of the bunch repetition frequency were demonstrated.

THE PRELIMINARY PHASE OF CTF3

The Preliminary Phase of CTF3 made maximum use of the existing hardware of the former LEP Pre-Injector (LPI) complex at CERN. Some major modifications had to be performed to adapt the installation to the new requirements of CTF3. The general layout of the facility is shown in Fig. 1 and a detailed description can be found in [3]. The machine was commissioned and operated between September 2001 and October 2002.

The CTF3 Preliminary Phase installation consists of a 3 GHz linear accelerator with a matching section, an injection line, and a combiner ring. The thermionic gun [4] of the linac produces up to seven electron pulses of 6.6 ns FWHM spaced by 420 ns, equivalent to the revolution period of the ring. The 3 GHz bunching system subdivides these pulses into trains of approximately 20 bunches each, spaced by 333 ps. The charge per bunch is about 0.1 nC, limited for the combination process by the beam-loading in the linac accelerating structures. The linac accelerates the bunches to an energy of about 350 MeV before entering a matching section to adapt the transverse Twiss parameters of the beam to the injection line optics. The following injection line is achromatic and isochronous at first order to avoid bunch lengthening.

The ring has a design circumference of 125.647 m, optimized for the combination where the condition

$$C = n\lambda_0 \pm \frac{\lambda_0}{N} \qquad (1)$$

has to be met between the ring circumference C and the bunch frequency multiplication factor N. λ_0 is the RF wave length in the linac and the deflectors, and n an integer. The frequency can be slightly detuned in order to switch between different combination factors from three to five.

BUNCH TRAIN COMBINATION BY RF DEFLECTORS

The injection into the ring is done using two horizontally deflecting RF structures. They are located in the ring with a horizontal betatron phase advance of π between them to create a time-dependent local closed bump of the reference orbit. The kick strength and direction vary rapidly with

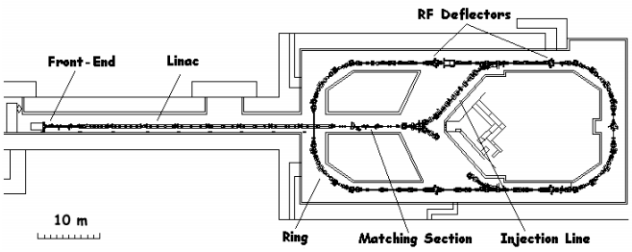

Figure 1: General layout of the CTF3 Preliminary Phase.

* tecker@cern.ch

† The research of A. Ferrari has been supported by a Marie Curie Fellowship of the European Community Programme "Improving Human Research Potential and the Socio-economic Knowledge Base" under contract number HPMF-CT-2000-00865.

time, allowing the interleaving of the bunches in the ring. Fig. 2 shows the principle of the injection with RF deflectors for a frequency multiplication factor four:

1. The bunches of the incoming train always receive the maximum kick from the RF deflector and are deviated onto the closed orbit in the ring.
2. With Eq. 1 fulfilled (for combination factor $N = 4$), the bunches arrive after one turn in the deflectors at the zero-crossing of the RF field, and stay on the equilibrium orbit. The second train is injected into the ring.
3. After a second turn, the first train bunches are deflected towards the opposite direction, the second train bunches arrive at the zero-crossing, and the third train is injected.
4. At the injection of the fourth train, the first and third train bunches arrive at the zero-crossing, and the second train bunches are kicked away from the septum. The four trains are now combined in one single train. The initial bunch spacing is reduced by a factor four and the current multiplied by the same factor.

For combination factors other than four, the phase of the deflecting field at the passage of the bunches and hence the trajectories between the two deflectors change accordingly.

The RF deflectors are short resonant, travelling-wave, iris-loaded structures with a negative group velocity. In order to obtain the nominal deflecting angle of 4.5 mrad for injection at 350 MeV, a power of about 7 MW is needed in each of the deflectors. They are powered by a common klystron with a phase shifter and variable attenuator in one

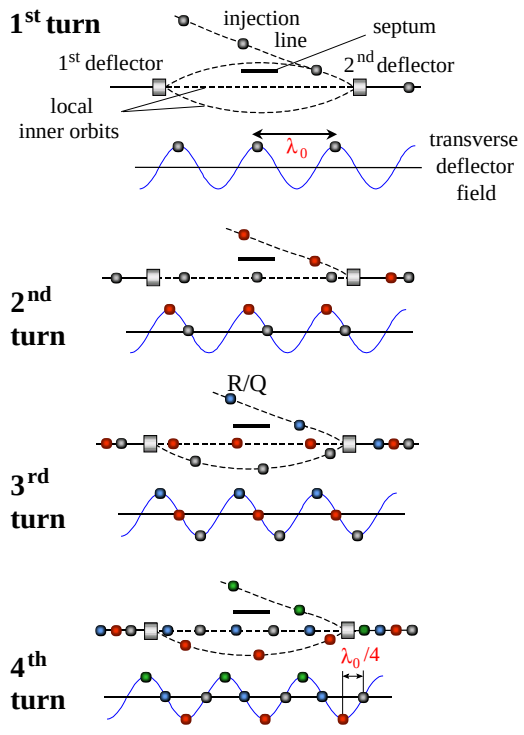

Figure 2: Bunch combination by RF deflector injection for a multiplication factor four.

of the RF network branches to allow relative phase and amplitude adjustments. Two different types of RF deflectors (built by CERN and INFN Frascati [5]) were used in two running periods of CTF3.

EXPERIMENTAL RESULTS

The linac and the combiner ring had been commissioned in 2001 [6]. The RF deflectors had been installed in the beginning of 2002. Several measurements were performed in order to prepare the bunch train combination [7]. The energy was measured after the bunching system and at the end of the linac. The beam optics was measured in the linac and found in good agreement with the design. The dispersion of the injection line was determined and one difference from the design was corrected empirically to render the line isochronous. The betatron tunes of the ring were determined for different operating conditions and were in excellent agreement with the MAD machine model. The dispersion of the ring was measured for a non-isochronous optics and showed to be very close to the model.

The bunch length is a very important issue for the combination process. The bunches must be kept short to limit the variation of the injection kick strength and the transverse extension in the injection region. Simulations have shown that about 6.5 ps rms is the maximum acceptable bunch length. The bunch length measured at the end of the linac was of the order of 3 ps rms. This imposes that both the injection line and the combiner ring have to be isochronous to avoid significant bunch lengthening. For the ring, this means that the momentum compaction factor α must smaller than 10^{-4}. A non-zero α also leads to a changing bunch distance over a number of turns in the ring due to the energy variation between the different bunches within a train created by beam loading in the linac.

The isochronicity of the ring optics was carefully tuned by changing the current in one quadrupole family while observing with a streak camera the time structure of the synchrotron light emitted in a bending magnet. Finally, the bunch distance did not change over 60 turns within the measurement error. The bunch length measured on the streak camera profiles was of the order of 4 ps rms, not changing over several turns and comparable with the one obtained at the end of the linac. Thus, within the resolution limit of the streak camera, no bunch lengthening was observed either in the injection line or the ring, proving the isochronicity as required for the combination.

The RF frequency has to be adapted for each combination factor since the path length in the isochronous ring is constant (see Eq. 1). A procedure was developed to optimize the RF frequency and both amplitudes and phases of the two RF deflectors. This procedure minimizes the injection error with respect to the closed orbit of the ring and is described in detail in [8]. A combination factor four was obtained with a frequency of $f_4 = 2.998\,585$ GHz. After the optimization, the bunch train combination showed a 100% combination efficiency. The charge multiplication could be

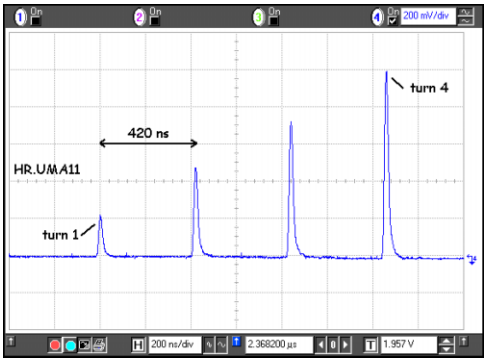

Figure 3: Intensity signal of a beam position monitor in the ring for a bunch combination by factor four.

observed on the intensity signal of beam position monitors in the ring. Fig. 3 shows that the charge increases each time a new train of bunches is combined with those circulating in the ring. The increase is not exactly linear due to pulse-to-pulse variations of the gun current.

The evolution of the time structure of the electron pulse was observed with the streak camera. Fig. 4 and 5 show typical images and corresponding intensity profiles.

For a combination factor five, the frequency was changed according to Eq. 1 and further optimized experimentally to $f_5 = 2.998\,715\,\mathrm{GHz}$. Again, a 100% combination efficiency could be obtained.

The combination performance was further studied by observing the bunch-to-bunch variations in transverse and longitudinal position [8]. Both could be minimised by the optimization procedure. Initially observed bunch spacing variations are due to the non-achromatic lattice at the observation point and could be reproduced by a linear optics model. These variations are compensated in the ejection region where the optics is achromatic.

An alternative method, based on beam frequency spectrum analysis, was also tested to monitor the frequency multiplication. A coaxial pick-up and its read-out electronics were designed and mounted in the ring to allow comparison of the amplitudes of five harmonics of the fundamental beam frequency (3 GHz) while combining the bunch trains. The commissioning of the monitor was a successful proof of principle for this new method [9].

R/Q

CONCLUSIONS

The bunch frequency multiplication has been successfully demonstrated at low charge in the Preliminary Phase of CTF3. Up to five bunch trains were combined without any measurable losses.

This proof of principle is a crucial step in the CLIC study. In the next stage of CTF3 [10], the bunch train combination will have to be shown at higher bunch charge (2.3 nC) and with longer pulses (140 ns). The CTF3 Preliminary Phase has been dismantled to allow the installation of a new linac in the building for the next stage.

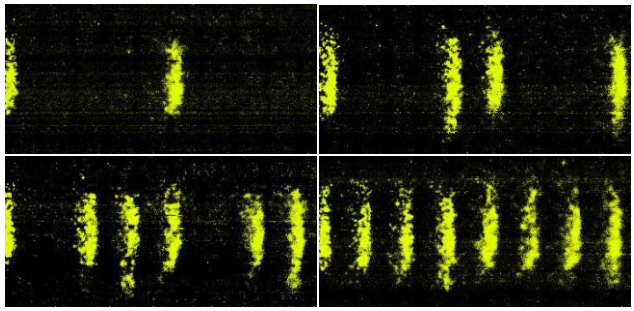

Figure 4: Bunch train combination of factor four, as observed with a streak camera. The horizontal axis represents time, the vertical corresponds to the horizontal position. The images are taken for one to four bunch trains injected.

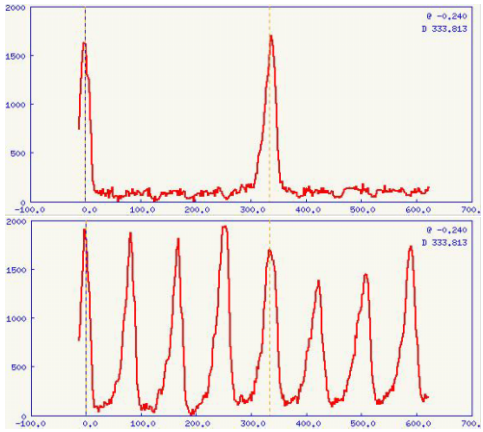

Figure 5: Longitudinal intensity profiles for a multiplication factor four. The horizontal axis is in ps. The two images correspond to injections of one and four bunch trains. Amplitude variations are again due to bunch current variations already present in the linac.

REFERENCES

[1] G. Guignard (ed.) *et al.*, "A 3-TeV e+ e- linear collider based on CLIC technology", CERN 2000-008.

[2] D. Allard *et al.*, "CTF3 Design Report. Preliminary Phase", CERN-PS-2001-072-RF.

[3] P. Royer, "Bunch frequency multiplication by RF injection into an isochronous ring", Ph.D. thesis, Université de Lausanne, Switzerland.

[4] G. Bienvenu *et al.*, "A Thermionic Electron Gun for the Preliminary Phase of CTF3", EPAC 2002, Paris, France.

[5] D. Alesini *et al.*, "RF beam deflectors for CTF3 combiner ring", EPAC 2002, Paris, France.

[6] R. Corsini *et al.*, "Status of the CTF3 commissioning", EPAC 2002, Paris, France, CLIC Note 522.

[7] R. Corsini *et al.*, "Report on the operation of the CTF3 Preliminary Phase, 8 Apr.-24 May 2002", PS/AE Note 2002-141.

[8] C. Biscari *et al.*, "Report on the third operation period of the CTF3 Preliminary Phase in 2002, 16 September - 25 October", PS/AE Note 2003-023.

[9] A. Ferrari *et al.*, "Development of a bunch frequency monitor for the Preliminary Phase of the CLIC Test Facility CTF3", DIPAC 2003, Mainz, Germany.

[10] G. Geschonke and A. Ghigo (ed.) *et al.*, "CTF3 design report", CERN/PS 2002-008 (RF).

START TO END SIMULATIONS FOR THE SPARX PROPOSAL

M. Biagini, M. Boscolo, M. Ferrario, V. Fusco, S. Guiducci, B. Spataro, C. Vaccarezza, M. Zobov
INFN-LNF, Frascati, ITALY
L. Serafini, INFN-Mi, Milan, ITALY
R. Bartolini, G. Dattoli, L. Giannessi, L. Mezi, M. Quattromini, C. Ronsivalle,
ENEA-Frascati, ITALY
E. Chiadroni, University of Rome II, Rome, ITALY
P. Emma, SLAC, Stanford, USA
J. B. Rosenzweig, UCLA, Los Angeles, USA

Abstract

We report in this paper the results of start to end simulations concerning the SPARX option based on an S-band normal conducting linac. One of the most critical systems is the bunch compressor. The effects on beam dynamics of a magnetic chicane system and a rectilinear RF compressor integrated in a high brightness photoinjector, are analyzed and compared in this paper.

INTRODUCTION

The SPARX proposal is devoted to the realization in Italy of a large scale ultra-brilliant and coherent X-ray source [1]. Two spectral complementary regions around 13.5 nm and 1.5 nm, are considered for the radiation source. A preliminary set of the required beam parameters are reported in table 1. Two basic schemes have been considered for the Linac, as shown in figure 1: the first one, the Hybrid Scheme, consists in an advanced high brightness photoinjector, with a RF compression stage [2], followed by a first linac (Linac 1) that drives the beam up to 0.5 GeV with the correlated energy spread required to compress the beam in the next magnetic chicane. The second linac (Linac 2) drives the beam up to 2.5 GeV while damping the correlated energy spread, taking profit of the effective contribution of the longitudinal wake fields provided by the S-band accelerating structures.

Table 1 – Beam Parameters

Beam Energy	2.5	GeV
Peak current	2	KA
Emittance (projected)	2	μm
Emittance (slice)	1	μm
Energy spread	0.1	%

In the Fully Magnetic Scheme the first compression stage is provided by a magnetic chicane after the Linac 1 at 350 MeV. An intermediate linac section, Linac 2, drives the beam up to 1 GeV. The next magnetic chicane compresses the beam up to the project requirements. The final Linac 3 brings the beam up to 2.5 GeV, while compensating the final energy spread of the beam.

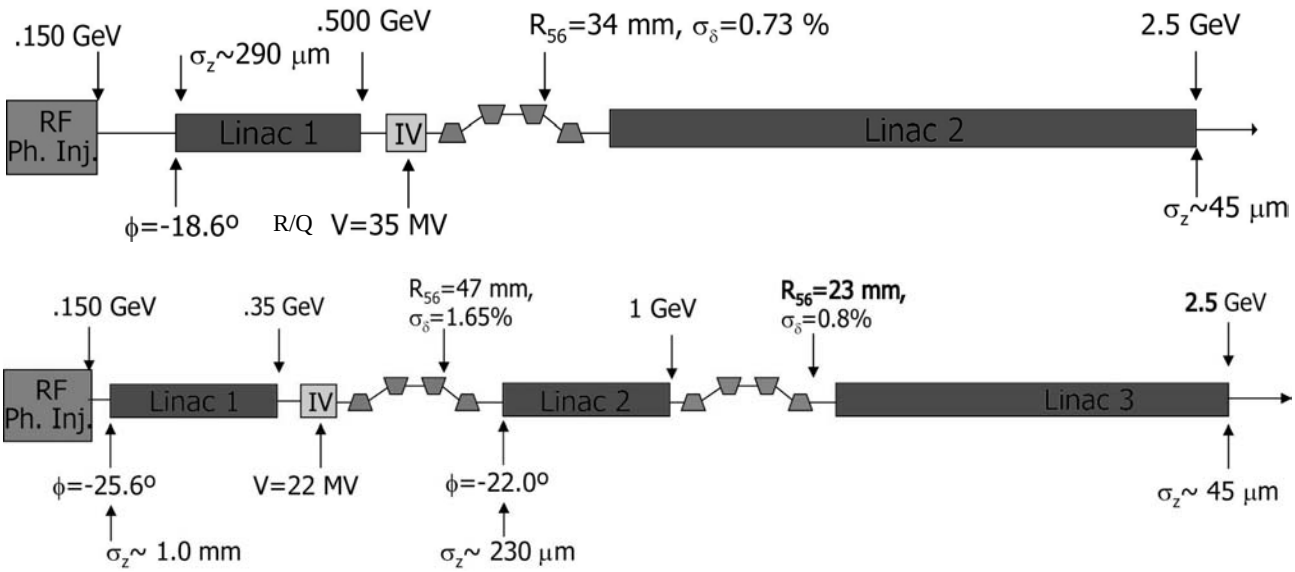

HYBRID SCHEME

The PhotoInjector design considers a 1 nC bunch, 10 ps long (flat top) with a 1.2 mm radius, generated inside a 1.6-cell S-band RF gun of the same type of the BNL-SLAC-UCLA one, operating at 140 MV/m peak field equipped with an emittance compensating solenoid (B=3090 G). Three standard SLAC 3-m TW structures each one embedded in a solenoid boost the beam up to 150 MeV. Applying the RF compression method, together with the proper setting of the accelerating phase and solenoid strength it is possible to increase the peak current while preserving the beam transverse emittance [2]. We have obtained, (Parmela [3] simulation), a bunch average current of 300 A with a normalised rms emittance below 1 μm, as shown in figure 2, using the parameter setting listed in table 2.

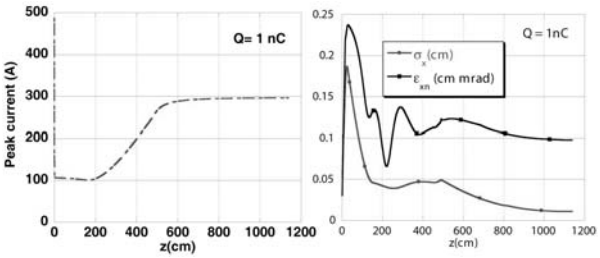

Figure 2: Parmela simulations of the peak current (left), rms norm.emittance and rms beam envelope (right), along the PhotoInjector structure.

Table 2

TW section	I	II	III
Gradient [MV/m]	15	25	25
Phase [Deg]	-86	-37	0
Solenoid field [G]	1120	1280	0

The Linac consists in a first accelerating section, Linac I, where 7 standard SLAC 3-m structures bring the beam up to an energy of .5 GeV. The accelerating phase is -18.6°, and the resulting energy spread is about 0.7%. A fourth harmonic cavity (11.424 GHz), follows, 60 cm long, in order to linearise the beam energy correlation. A magnetic chicane with R_{56} = 34 mm, about 15 m long, compresses the beam from 290 μm to 45 μm. A second accelerating section, Linac II , with 34 SLAC structures, in which the beam travels on crest, brings the beam energy up to 2.5 GeV and remove the energy spread .

FULLY MAGNETIC SCHEME

The PhotoInjector system consists of a 1.6 cell RF gun operated at S-band and high peak field on the cathode, (120 MV/m), generating a 6 MeV beam. The gun solenoid field is B=2730 G, and the injection phase is 33°. The beam is then focused and matched into 2 accelerating sections of the SLAC type, as described in [4]. Our simulations using PARMELA indicate that we can generate in this way a beam at 155 MeV with a rms correlated energy spread of 0.2%, and a rms norm. emittance of 0.6 μm (at 1.0 nC bunch charge and I = 90 A peak current). The slice energy spread and the slice norm. emittance, calculated over a 130 μm slice length, are well below 0.04% and 0.5 μm respectively, all over the bunch.

In the first accelerating section, Linac I, four standard SLAC 3-m structures bring the beam energy up to .35 GeV. The accelerating phase is -25.6°, and the resulting energy spread is about 0.17%. A fourth harmonic cavity follows in order to linearise the beam energy correlation. A magnetic chicane, about 3m long, with R_{56} = 47 mm compresses the beam from 1 mm to 230 μm. A second accelerating section, Linac II , with ten SLAC structures, operating at 22° off crest, accelerates the beam up to 1 GeV with energy spread 0.8%. The second chicane, R_{56} = 23 mm, 15 m long, compresses the beam up to 45 μm. In the third linac section, Linac III, twenty seven structures, accelerating the beam on crest, bring the beam energy up to 2.5 GeV and compensate the energy spread

TIMING JITTER ANALYSIS

One of the relevant aspects in the SPARX project is the sensitivity of the compression system to the laser pulse temporal jitter [5]. The performances of the two proposed schemes have been analysed and compared adding a 1° phase error at the RF gun injection stage.

The two channels have been optimized, with the code Litrack [6], to obtain the minimum sensitivity of the compressed beam properties to the phase error. For the hybrid scheme the optimized on has been performed on the channel downstream the RF compression stage, looking for the best combination of the relative phase of the first linac section, the X-band cavity voltage and the R_{56} value of the magnetic chicane. The same has been done for the purely magnetic channel regarding the parameters of the first two linac sections, the X-band and the two magnetic chicanes. The results are reported in table 3 and in figures 3 and 4. It's worth to notice that with the optimized Hybrid scheme in all of the three cases the final peak current is higher than 2 kA, and with the Purely Magnetic scheme, we have two cases with 2 kA and one with the peak current 10% lower.

Table 3

	Hybrid	**F. Magnetic**
Δϕ (ps)	I_{peak}(kA)	I_{peak}(kA)
0	2.0	2.0
+1	1.9	1.8
-1	2.4	2.3

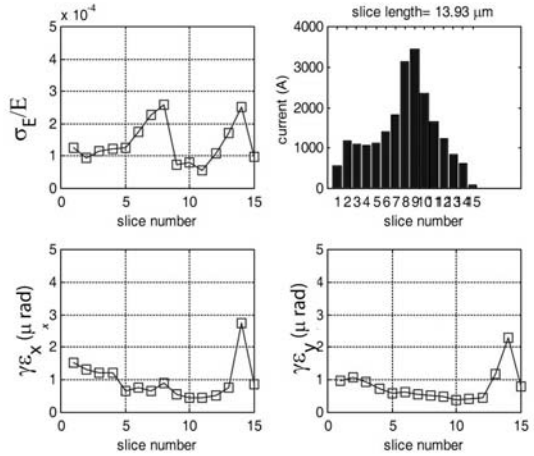

Figure 3: Slice analysis of the beam properties at the exit of the linac, for the hybrid reference case.

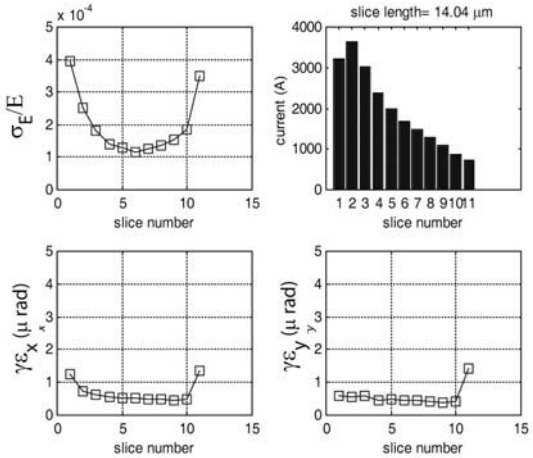

Figure 4: Slice analysis of the beam properties at the exit of the linac, for the fully magnetic reference case.

THE FEL SASE SOURCE

The beam quality has been tested by simulating the FEL process at the wavelength of 1.5 nm with the beam parameters obtained at the end of the last compression stage. The simulations have been done with the time dependent version of PERSEO [7]. The beam has been longitudinally "sliced" in five regions where the average parameters (emittance, energy, energy spread, current) have been calculated. The parameters of the slice with the higher current have been selected for the simulation. In table 4 a list of the "best slice" beam parameters for each case are shown. In table 5 the saturation length in presence of ±1° of phase jitter are reported for both schemes. The hybrid scheme with a phase jitter of +1° shows overcompression effects, resulting in more than 2 μm x-emittance. The magnetic saturation length is in this case of about 36 m.

Table 4

Case	I_{peak} (A)	ε_{nx}(m-rad)	ε_{ny}(m-rad)	γ	σ_E/E
Hybrid Reference	2790	0.83E-06	0.49E-06	4977	1.82E-04
Hybrid +1 °	2230	0.95E-06	0.51E-06	4982	5.53E-04
Hybrid -1 °	3330	2.13E-06	0.66E-06	4977	5.64E-04
Magnetic Reference	3237	0.84E-06	0.56E-06	5038	3.49E-04
Magnetic -1 °	2748	0.84E-06	0.62E-06	5038	2.80E-04
Magnetic +1 °	3744	1.10E-06	0.56E-06	5038	4.60E-04

Table 5

Case	Sat. L (m) (Steady State)	Sat. L (m) (Time Dependent)
Hybrid Reference	18.7	19.5
Hybrid +1 °	23.3	23.6
Hybrid -1 °	36.5	36.7
Magnetic Reference	18.5	19.0
Magnetic -1 °	19.6	20.5
Magnetic +1 °	19.9	20.2

CONCLUSIONS

We have analysed the effects of a phase jitter (±1°) on the SPARX beam quality considering two different concept for compression schemes,. The parameters have been set to obtain an equivalent compression factor between the two schemes. The slice parameters in terms of emittances, energy spread are comparable. The purely magnetic compression provides a more linearised longitudinal phase space which could in principle allow a further compression. We expect to obtain similar results also in the hybrid scheme with the IV harmonic cavity located upstream the RF compressor. The beam quality have been tested with time dependent PERSEO simulations showing a slightly lower sensitivity to phase jitter for pure magnetic compression. The low number of macroparticles considered in the ELEGANT simulations doesn't allow a correct representation of collective effects arising from the CSR coupling. A further effort in this direction is required to complete the analysis.

REFERENCES

[1] D. Alesini, et al. “Conceptual Design of a High-Brightness Linac for Soft X-ray SASE-FEL Source”, to be published on Nucl. Instr. and Meth. A
[2] M. Boscolo et al., proc EPAC02, p 1762, Paris 02
[3] J. Billen, “PARMELA”, LA-|UR-96-1835, 1996.
[4] M. Biagini et al., “Beam Dynamics studies for the SPARC project”, these conference
[5] P.J. Emma, proc. EPAC-02, p. 49 Paris 02.
[6] P.J. Emma , private communication
[7] L. Giannessi, http://www.perseo.enea.it

DAΦNE BEAM TEST FACILITY COMMISSIONING

G. Mazzitelli*, A. Ghigo, M.A. Preger, F. Sannibale, P. Valente, G. Vignola
Laboratori Nazionali di Frascati dell'INFN, Frascati, Italy

Abstract

The DAΦNE Beam Test Facility (BTF) is a beam transfer line optimized to produce single electrons and positrons mainly for high-energy detectors calibration in the energy range between 20 and 800 MeV. The BTF has been successfully commissioned in February 2002, and started operation in November. The scheme of operation, the commissioning results, as well as the first users' experience are presented.

DESCRIPTION OF THE DAΦNE BTF

The Beam Test Facility (BTF) has been designed [1] to provide a defined number of particles in a wide range of multiplicities and energies, mainly for detector calibration purposes, such as energy calibration and efficiency measurements (in single electron mode), and also for beam diagnostics devices and detector aging (at higher intensities).

The BTF is part of the DAΦNE accelerator complex, consisting of a double ring electron-positron collider, a high current linear accelerator (LINAC), an intermediate damping ring (Accumulator) and a system of 180 m transfer lines connecting the four machines. The LINAC delivers electrons with energy up to 800 MeV, with a typical current of 500 mA/pulse, or positrons with energy up to 550 MeV, with a typical current of 150 mA/pulse; the pulse duration can be adjusted in the range $1 \div 25$ ns with a maximum repetition rate of 50 Hz. When injecting for operation of the main rings at the ϕ resonance, the beam energy is 510 MeV.

The minimum LINAC beam current that can be conveniently measured by the DAΦNE current monitors is $I \approx 1$ mA, corresponding to $\approx 10^8$ electrons/pulse, so that it is thus necessary to strongly reduce the number of particles to reach the few particles range. The reduction of the particle multiplicity can be achieved with different methods, the one chosen for the BTF operation is the following[2]: first the LINAC beam is intercepted by a (variable depth) target in order to strongly increase the energy spread of the primary beam; then the outcoming particles are energy selected by means of a bending magnet and slit system. The energy selector only accepts a small fraction of the resulting energy distribution, thus reducing of the number of electrons by a large and tunable factor. The target is shaped in such a way that three different values of depth can be selected by inserting it into the beam-pipe, corresponding to $1.7, 2.0, 2.3\ X_0$.

The attenuated beam is transported by a ≈ 12 m transfer line to the BTF hall, where the experimental set-ups can be installed; at the end of the BTF line a second bending magnet allows to use two separate test lines: one directly from the straight section, the other from the magnet at 45°. A schematic view of the BTF layout is shown in Fig. 1.

Due to the momentum dispersion introduced by the bending magnet, the relative energy spread $\Delta E_{\rm sel}/E_{\rm sel}$ is essentialy determined by the magnet/collimators configuration[1]; in the standard BTF operation for a wide range of slit apertures a resolution better than 1% can be obtained.

The number of transported electrons (or positrons) can be adjusted in a wide range, down to single particle, and is well below the sensitivity of any standard beam diagnostics device, so that many different particle detectors have been used to monitor the beam characteristics.

The experimental area extendes over a 100 m^2 area hall, surrounded by shielding walls of (movable) concrete blocks; a 20 ton crane and a remotely controlled, motorized trolley are available. A number of coaxial cables are stretched between the experimental hall and a dedicated control room, where the BTF beam (and user apparata) can be fully steered. The facility is fully equipped with a complete DAQ, both VME and CAMAC, with NIM electronics and HV modules available for the users.

BEAM COMMISSIONING

During 2002 the BTF has been successfully commissioned and started operation, delivering beam to the first user experiments, from Nov. 2002 to May 2003[3]. Two different operation modes of the facility have been successfully implemented:

- "parasitic": when the DAΦNE collider is working for the main experiments, the LINAC can deliver electron/positron beams to the BTF only between two injection cycles for the main rings. The LINAC setting was optimized to provide a 510 MeV energy, $4 \div 5$ mA intensity beam, with a repetition rate of 24 Hz (+1 shot to the spectrometer line for LINAC energy measurement), and the pulse duration was the same as for injection in the accumulator, ≈ 10 ns. With a typical collimator setting of 2 mm total aperture, both for the upstream and downstream slits and with the target depth set to 1.7 X_0, only a few electrons reach the diagnostic detectors.

- "dedicated": when there are no collisions in the DAΦNE main rings the LINAC beam can be continuously delivered to the BTF. In this case is possible to change the LINAC energy in order to optimize the

* giovanni.mazzitelli@lnf.infn.it

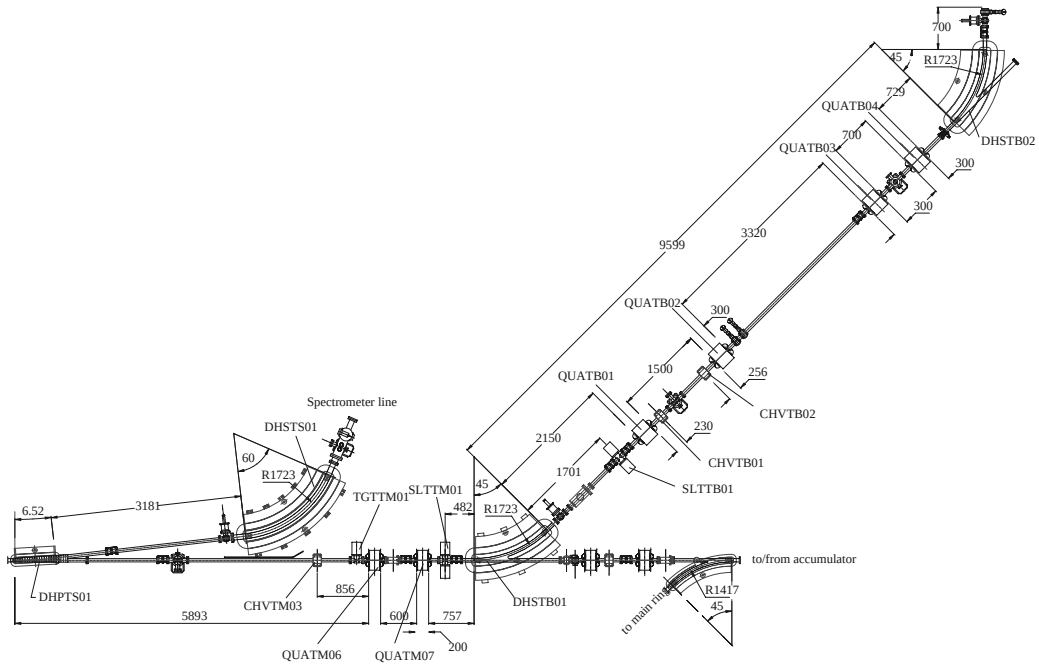

Figure 1: Layout of the Beam Test Facility.

energy/multiplicity of the BTF beam; moreover, the pulse duration can be also changed.

The facility has been operating both in the single electron production scheme and in the high multiplicity operation mode, according to the different user requirements. At low multiplicity a calorimeter has been used as main diagnostic device. The detector is a lead/scintillating fibers calorimeter (developed for the KLOE experiment[4]), with single side photomultiplier readout, with good energy resolution (7% at 500 MeV).

Due to the good energy resolution of the calorimeter (anyhow still worse than the intrinsic beam-line energy acceptance) the number of produced electrons can be counted simply by measuring the total deposited energy E: $n = E/E_1$, where E_1 is the energy deposited by a single electron. An example of ADC spectrum (pedestal subtracted) is shown in Fig. 2, for a selected energy of $E_{\rm sel} = 442$ MeV: the individual peaks corresponding to $0, 1, \ldots, n$ electrons can be easily identified.

The most effective way to change the average number of particles in the beam is to change the selected energy $E_{\rm sel}$; in particular, at the **same** LINAC energy and intensity and with the **same** collimator settings, the multiplicity increases by decreasing the chosen $E_{\rm sel}$. In addition, the multiplicity can be tuned by changing the aperture of the upstream and/or downstream collimators. In this case the energy resolution of the selector will be also affected by a relatively small amount, in any case well below the intrinsic resolution of our calorimeters. In particular, the measured multiplicity increases by increasing the slits aperture until the intrinsic beam spot size is exceeded.

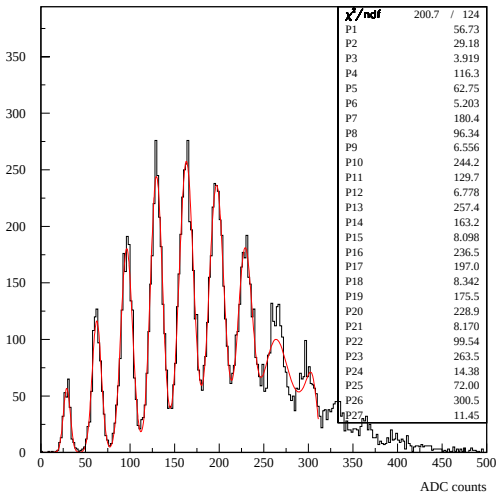

Figure 2: Counting electrons in the calorimeter: charge spectrum for $E_{\rm sel} = 442$ MeV.

Above ≈ 20 particles the calorimeters are no longer effective due to saturation effects. In order to have a diagnostics device in the $\overline{n} = 100$-1000 range (and higher), a detector has been developed and tested in collaboration with the AIRFLY group [5, 6], based on the Cerenkov radiation emission.

Another important parameter is the beam energy, that can be chosen by changing the current of the energy selector dipole magnet. The average measured energy of the single electron signal in the calorimeter is proportional to the incoming beam energy $E_{\rm sel}$ as shown in Fig. 3.

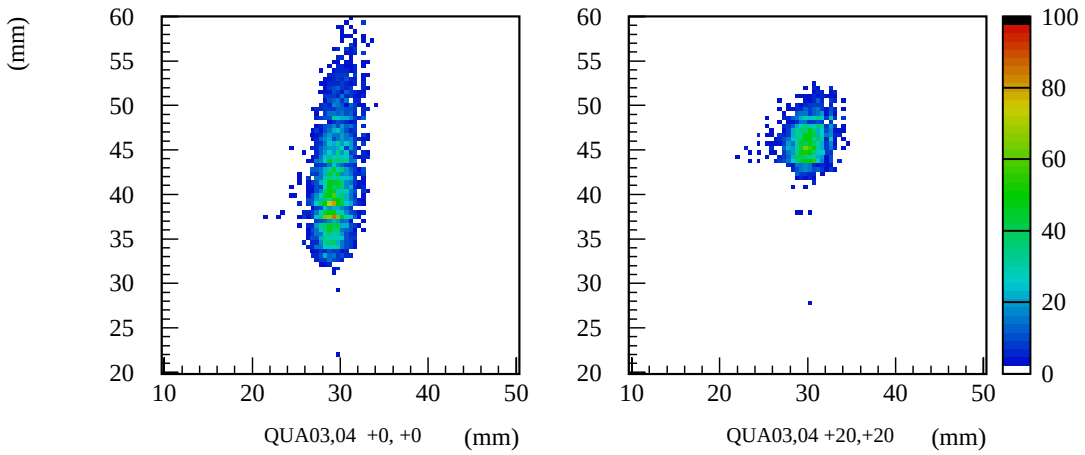

Figure 4: Beam spot measured by the AGILE silicon tracker: on the left for defocussed beam (last vertical and horizontal quadrupoles off); on the right for optimized optics ($\sigma_x \approx \sigma_y \approx 2$ mm).

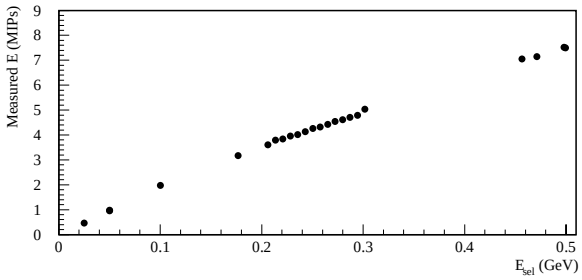

Figure 3: Total energy deposited in the calorimeter by a single electron as a function of the selected beam energy $E_{\rm sel}$.

The single electron beam spot size has been measured profiting of the high spatial resolution of the silicon microstrip tracker of the AGILE gamma-ray experiment [7]. An example of the beam spot measured by the silicon microstrip monitor is shown in Fig. 4: a $\sigma_x \approx \sigma_y \approx 2$ mm spot has been measured with an optimized optics, defocussed optics have been also studied for detector efficiency testing purposes.

Many user experiments were carried out since Nov. 2002, both in single electron mode and at high multiplicity. The single electron mode has been mainly used for testing particle detectors, while the AIRFLY experiment (measuring the air fluorescence yield) has been the main user of the high multiplicity beam: a wide range of particle multiplicity has been exploited, spanning from 10 to more than 1000 electrons/pulse. In both cases the full energy range of the BTF beam has been spanned, up to the maximum LINAC energy ($\approx$ 800 MeV), and also at very low energy (as low as 25 MeV).

Many different settings for BTF beam, for various energy/multiplicity/beam-size configurations have been optimized. The desired beam characteristics were in general easily tunable and the settings showed a very good reliability. Moreover, some diagnostic devices have been integrated in the DAΦNE control system in order to provide an easy user interface.

CONCLUSIONS

The BTF has been operational during the second half of year 2003, both in parasitic and dedicated mode, giving beam to a number of experimental users in a wide range of energy and particle multiplicity. It demonstrated to be easily tunable and very reliable both from the point of view of the desired particle number (from single electron mode to $\approx$ 1000) and energy setting. In order to overcome the present limitations imposed by the DAΦNE collider experiments operation and to largely improve the duty-cycle, we plan to upgrade the facility [8]; a complete separation between the DAΦNE transfer lines to the Main Rings and the BTF channel will allow to operate in the BTF mode with the only limitations of the LINAC switching time and the time spent for filling the Main Rings. An upgrade of allowed dose, up to 10^{10} particles/s, will also permit to use the BTF for testing of standard beam diagnostic devices.

REFERENCES

[1] F. Sannibale, G. Vignola, DAΦNE Techical Note **LC-2** (1991).

[2] L. Rinolfi *et al.*, *Single electron beams from the LEP preinjector*, in Proceedings of PAC 89, Chicago (1989) 298.

[3] G. Mazzitelli, P. Valente, *Commissioning of the DAΦNE Beam Test Facility*, LNF-03-003(P).

[4] M. Adinolfi *et al.*, Nucl. Instrum. Meth. **A482** (2002) 364.

[5] P. Privitera *et al.*, *AIRFLY Letter of Intent*, INFN Gr. V, unpublished.

[6] G. Mazzitelli *et al.*, *Beam Instrumentation for the Single Electron DAΦNE Beam Test Facility*, DIPAC 2003.

[7] M. Prest *et al.*, Nucl. Instrum. Meth. **A501** (2003) 280.

[8] G. Mazzitelli *et al.*, DAΦNE Techical Note **BTF-1** (2003).

FEASIBILITY STUDY OF A 2 GeV LEPTON COLLIDER AT DAFNE

G. Benedetti, D. Alesini, M. E. Biagini, C. Biscari, R. Boni, M. Boscolo, A. Clozza, G. Delle Monache, G. Di Pirro, A. Drago, A. Gallo, A. Ghigo, S. Guiducci, M. Incurvati, C. Ligi, F. Marcellini, G. Mazzitelli, C. Milardi, L. Pellegrino, M. A. Preger, P. Raimondi, R. Ricci, C. Sanelli, M. Serio, F. Sgamma, A. Stecchi, A. Stella, C. Vaccarezza, M. Vescovi, M. Zobov
LNF-INFN, Frascati, Italy

Abstract

While the main advances in the Standard Model probing require the construction of very high-energy colliders, many open questions still remain which can be answered by exploring low and medium energy regions. In this framework we are investigating the possibility of upgrading the ϕ-factory DAϕNE [1] from the energy of 1.02 *GeV* c.m. up to the neutron-antineutron threshold (about 2 *GeV* c.m.) using the existing systems and structures. The luminosity required by the experiments for a *light quark factory* is of the order of few 10^{31} cm^{-2} s^{-1}, easily achievable in the particle factory era. The very first results of the feasibility study are presented.

ENERGY UPGRADE OF THE FRASCATI FACTORY: GENERAL PROJECT

In the discussion about the future plans for the Frascati e^+e^- factory, one of the possibilities the DAϕNE team is considering is the upgrade of the collider energy for new experiments up to about 2 *GeV* c.m. The hypothesis called DAFNE2 (Double Annular Frascati e^+e^- factory for Nice Experiments at 2 *GeV*) is aimed at the measurement of the form factors of the nucleon and the QCD excited states in the 1.2 to 2–2.5 *GeV* c.m. energy range [2]. This experimental program can be realized with the FINUDA [3] detector at a solenoid field of 0.3 *T*.

Table 1: DAFNE2 Parameters

Energy E_0	1.0 *GeV*
Luminosity L	$1\cdot10^{32}$ s^{-1} cm^{-2}
Circumference C	97.69 *m*
Emittance ε	$0.5\cdot10^{-6}$ *rad m*
Coupling $\kappa = \varepsilon_x/\varepsilon_y$	0.009
Beta functions at IP β_x^*/β_y^*	1.5 / 0.025 *m*
Crossing angle at IP θ_x^*	±15 *mrad*
Bunch width at IP σ_x^*/σ_y^*	0.95 / 0.008 *mm*
Bunch natural length σ_z	13.9 *mm*
Linear tune shift ξ_x / ξ_y	0.014 / 0.024
Betatron tunes ν_x / ν_y	5.15 / 5.21
Momentum compaction α_c	0.009
Number of bunches	30
Particles per bunch	$3\cdot10^{10}$
Beam current I_{tot}	450 *mA*

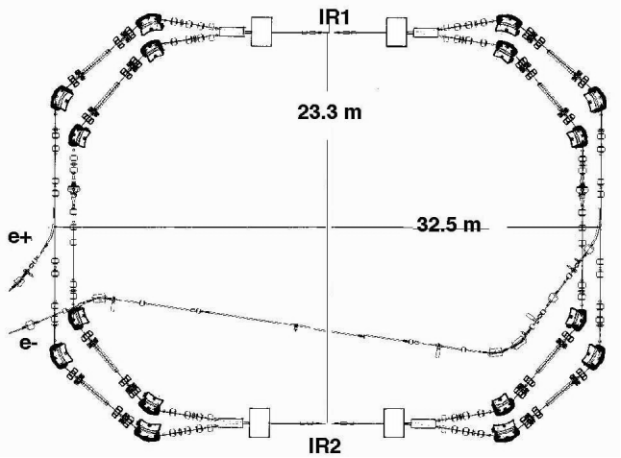

Figure 1: Main Rings layout.

DAFNE2 can use without any change the DAϕNE injection system (linac, damping ring and transfer lines) at 0.51 *GeV* and the two Main Rings with limited changes in the hardware to reach 1–1.25 *GeV* per beam.

Design Parameters

The experimental luminosity requirements are not critical for DAFNE2. This allows choosing the machine parameters with enough freedom, exploiting our commissioning know-how. We have worked out new parameters at the beam collision energy of 1 *GeV*.

Choosing an emittance $\varepsilon = 0.5\cdot10^{-6}$ *rad m* compatible with the ring aperture, a vertical beta function at the Interaction Point (IP) and a coupling factor already achieved, the linear tune shift is ξ_x / ξ_y = 0.014 / 0.024, below the limit achieved by DAϕNE.

The horizontal crossing angle at the interaction point is ±15 *mrad*, corresponding to a Piwinsky's angle:

$$\phi = \theta_x^* \frac{\sigma_L}{\sigma_x^*} = 0.22$$

which has already been exceeded in the existing factories.

The chosen number of bunches is 30 so that, leaving the harmonic number h = 120 unchanged, we can inject both electrons and positrons out of collision and collide the two beams by performing a RF phase jump [4] after having ramped the beam energy to 1 *GeV*.

Once fixed such parameters (Table 1), a luminosity of $1\cdot10^{32}$ s^{-1} cm^{-2} is straightforward to achieve with 15 *mA* per bunch and a total current of 0.45 *A*.

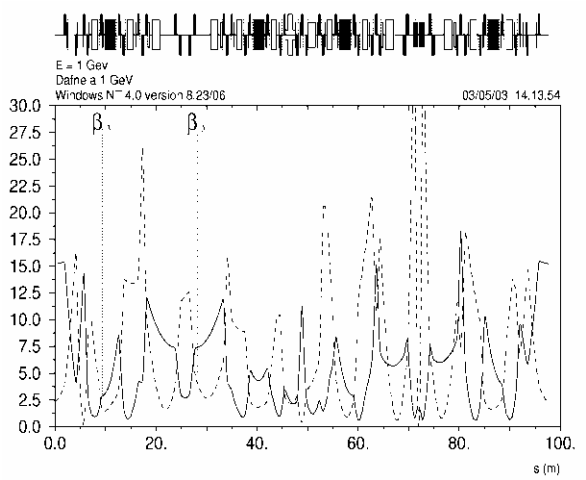

Figure 2: DAFNE2 ring beta functions calculated by MAD.

MAIN RINGS

The design of the two collider Main Rings is unchanged (Figure 1): two different rings for positrons and electrons with two 10 *m* long Interaction Regions where the opposite beams travel in the same vacuum chamber. Four wigglers per ring are installed in the arcs. The existing vacuum chamber is reused.

The experiment FINUDA is in the Interaction Region 2 (IR2) and in the opposite Interaction Region (IR1) two quadrupole doublets are installed: a lattice already used when only the KLOE detector was installed [5].

More study has to be done on the energy ramping, to be performed keeping the betatron tunes constant.

Optics

The main optical features at 1 *GeV* are (Figure 2):

- Only one low beta insertion in IR2, where the experimental detector is housed and the positron and electron beams collide at a horizontal angle of ±15 *mrad*.
- In IR1, four FDDF quadrupoles allow to separate the two beam trajectories with a vertical bump of ±1 *cm*.
- Horizontal and vertical beta functions in the four achromat arcs, where the dispersion is higher, are separated to correct both horizontal and vertical chromaticities with chromatic sextupoles.
- The horizontal beta function and the dispersion are shaped in such a way that the natural emittance does not change from 0.51 to 1 *GeV* as explained in the next section.

Interaction Region 2

The low beta insertion is realized with four FDDF quadrupoles housed inside the experimental detector (Figure 3). Since they must be powered for variable beam energy, the only solution to fit them inside the detector is developing superconducting quadrupoles as for example at upgraded HERA [6]. Two further doublets outside the detector are realized with conventional quadrupoles.

The FINUDA solenoid field integral of 0.3 *T* x 2.4 *m* at the collision energy rotates the beam by an angle of 6° around the longitudinal axis. The coupling at the Interaction Point and outside IR2 is corrected with the rotating frame method [7]: each quadrupole is rotated around its longitudinal axis following the rotation of the beam and two compensating solenoids 0.36 *T* x 1 *m* provide cancellation of coupling outside the IR. The solenoid fields and the quadrupole rotation angles are fixed. At the injection energy of 0.51 *GeV* the non vanishing coupling from mismatched quadrupole rotation angles can be useful to have a long beam lifetime during ramping and can be controlled with the skew quadrupoles in the ring.

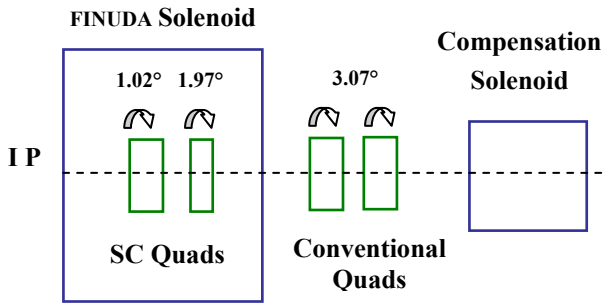

Figure 3: half Interaction Region 5 *m* long layout: from the Interaction Point (IP) to the splitter magnet.

Synchrotron Radiation and Emittance

The synchrotron radiation loss per turn depends on the energy and on the bending radius in dipoles as:

$$U_0 = C_\gamma \frac{E^4}{2\pi} \oint \frac{ds}{\rho^2}$$

The wigglers are useful at the injection energy to increase synchrotron radiation and decrease damping times. From 0.51 to 1 *GeV* the wiggler field is kept constant, since it is already near saturation and the synchrotron radiation from the energy increase is high enough to improve damping times (Table 2).

The emittance in electron storage rings depends on the second power of the energy according to:

$$\varepsilon = C_q \gamma^2 \frac{< \mathrm{H} / |\rho|^3 >}{J_x < 1/\rho^2 >}$$

and to have constant emittance at different energies the dispersion invariant:

$$\mathcal{H} = \gamma_x D^2 + 2\alpha_x DD' + \beta_x D'^2$$

is fairly reduced by changing the Twiss parameters in the arcs when the energy goes from 0.51 to 1 *GeV*.

Table 2: Energy loss with and without wigglers

without / with Wigglers		0.51 GeV	1 GeV
U_0	(*keV/turn*)	4.3 / 9.3	64.0 / 83.5
τ_x	(*ms*)	68 / 40	11 / 8.6
τ_E	(*ms*)	41/ 31	5.0 / 3.5

Table 3: RF System and Bunch Parameters

RF peak voltage V_{RF}	250 *kV*
RF frequency f_{RF}	368.26 *MHz*
Energy loss U_{rad}+U_{paras}	83.5 +6.5 *KeV/turn*
RF power P_{beam}+P_{wall}	40.5 + 17.5 *kW*
Synchr. frequency f_{syn}	11.7 *kHz*

Magnets

Eight dipoles are installed in each ring: four 0.99 *m* long magnets with a 40.5° bending angle and four 1.21 *m* long with a 49.5° angle. The bending field in present magnets at 0.51 *GeV* is 1.2 *T* and the maximum field is 1.7 *T*, insufficient to reach 1 *GeV*: new stronger dipoles are needed.

The existing vacuum chamber puts constraints on the dipole geometry. With a different shape of the polar shoe, the same gap height and 10% longer magnets, we expect to achieve the needed field of 2.2 *T* with a $\Delta B/B = 2 \cdot 10^{-4}$ field quality in the ±3 *cm* range, using a ferromagnetic alloy with higher saturation limit to realize the DAFNE2 dipoles. More work and simulations are in progress to study the features and the quality of such magnets.

Existing quadrupoles and sextupoles allow doubling the ring energy, some quadrupoles reach saturation, but we assume to avoid it with further optics optimisation.

RF Parameters and longitudinal bunch distribution

The DAΦNE RF cavity cooling system can withstand a maximum accelerating field of 350 *kV*, corresponding to a RF power loss of 35 *kW* on the cavity walls, while the maximum RF power the klystron can supply is 150 *kW*. The RF power to be delivered to the beam is given by $P_{beam} = V_{loss}\, I_{beam} \approx 40.5$ *kW*, assuming 90 *keV/turn* of total losses (including the parasitic ones). Since the required accelerating voltage is 250 *kV* corresponding to a RF wall dissipation of ≈17.5 *kW*, the existing RF system is completely compatible with the required specifications.

Bunch lengthening has been estimated by performing a multiparticle tracking. Using the impedance estimates and correspinding wake fields calculated for the present vacuum chamber [8] in the turbulent microwave threshold calculations and in the bunch lengthening simulations, the rms bunch length increases from the natural value of 13.9 *mm* (Figure 4) to only 15.9 *mm* at 15 *mA* per bunch, while the energy spread remains constant indicating that the microwave instability threshold is not reached at the nominal bunch current.

Lifetime and background

Background and beam lifetime at DAΦNE are strongly dominated by Touschek scattering [9]. Touschek lifetime is a complicated function of machine parameters: at the larger energy and RF voltage of DAFNE2 it will be less critical than at the present energy. In fact with the parameters in Tables 1 and 3 τ_{tou} comes out to be 650 *min* as calculated by MAD with longitudinal acceptance dominated by RF. Further quantitative simulations will be done with the programs developed and used for DAΦNE that consider the physical aperture of the vacuum chamber along the rings.

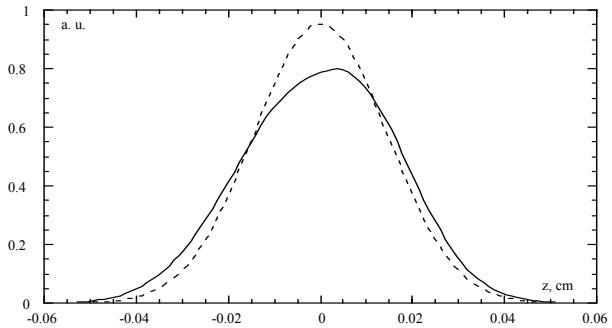

Figure 4: Charge density bunch distribution at zero current (dashed line) and at 15 *mA/bunch* (solid line).

Vacuum System

Present layout can withstand the new configuration. In fact in DAFNE2 (0.45 *A* and 1 *GeV*) synchrotron radiated photon flux is $1.8 \cdot 10^{20}$ *phot/s* corresponding to a power of 38 *kW,* while the existing vacuum chamber is designed for a synchrotron radiation power of 50 *kW*.

Feedback System

No change is needed for the transverse feedback if the betatron tunes stay constant during the energy ramping. The longitudinal feedback can follow the synchrotron frequency variation in a large range with eight synchronizable filters. Timing is not critical with a synchronous RF phase up to 100 *ps* (the RF phase is 70 *ps* at 250 *kV*).

REFERENCES

[1] G. Vignola and DAΦNE Project Team, "DAΦNE: The first Φ-Factory", EPAC'96, Sitges, June 1996.

[2] R. Baldini, "Unknown for ever?", Accelerator Division–LNF seminar, Frascati, January 2003, www.lnf.infn.it/acceleratori/

[3] The FINUDA Collaboration, "FINUDA,a detector for nuclear physics at DAΦNE", LNF Internal Note LNF-93/021, May 1993.

[4] A. Gallo et al., "Operational Experience with the DAΦNE Radio Frequency Systems", PAC'99, New York, Nov. 1999.

[5] C. Biscari, "Detuned Lattice for Main Rings", DAΦNE Technical Note L-32, 2001.

[6] B. Parker and al., "Superconducting Magnets for use inside the HERA ep Interaction Regions", EPAC'98, Stockholm, June 1998.

[7] M. Bassetti et al., "Solenoidal field compensation", 14th ICFA Beam Dynamics Workshop, Frascati, Oct. 1997.

[8] M. Zobov et al., KEK Proceedings 96-6, August 1996 (A), pp. 110-155.

[9] M. Boscolo et al., "Simulations and Measurements of the Touschek Background at DAΦNE", EPAC'02, Paris, June 2002.

BEAM DYNAMICS STUDIES FOR THE SPARC PROJECT

M. Biagini, M. Boscolo, M. Ferrario, V. Fusco, S. Guiducci, M. Migliorati, Vaccarezza,
INFN-LNF, Frascati, ITALY
L. Serafini, INFN-Mi, Milan, ITALY
R. Bartolini, L. Giannessi, M. Quattromini, C. Ronsivalle, ENEA-Frascati, ITALY
C. Limborg, SLAC, Stanford, USA, J. B. Rosenzweig, UCLA, Los Angeles, USA

Abstract

The aim of the SPARC project, is to promote an R&D activity oriented to the development of a high brightness photoinjector to drive SASE-FEL experiments. We discuss in this paper the status of the beam dynamics simulation activities.

INTRODUCTION

The SPARC photoinjector has to drive a SASE FEL experiment at 530 nm [1]. To meet the FEL requirements a high brightness electron beam has to be generated, accelerated up to 155 MeV and transported up to the entrance of the undulator, minimizing the emittance and energy spread degradation due to correlated space charge and wake field effects. In order to saturate the FEL radiation in the planned 15 m long undulator, and to additionally allow generation of higher harmonics, the design beam parameters are very rigorous: normalized emittance ε_n < 1 μm, relative energy spread $\Delta\gamma/\gamma$ < 0.1 % and peak current I ~ 90 A. Fortunately, such parameters have to be reached only on the scale of the FEL cooperation length, which in our case is less than 300 μm.

START TO END SIMULATIONS

The accelerator consists of a 1.6 cell RF gun operated at S-band with a peak field on the cathode of 120 MV/m and an incorporated metallic photo-cathode followed by an emittance compensating solenoid and three accelerating sections of the SLAC type (S-band, travelling wave). A transfer line made with two triplets allows the matching with the undulator optics (see Fig. 1). A start-to-end simulation of the beam dynamics from the injector through transfer line and undulator system has been performed by means of the codes PARMELA [2] and GENESIS [3].

We take as our example the most conservative system that is to be encountered, one with no velocity bunching [1], and a relatively low energy of 155 MeV (consistent with either low gradient, three TW section operation, or high gradient, two TW section operation). The temporal profile of the bunch has been taken uniform over 11.5 ps with a rising time of 1 ps, a laser spot on the cathode of 1 mm and a 1 nC charge, with a 35 degree launch phase in the gun, 0.27 T of solenoid field and on-crest acceleration in the linac. We decided to place a set of coils around the first accelerating structure (700 G), to provide additional flexibility in the choice of the accelerating gradient (25 MV/m in the simulations).

The transverse emittance compensation process is visible in figure 2: the emittance reaches an absolute maximum in the centre of the solenoid and it is reduced to a minimum in the drifting section, then begins again to increase. The booster entrance is located at the envelope laminar waist corresponding to an emittance relative maximum [4]. The emittance oscillation is driven by a properly matched accelerating field [5] down to an absolute minimum (~0.6 μm) at the linac exit where the average bunch energy is 155 MeV, high enough to damp space charge forces. The estimated thermal emittance (0.3 μm), included in the simulation, results to be in the present design the main contribution to the total emittance.

As expected, the emittance along the transfer line and in the undulator is not anymore affected by space charge effects even when the beam has to be focused to a very small spot (~55 μm) to meet the undulator matching conditions.

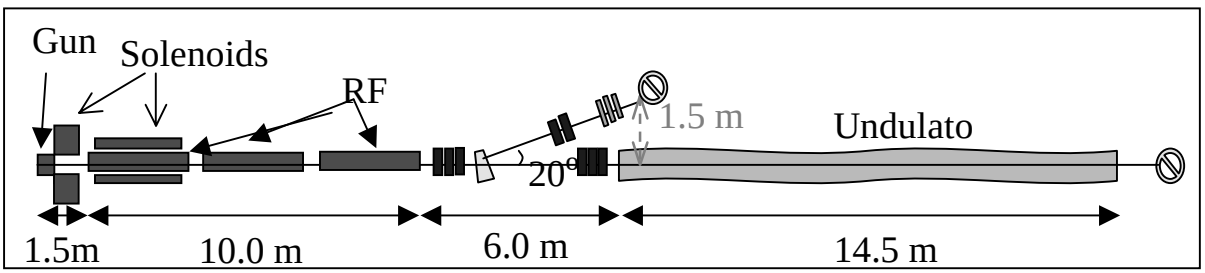

Figure 1: Schematic layout of SPARC phase 1

Transverse and longitudinal phase spaces at the entrance of the undulator are shown in figure 3. Despite some halo observed in the transverse phase space related to the bunch tails mismatch, the core of

the bunch is very good behaved, having a 0.6 μm rms normalized emittance in both planes.

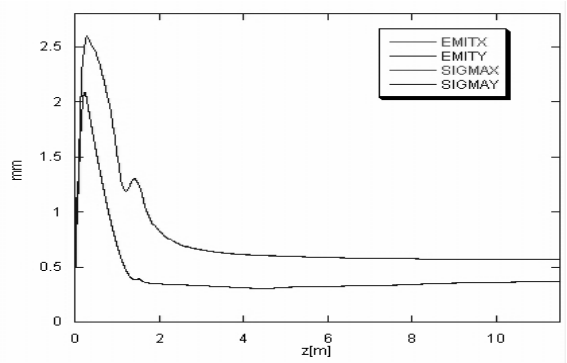

Figure 2: PARMELA simulation of the rms normalized emittance and bunch envelope evolution along the SPARC injector up to 11.5 m.

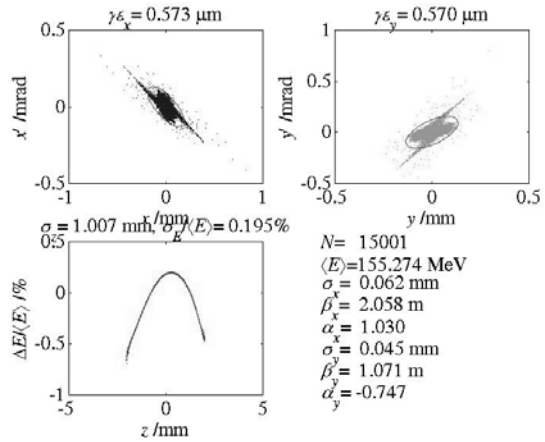

Figure 3: Transverse and longitudinal phase spaces at the entrance of the undulator.

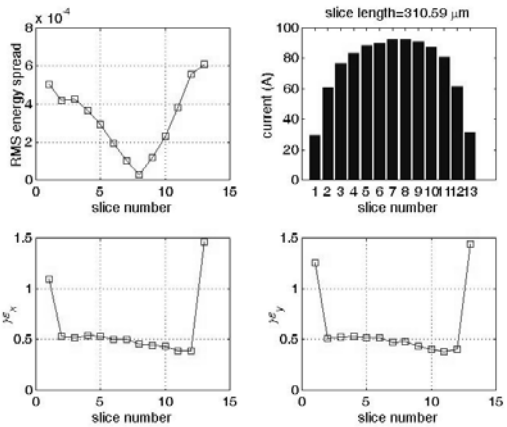

Figure 4: Slice analysis of beam properties at the undulator entrance.

The longitudinal phase space shows the typical energy phase correlation induced mainly by the RF field, with little contribution from longitudinal space-charge, having relative rms energy spread lower than 0.2% as required. The slice analysis performed at the undulator entrance is shown in figure 4. Slice emittance and energy spread are well below the nominal design values for more than 85% of the bunch length. The slice peak current is above 60 A in the same region.

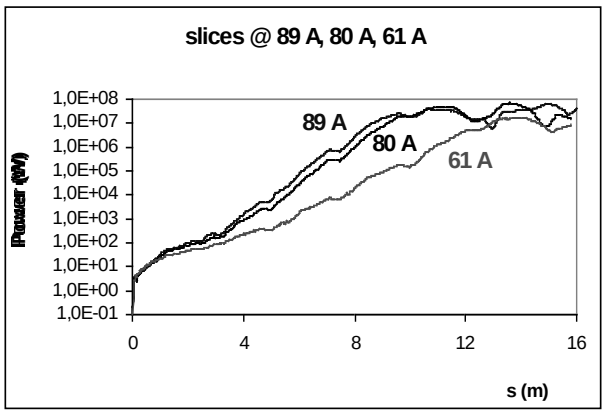

Figure 5: GENESIS simulations of the FEL for three representative slices along the bunch.

The analysis of the FEL performance has been performed with the code GENESIS, taking in to account three representative slices along the bunch provided by PARMELA, showing that even the radiation emitted by the slices closer to the tails that contain a lower local value of the current (61 A) can reach saturation as shown in figure 5.

SENSITIVITY STUDIES

Once the nominal parameters are set we have to provide also stable operation and tolerate some jitter in the nominal value of the parameters . In this section we discuss only two selected topics of such studies performed thus far, in which cathode emission uniformity, laser beam ellipticity, laser centroid offset, laser time structure, and solenoid field errors have been explored.

The effects of cathode's dishomogeneities [6] have been tested by simulating, using the code TREDI [7], a zone on the cathode with reduced quantum efficiency QE. We have assumed a circular QE "hole" with a surface 10% of the nominal bunch spot, centered half-way of the bunch radius. The results suggest that localized inhomogeneities do not dramatically degrade the emittance, growing by $\Delta\varepsilon_{x(y)} \approx 10\%\,(15\%)$ for QE $\approx$ 70% as reported in figure 6. This analysis will be further extended to the cases of randomly distributed ("spotty") inhomogeneities, which better describe the behavior of real cathodes.

Flat top laser pulses with rise times shorter than1 ps are required in order to avoid emittance degradation [8], as shown in figure 7.

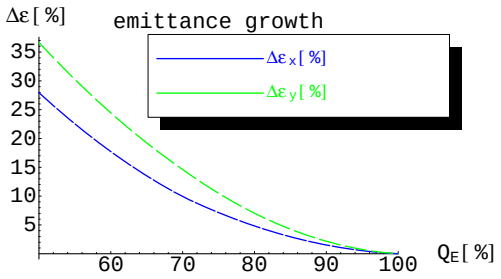

Figure 6: **:** Emittance growth as a function of Q_E .

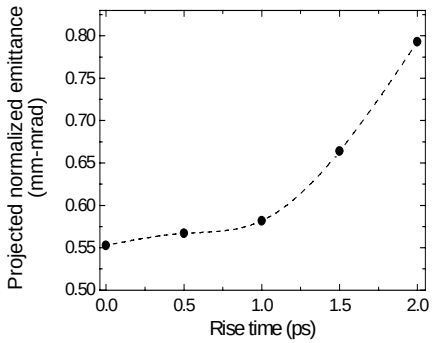

Figure 7: **:** Norm. rms emittance versus rise time.

But laser pulse shaping with short rise time may result in the formation of longitudinal ripples. Therefore, the effect of a laser pulse with longitudinal ripples has been investigated. The beam is assumed to be transversely uniform in these studies. The striking result is that even with a 30% of longitudinal irregularity the beam emittance degradation is limited to 6%. This result can be interpreted as if the space-charge force induces a compensation of the longitudinal irregularity. This hypothesis is justifed by PARMELA simulation results. In figure 8 the evolution of longitudinal beam distributions are displayed. At the cathode the temporal spectrum has a 30 % ripple overlapped on a square pulse, the relative energy spread is zero. As the beam goes through the gun and drifts the temporal oscillations transform in energy oscillations. At the entrance of the first acceleration structure (at z=150 cm) the beam has lost the temporal ripples, which have converted into energy variations through a fractional plasma oscillation. These energy ripples do not have any notable effect to the rms energy spread at the end of the linac, as they are soon suppressed inside the first accelerating structure. These results indicate that the shape of the laser pulse should be square with a very small rise time, whether a smooth temporal profile is not a stringent requirement.

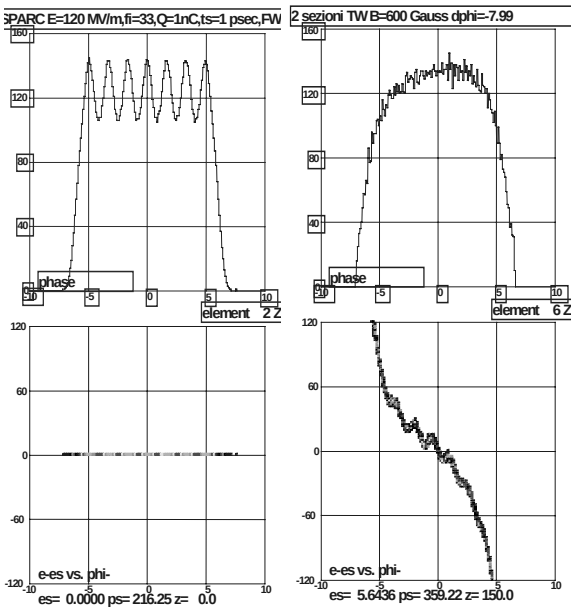

Figure 8: : Longitudinal beam distribution: phase and energy spectrum in the upper and lower plots, respectively. Left plot: initial distribution at cathode (z=0 m); right plot: beam at z=1.5 m.

CONCLUSIONS

Start to end simulation of the optimal SPARC working point have shown that we can meet the FEL requirements with a reasonable parameter set. The requirements on the longitudinal and transverse profile of the laser pulse, the phase jitters, the laser pointing stability have been set. Preliminary sensitivity studies have not shown dramatic concerns about the possibility of stable operation. A more systematic [9] study is in progress .

REFERENCES

[1] L. Palumbo et al., "The SPARC Project: A High-Brightness Electron Beam Source to Drive a SASE-FEL Experiment at LNF", this conference.
[2] J. Billen, "PARMELA", LA-|UR-96-1835, 1996.
[3] S. Reiche, Nucl. Instrum. & Meth. A429,243 (1999).
[4] M.Ferrario et al., "HOMDYN Studies for the LCLS RF Photoinjector", Proc. of ICFA Workshop on the Physics of High Brightness Beams, UCLA, Nov. 1999
[5] L.Serafini,J.Rosenzweig,*Phys. Rev. E* **55**(1997) 7565
[6] F. Zhou et al.,PRST-AB, V. 5, 094203 (2002).
[7] L. Giannessi, M. Quattromini, Submitted to PRST AB (2003).
[8] J. Yang, J. of Appl. Phys., V. 92, N. 1, (2002)
[9] C. Limborg, "New optimization for the LCLS photo-injector", Proc. Of EPAC-02, Paris 2002.

STUDY AND DESIGN OF ROOM TEMPERATURE CAVITIES FOR A RF COMPRESSOR PROTOTYPE

David Alesini[+], Franco Alessandria[*], Alberto Bacci[*], Carlo De Martinis[*] , Massimo Ferrario[+], Alessandro Gallo[+], Dario Giove[*], Fabio Marcellini[+], Marco Mauri[*], Luca Serafini[*]

[+]*INFN-LNF-Frascati* , [*]*INFN-Milan and University of Milan*

Abstract

The generation of high brightness electron beams with sub-ps bunch lentgh at kA peak currents is a crucial requirement in the design of injectors for Linac based X-Ray FEL's. In the last years the proposal to use a slow wave RF structure as a rectilinear compressor in this range of interest, to overcome the difficulties related to magnetic compressors, has been widely discussed in the accelerator physics community. In this paper the results in the design and study of a 3 GHz model structure will be presented.

INTRODUCTION

The need to produce high brightness electron beams delivered in short (sub picosecond) bunches has been driven recently by the demands of X-Ray SASE FELs, which require multi-GeV beams with multi-kA peak currents and bunch lengths in the 100-300 fs range, associated to normalized transverse emittances as low as few mm mrad. The strategy to attain such beams is based on the use of RF Linacs in conjunction with RF laser driven photo-injectors and magnetic compressors. The formers are needed as sources of low emittance high charge beams with moderate currents, the latter are used to enhance the peak current of such beams up to the design value of 2-3 kA by reduction of the bunch length achieved at relativistic energies (> 300 MeV). Nevertheless the impact of magnetic compressors on the beam dynamics is quite relevant, with tendency to reduce the performances of the whole system in terms of the final beam brightness achievable [1].

In the last years, developing a previous work about a plasma buncher scheme, alternative option of compression based on slow wave RF fields has been proposed [2]. The basic idea is to develop a rectilinear RF compressor that works indeed as a standard accelerating structure which simultaneously accelerates the beam and reduces its bunch length.

RF RECTILINEAR COMPRESSOR THEORY

The great advantage of a rectilinear scheme is obviously the absence of curved path trajectories, in addition to the fact that compression is applied at moderate energies (from 10 to 100 MeV) leaving the Linac free from any further beam manipulation.

We briefly report the basic elements of the theory of RF compressor as outlined in ref.2.

The interaction between an electron and the longitudinal component E_z of the RF field in a RF travelling wave structure is described by the Hamiltonian

$$H = g - b_r\sqrt{g^2 - 1} - a\cos x$$

where $g = 1 + \frac{T}{mc^2}$ is the normalized energy of the electron, $x = (wt - kz - y_0)$ is the phase of the wave as seen by the electron (y_0 is the injection phase) and $a = \frac{eE_0}{2mc^2k}$ is a dimensionless parameter which represents the accelerating gradient.

If we consider a wave whose phase velocity is slightly lower than c, we have that $k = k_0 + \Delta k = \frac{w}{c} + \Delta k$ (where the detuning parameter is small i.e. $\Delta k << k_0$) and we can write for the resonant beta and gamma the expressions $b_r = 1 - \frac{c\Delta k}{w}$ and $g_r = \sqrt{\frac{w}{2c\Delta k}}$.

The behaviour of the RF compressor may be easily understood looking at the phase contour plots in the [?,?] phase space. As an example we have considered a wave of amplitude a = 0.65 and resonant gamma $?_r$ = 24. This corresponds to a wave phase velocity of b_r =0.999.

In fig. 1 we plot a phase-space diagram showing that particles injected with a phase equal to –p/2 and an energy smaller than the resonant one, will slip back in phase while accelerated up to ? = $?_r$. Due to the nature of phase lines the bunch will have a phase spread (i.e. a bunch length) smaller than the initial one. For the same reason a further acceleration would clearly tend to de-compress the bunch.

The figure of merit for the compression process may be defined as the ratio between the initial phase spread and the final one at the extraction. Values in excess of 10 may be reached in such a scheme. A proper matching of the beam into the accelerating section and an additional focusing provided by external solenoids has been shown by simulation to obtain a proper preservation of the transverse emittance as discussed in Ref. [3]

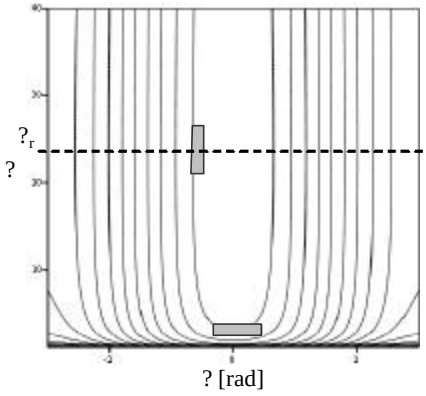

Fig. 1 Phase space plots of a slow RF wave

DESIGN OF CELLS FOR A SLOW WAVE RF COMPRESSOR

In the last year preliminary experimental investigations have been carried out using speed of light linac sections, which showed the validity of the velocity bunching concept[3]. In such a frame our group started an experimental activity aimed at the development of cells for the construction of a slow wave TW structure which can be used as a RF compressor. Table 1 shows the main parameters which we took as a reference for our investigations:

Parameter	Value
Frequency of the wave structure	2856 MHz
Linac structure	TW
Accelerating gradient	20 MV/m
Initial energy	6 MeV
Extraction energy	16 Mev
Compression factor	7
RF pulse repetition rate	1÷10
Bunch length	10 ps

Table 1 Reference parameters for the study of the RF compressor

The required compression factor calls for the availability of a structure able to control the phase velocity in the range between 0.999 c and c. In an iris loaded TW structure the equation:

$$(dvf / vf) = (df / f) (1 - vf / vg)$$

shows that the v_f can be controlled by changing the excitation frequency or, in a equivalent way, by detuning the structure. A suitable approach may be that to use a thermal control process that change the v_f at a fixed exciting frequency. The feasibility of such an approach has been initially studied referring to the typical parameters of a SLAC structure. The results obtained show that a change of the order of 1‰ of the phase velocity is equivalent to a variation of the order of 0.6 °C in the temperature of the structure. This calls for a system able to control in real time the temperature with a resolution of the order of 0.06°C under a RF power load of the order of ~ 1.5 kW. We evaluated that it would be too much difficult to achieve such a performance and we tried to approach the problem with a new cell design. The goal was to obtain a structure able to decrease of a factor of 3 the thermal sensitivity, so that the required phase velocity modulation will ask for a temperature variation of the order of 2 °C. The fact that the required accelerating gradient is lower with respect to a standard SLAC structure gave us a certain degree of freedom in the design as far as the shunt impedance figure is involved. Table 2 shows the main parameters of the new structure (referenced as ALMA 3) which we propose for the RF compressor:

	SLAC Mark IV	Alma 3
Cell radius (mm)	41.24	42.60
Iris radius (mm)	11.30	15.40
Disk thickness (mm)	5.84	5.90
Cell length	35	35
Frequency (MHz)	2856	2856
Mode	2π/3	2π/3
Q	13200	13084
Shunt impedance (MOhm/m)	53	41
Vg/c	0.0122	0.0341
?T (equivalent to 1‰ Vf)	0.6 °C	2.0 °C
Tuning ring capability (MHz)	-	18
Tuning rod capability (kHz)	-	200

Table 2 Main parameters of the Alma 3 TW structure

The mechanical design of the cell has been carried out in a complete fashion taking into account the requirements due to the cooling system and to the brazing process to join cells to give the final structure.

At the same time, at least for the first prototypes, we add frequency control capabilities to the cells both during the mechanical machining (using a tuning ring) and after the brazing (using a set of tuning rods). Such a feature has been foreseen to allow to control the influence of the achievable mechanical tolerances on the frequency response of the cells (a tolerance of 0.01 mm in the cell diameter gives an uncertainty of 370 kHz in frequency) and to provide a tuning tool for field adjustment.

The thermal control of this structure will be obtained using 8 channels for water flow. These channels have been machined within the cells body to provide a better heat exchange. The behaviour of this design has been verified under the expected RF power load using the finite element code Ansys. The results of this analysis show that the system will be suitable to match our requirements (fig. 2). The so far obtained thermal sensitivity allows to use a refrigeration unit with a control capability of the order of 0.1°C@45°C operating point. Such units are commercially available and we plan to use one of these as the basic building block of the thermal control setup.

To prove the reliability of the design and to gain experience on such a structure we machined a 4 cells aluminum prototype. The cells were stacked together using stainless steel threaded rods.

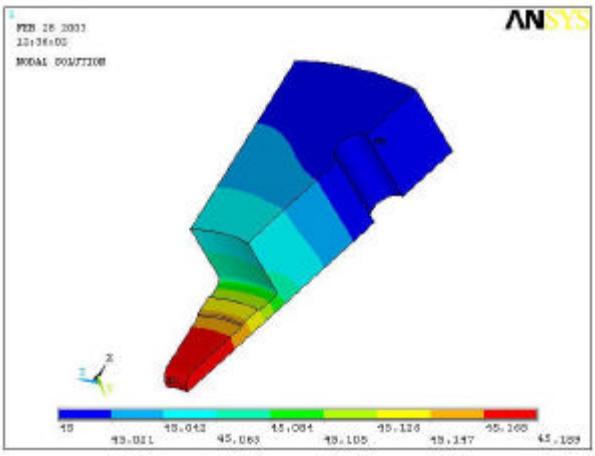

Fig. 2 Ansys simulation of the thermal behaviour of the ALMA 3 structure

The machining of these cells was simplified with respect to the final ones removing the cooling channels and the brazing grooves. The mechanical tolerances obtained were quite close to those required and this allowed to carry out significant measurements both on the single cell and on the set of the four cells.

The resonant frequency measurements on the single cells were in very good agreement with the expected values obtained with the code Superfish and confirmed the influence of the mesh value adopted in the numerical analysis (0.15 mm which gave us a frequency accuracy of the order of 100 kHz). For the sake of simplicity we started considering this assembly as a SW structure giving us the opportunity of sampling the dispersion curve at 4 points and to check field profile (Fig. 3).

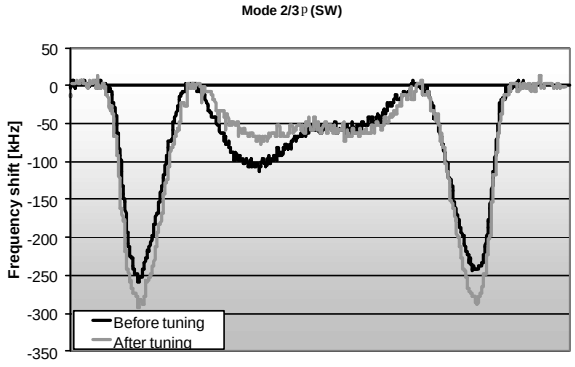

Fig.3 Measurements of the ALMA 3 structure accelerating field

The dispersion curve as a function of the cells temperature was measured using a test bench based on a laboratory oven. The internal size of the oven allows to position the 4 cells stack along with RF probes and temperature sensors to characterize the oven behaviour and to measure the cells temperature. Measurements were carried out in the range between 25 and 45 °C. The oven stability was of the order of 0.1 °C. The results (Fig. 4) proved a good agreement with the predicted behaviour of the phase velocity and gave the final validation of the whole design.

At the same time that we carry out the above described measurements, the OFHC copper to be used for the machining of a new 9 cells prototype has been forged by an Italian company according to our specifications. Great care has been taken to the control and measurement of the grain size of the bulk material (< 100 µm) in order to match the requirement for the brazing procedure. This process will be carried out at CERN and the whole cycle has been defined in agreement with CERN specialists.

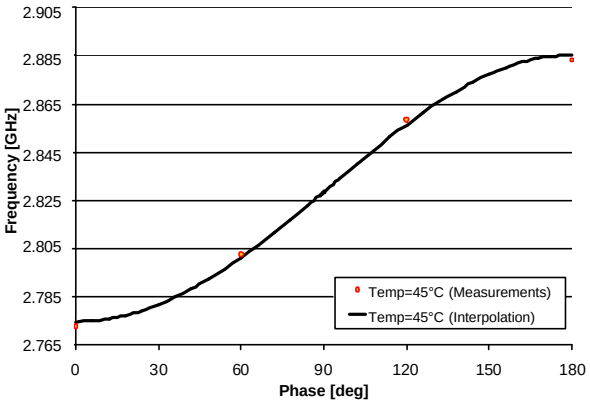

Fig. 4 Measurements of the ALMA 3 structure dispersion curve

CONCLUSIONS

The design of a new cell for a RF compressor working in the S-band has been completed and the measured performances of a first aluminum prototype have proven the feasibility of such an approach.

At this time the machining of the copper cells has been started and we plan to have a 9 cells brazed structure within the end of June 2003.

ACKNOWLEDGEMENTS

We would like to acknowledge very helpful discussions with M. Vretenar and S. Mathot (CERN), R. Boni (INFN-LNF) and the valuable support received in the experimental work by Luigi Gini and Carlo Uva (INFN-Milan) and Luciano Grilli (University of Milan).

REFERENCES

[1] P.Emma "Accelerator Physics Challenges of X-Ray FEL SASE Sources", EPAC2002, Paris, June 2002, p. 49

[2] L. Serafini et al. "Ultra-short Bunch Generation with a Rectlinear Compressor", PAC2001, Chicago, June 2001, p. 2242.

[3] M. Ferrario et al. "Recent Advances and Novel Ideas for High Brightness Electron Beam Production Based on Photo-Injectors" INFN-LNF 03/06P– 5 May 2003

DESIGN OF OTR BEAM PROFILE MONITORS FOR THE TESLA TEST FACILITY, PHASE 2 (TTF2)

K. Honkavaara*, A. Brenger, R. Fischer, D. Nölle, K. Rehlich, DESY, 22603 Hamburg, Germany
L. Cacciotti, M. Castellano, G. DiPirro, M. Raparelli, R. Sorchetti, INFN-LNF, 00044 Frascati, Italy
L. Catani, A. Cianchi, INFN-Roma 2, 00133 Roma, Italy

Abstract

The TESLA Test Facility is being extended to an electron beam energy of 1 GeV to drive a new Free Electron Laser facility. 24 beam profile monitors based on optical transition radiation (OTR) will be used along the linac. Their design is a challenging task, since the system has to measure transverse electron beam sizes from millimeter scale down to 50 μm with a high resolution. This paper describes the design of the beam imaging system, the readout system as well as the mechanical construction.

INTRODUCTION

The TESLA Test Facility (TTF), Phase 1 [1] operated at DESY until November 2002 to perform various tests and experiments related to the TESLA linear collider project [2] as well as to serve as a Free Electron Laser [3, 4]. Presently TTF is being extended to a new Free Electron Laser facility (TTF2-FEL) [5]. In the first stage, five accelerating modules having eight 9-cell superconducting TESLA cavities each are installed, later two more modules can be added. Electron beam energies up to 1 GeV can be achieved. A sketch of the TTF2 linac is shown in Fig. 1.

The requirements for beam profile diagnostics are demanding. Beam profile monitors have to measure transverse electron beam sizes from millimeter scale down to 50 μm (sigma) with a high resolution. These monitors will be based on the use the visible part of the transition radiation spectrum, i.e. the optical transition radiation (OTR), providing a fast single shot measurement with a linear response. OTR was already used at TTF1 for beam transport optimization and beam characterization [6]. However, in order to meet the more strict requirements of TTF2, several improvements to the old monitor system have been made. The OTR beam profile monitor system is realized, as at TTF1, mainly by INFN-LNF and INFN-Roma 2, in collaboration with DESY.

OTR MONITORS AT TTF2

Totally 27 beam profile monitors will be installed along the TTF2 Linac (Fig. 1). Most of them (24) are equipped with an OTR screen, three monitors in the RF-gun section have Ce:YAG screens. Eight of the OTR monitors are combined with a wire scanner.

* katja.honkavaara@desy.de

Profile monitors have multiple tasks. They provide online beam images and profiles to optimize the beam transport through the linac. They are also used for the characterization of the beam: measurements of the transverse beam shape and size, emittance measurements using both the quadrupole scan and the four screen methods, as well as energy spread measurements in dispersive sections. The resolution of the monitor has to be sufficient to measure beam sizes down to 50 μm. In addition the system has to be robust, remote controlled, and have a possibility to change the magnification of the imaging optics and the attenuation of the OTR signal. Furthermore, because TTF2-FEL will serve as a user facility, reliability is an important aspect.

OTR monitors are based on measuring backward optical transition radiation emitted by a screen inserted into the beam with an angle of 45° with respect to the beam direction. A sketch of the monitor is shown in Fig. 2, and the different components are described below. OTR monitors in the bunch compressors have a special design, and they are not discussed in this paper.

VACUUM CHAMBER AND MOVER

A standard OTR vacuum chamber is a 7-way cross having three view ports. Fused silica (DUV-200) is used at the OTR output window because of its radiation hardness and good transmittance at the visible wavelengths. The opposite port is used for alignment purposes and has a normal glass window. The third view port is a small glass window at 45° with respect to the beam direction allowing to illuminate the screen from the front.

Eight of the monitors are combined with a wire scanner providing complementary measurements of the beam profile. Both devices are mounted into the same vacuum chamber. Ideally the screen and the wire should be in the same longitudinal position, but in order to avoid an accidental collision between them, they are separated in the beam direction by 25 mm. In order to have space to the wire scanner actuator, the opposite view port is lacking in these chambers.

An OTR screen is inserted into the beam by a stepper motor actuator. This mover is similar to the movers used at TTF1, but some mechanical parts are redesigned to improve its stability. The moving range is 100 mm, and the absolute screen position is read out by a potentiometer. For compatibility reasons, the motor driver is the same as used for other stepper motors at TTF2.

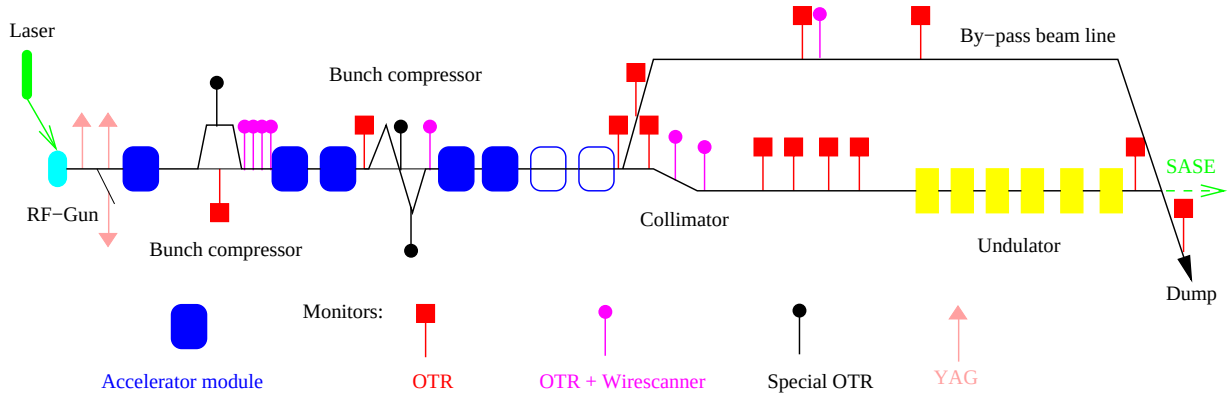

Figure 1: Schematic overview of the TTF2 linac (not to scale). Beam direction is from left to right, the total length is about 250 m. Different beam profile monitors along the linac are indicated.

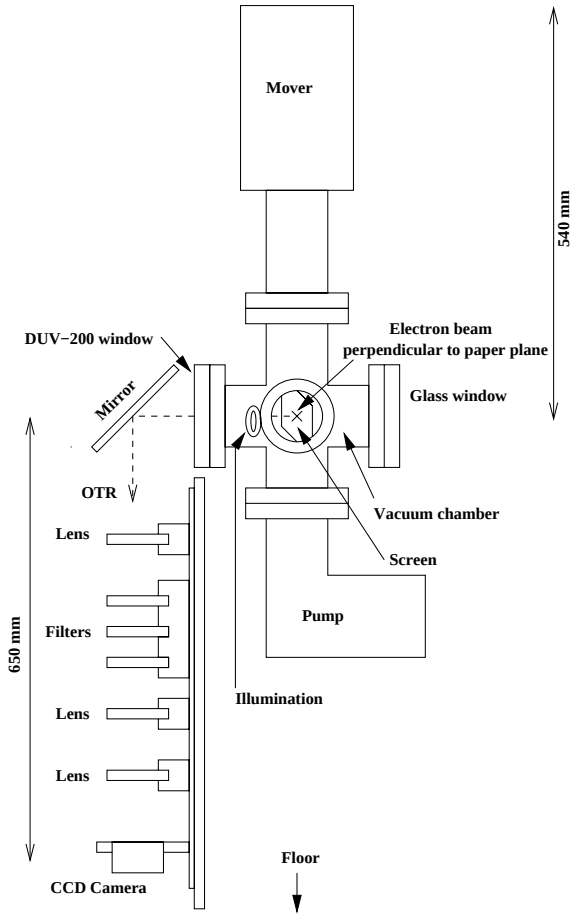

Figure 2: Sketch of a standard TTF2 OTR monitor (not to scale).

SCREENS

At TTF1, kapton foils with an aluminium coating were used as OTR screens. These screens showed cracks in the Al coating after some time of use. Our understanding is that the beam heats the screen and due to different thermal expansion, the Al coating cracks. One silicon screen with an aluminium coating was used as well. No visible damage is seen on this screen.

At TTF2, due to smaller beam sizes, the charge density on the screen will be even higher than at TTF1. Even if the number of electron bunches per macropulse will be limited to only a few, the charge density on the screen may be sufficient to destroy it even by a single shot. Therefore the screen material has to be carefully selected. So far, two materials, silicon and aluminium, have been studied. Other possibilities are tungsten, titanium and beryllium. According to EGS4 simulations [7] with a round gaussian beam distribution of σ = 50 μm, a silicon screen stays below its stress limit, when the charge per macropulse is less than about 110 nC. For aluminium the corresponding value is about 10 nC. The light emission efficiency of these two materials has been measured at TTF1: The number of photons detected by the same standard CCD camera was about four times less for polished silicon than for aluminium.

Because of the significant difference in the light emission, it has been decided to mount two screens in all the monitors: a 350 μm thick polished silicon screen and a silicon screen with a 40 nm aluminium coating. The size of both screens is 30 mm x 30 mm, and they are mounted on a common screen holder made of stainless steel. Between the two screens, on the same plane, are marks to adjust and calibrate the imaging optics.

OPTICAL SET-UP

A sketch of the optical system used to image the OTR light to the CCD camera is shown in Fig. 2. This system consists of a mirror deflecting the OTR light downwards, three achromatic doublets, three neutral density filters, and a CCD camera. The components are mounted on two rails on a stainless steel plate. The plate will be fixed to the support structure of the linac. The optical system is protected against the stray light, and the CCD camera is shielded with lead to reduce radiation damage.

Both, lenses and filters can be remotely moved transversally in or out of the optical axis. Only one lens is inserted

at any time. Focal lengths of the lenses are 250 mm, 200 mm and 160 mm providing nominal magnifications of 1, 0.38 and 0.25, respectively. The filters have transmission of 10 %, 25 % and 40 %, and any combinations of them can be used. The camera is a digital CCD camera (Basler A301f) with a firewire interface (IEEE1394). The sensor size of the camera is 658 x 494 pixels with a pixel dimension of 9.9 μm x 9.9 μm.

The initial adjustment of the optical set-up is done on an optical table. The optical axis is defined with a help of a He-Ne laser and small diaphragms. The correct position of the lenses is searched by automatically measuring the contrast on a calibration target. When the correct position of the lenses and the camera is found, their position is fixed. On the beam line, the distance of the whole system from the screen is adjusted with the help of the marks on the screen holder. The same marks are used to calibrate the magnification.

The resolution of the optical system was studied by measuring the Modulation Transfer Function (MTF). The resolution can be improved significantly by using a diaphragm reducing geometrical aberrations. In order to define the limiting resolution of the system, an edge profile of a black rectangle on the calibration target was taken. A gaussian point spread function (PSF) convoluted with a step function was fitted to the measured profile. From the fit the gaussian width (σ) of the PSF can be determined. A value of σ = 10 μm was obtained with a diaphragm of a diameter of 20 mm (magnification of 1). Without a diaphragm, the corresponding value was σ = 30 μm.

The highest resolution is required when the beam size is expected to be small. This is the case at the high beam energies, in the case of TTF2 after the full acceleration, when the beam energy is of the order of 1 GeV. At high energies OTR is well collimated and therefore the intensity cut by a diaphragm is small. Thus this technique can be used to improve the resolution in the high energy section of TTF2.

READ OUT-SYSTEM

The beam images are captured by digital CCD cameras. All the cameras are connected to a computer running control and acquisition software. This computer acts as a image server controlling the cameras and providing live beam pictures for monitoring, on-line beam profiles and beam widths, as well as high-resolution images for measurements, and low-resolution images for documentation. It also takes care of the communication with the TTF2 control system. A more complete description of the image server is in Ref. [8].

Digital IEEE1394 (firewire) cameras have been chosen, because they offer, at a cost comparable to their analog counterparts, several advantages, like full frame resolution, remote gain and shutter control and a triggered acquisition mode. A further advantage is a simpler cabling topology, because only a firewire link and a trigger are required, no videomultiplexer nor frame grabber is needed. On the other hand, there is no experience with a large digital camera system. The connection of almost 30 cameras distributed along the linac can be complicated, because the maximum length of standard firewire connections is only about 5 m. One possibility is to use glass fiber optical links and optical repeaters for long distance connections and hubs to connect locally the cameras via firewire links. Another solution is to replace the optical repeaters by compact PC104 computers connected to the image server via a local ethernet. In this solution each computer controls a limited number of cameras. The final solution for TTF2 is still under investigation.

STATUS AND OUTLOOK

All the vacuum components of the beam profile monitors are ready and the mounting of the OTR chambers in the linac will start this summer. The prototype phase of the optical set-up is successfully finished, and the first optical set-ups will be installed and commissioned soon. The test of the digital camera system continues and the decision of the final solution for the connection scheme will made within a few months. The complete OTR beam profile monitor system is expected to be in operation early 2004.

ACKNOWLEDGMENT

We like to thank our colleagues at DESY and at INFN for the technical support. Special thanks are due to S. Schreiber for many valuable discussions.

REFERENCES

[1] TESLA-Collaboration, ed. D.A. Edwards, “TESLA Test Facility Linac – Design Report”, DESY Print March 1995, TESLA 95-01.

[2] R. Brinkmann et al, “TESLA Technical Design Report, Part II The Accelerator”, DESY 2001-011, http://tesla.desy.de/new_pages/TDR_CD/PartII/accel.html

[3] J. Andruszkow et al., “First Observation of Self-Amplified Spontaneous Emission in Free-Electron Laser at 109 nm Wavelength”, Phys. Rev. Lett. 85 (2000) 3825-3829.

[4] V. Ayvazyan et al, “Generation of GW radiation pulses from a VUV Free-Electron Laser operating in the femtosecond regime”, Phys. Rev. Lett., 88 (2002) 104802.

[5] “SASE FEL at the TESLA Facility, Phase 2”, TESLA-FEL note 2002-01, DESY, June 2002.

[6] M. Castellano et al, “OTR Measurements for the TTF Commisioning”, Proceedings of DIPAC 1997 - LNF-97/048(IR) 195, 1997.

[7] V. Balandin and N. Golubeva, “Survival and Thermal Heating of materials for the OTR Screen at the TTF phase 2”, TESLA note in preparation.

[8] L. Catani, A. Cianchi, G. Di Pirro, “A Beam Image Server For TTF2”, Proceedings of PCaPAC 2002, Frascati (Roma) October 2002.

STUDY OF A LOW IMPEDANCE BEAM POSITION MONITOR FOR SHORT BUNCHES

D. Alesini, B. Spataro, C. Vaccarezza, LNF-INFN, Frascati (Rome), Italy
C. D'Alessio, A. Mostacci, L. Palumbo, University "La Sapienza", Rome, Italy

Abstract

A low coupling impedance beam position monitor based on microwave spectroscopy is proposed. A coaxial cavity is coupled to a circular beam pipe through four small longitudinal slots. Displaced beams excite TE cavity modes that can be detected by two antennas. Applying the modified Bethe's theory, the TE_{111} mode power has been derived as a function of the beam displacement. An aluminium prototype has been constructed with the support of numerical (HFSS) simulations. Bench measurements using a coaxial wire excitation show good agreement with both theoretical and numerical expectations.

1 INTRODUCTION

Different methods to measure beam position inside the pipe have been proposed either in the time domain than in the frequency domain. In this paper we describe a beam position monitor (b.p.m.) that measures the beam position detecting the resonant field excited by the bunch train in a coaxial cavity. The coaxial cavity is coupled to the beam pipe through four identical slots (see Fig. 1) having the longer side (l) in the beam direction that assure a small coupling impedance of the whole device [1]. The length of the cavity is chosen in order to excite a transverse TE mode. The beam position inside the pipe can be calculated by probing the field in the cavity with a small antenna.

We will describe and compare three different methods to evaluate the signal in the cavity as a function of the beam displacement. The first one is an analytic approach based on the modified Bethe's theory [2]. The second one is based on HFSS [3] simulations and the third one is based on the wire measurements method [4] made on an aluminium prototype.

2 ANALYTICAL APPROACH RESULTS

A sketch of the beam position monitor is shows in Fig.1 with the dimensions of the prototype shown on Table 1.

Considering a bunch train traveling off-axis at a distance r_0 with respect to the center of the beam pipe, the total density current in z=0 can be expressed by the summation:

$$J(t)=\left[\sum_{k=-\infty}^{+\infty} I(t-kT_0)\right]\frac{\delta(r-r_0)}{\pi r_0}\sum_{m=0}^{\infty}\frac{\cos[m(\varphi-\varphi_1)]}{1+\delta_{m0}} \quad (1)$$

where $I(t)$ is the current distribution of the single bunch, T_0 is the bunches spacing and c is the velocity of light. The spectrum of the beam current is:

$$\sum_{k=-\infty}^{+\infty} I(t-kT_0) = I_0 + \sum_{p=1}^{+\infty}\tilde{I}_p\cos(p\omega_0 t) \quad (2)$$

where $\omega_0 = 2\pi/T_0$, I_0 is the average beam current and $\tilde{I}_p$ is the amplitude of the Fourier component at $p\omega_0$ [5]. By assuming a Gaussian bunch distribution we obtain:

$$I(t)=\frac{I_0 T_0 c}{\sqrt{2\pi}\sigma_z}e^{-\frac{1}{2}\left(\frac{z}{\sigma_z}\right)^2} \Rightarrow \tilde{I}_p = 2I_0 e^{-\frac{1}{2}\left(\frac{\sigma_z}{c}\right)^2 p^2\omega_0^2} \quad (3)$$

where σ_z is the rms bunch length.

If a dipole mode of the cavity is tuned in order to resonate at one of the frequencies of the beam power spectrum lines ($\tilde{I}_n$), the average powers extracted by two probes coupled with the two azimuthal polarities (φ_0 and $\varphi_{\pi/2}$) can be expressed as a function of the beam current and transverse displacement in the general form:

$$\begin{cases} P^{(0)} = \underline{P}(\omega_r, r_0, \varphi_1)\tilde{I}_n^2 \\ P^{(\pi/2)} = \underline{P}(\omega_r, r_0, \varphi_1 - \pi/2)\tilde{I}_n^2 \end{cases} \quad (4)$$

Knowing by theory, simulations or calibrating measurements the coefficient $\underline{P}$, the previous system of equations (for a given power spectrum lines $\tilde{I}_n$) allows to calculate, in principle, the values of r_0 and φ_1.

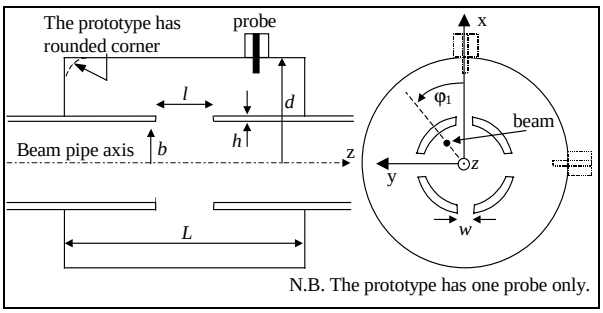

Figure 1: sketch of the beam position monitor.

Table 1: prototype dimensions (mm)

d	30
b	10
L	52
w	2
l	5
h	1

The TE_{111} mode with the polarity φ_0, according to the modified Bethe's theory, dissipates an average power given by [2]:

$$P_{Th.}^{(0)} = \frac{1}{2}\frac{R}{Q}Q_0\cos(\varphi_1)^2 r_0^2\tilde{I}_n^2 \quad (5)$$

where R/Q is given by:

$$\frac{R}{Q}=\frac{4\omega_r\mu A^2\alpha_E^2}{\left(1-2\alpha_E(1+Q)A^2\right)^2+\left(1-2\alpha_E A^2\right)^2} \quad (6)$$

where ω_r and Q_0 are the resonant angular frequencies and the quality factor of the TE_{111} mode, α_E is the electrical polarizability of the single slot and the A coefficient is given by the following integral:

$$A=\frac{\omega_r L\tilde{J}_1(b)}{b\pi c}\left[\int_b^d \frac{L\pi}{2}\left(k_t^2\left(\tilde{J}_1'\right)^2 r+\frac{\left(\tilde{J}_1\right)^2}{r}+\frac{k_t^4L^2}{\pi^2}\left(\tilde{J}_1\right)^2 r\right)dr\right]^{-\frac{1}{2}} \quad (7)$$

with $\tilde{J}_1(r)=J_1(k_t r)-Y_1(k_t r)J_1'(k_t b)/Y_1'(k_t b)$, the prime denote the total derivative with respect to the argument and $k_t=\sqrt{(\omega_r/c)^2-(\pi/L)^2}$.

Considering the prototype dimensions, one obtains the values of ω_r, Q_0 and R/Q reported in Table 2 (first column).

The value of the normalized power $P_{Th.}^{(0)}/Q_0\tilde{I}_n^2$ as a function of r_0 for $\varphi_1=0$ is plotted in Fig. 2 and compared with the simulation and measurement results (described in the next section). In Fig. 3 the same quantity is plotted as a function of φ_1 for r_0=0.6 mm.

Table 2: theory, simulations and measurements results

	THEORY	**HFSS**	**MEAS**
ω_r [GHz]	3.78	3.74	3.74 (tunable)
Q_0	9600	9100	3500
R/Q [mΩ]	36	31	39

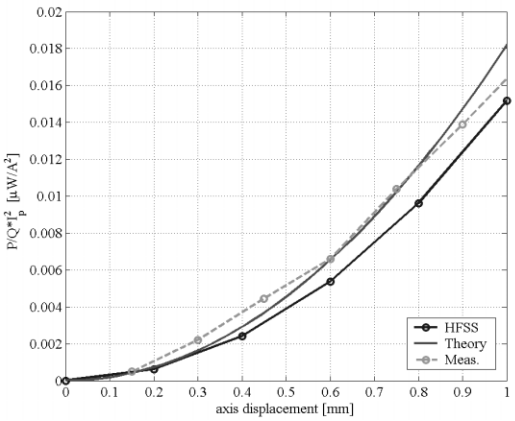

Figure 2: $\underline{P}^{(0)}/Q\tilde{I}_p^2$ as a function of r_0 for φ_0=0.

3 SIMULATION RESULTS

To compare the analytical results with the numerical simulations, we have studied the coupling impedance of the cavity for the TE_{111} mode as a function of the transverse displacement r_0 and φ_1. We have, therefore, calculated the longitudinal shunt impedance of the mode (R_s) for different axial positions, using the Eigenmode Solver of HFSS.

The HFSS model is shown in Fig. 4 with the obtained E field lines. It is only 1/8 of the structure with proper magnetic and electric boundary conditions on the symmetry planes. The average dissipated power in the cavity corresponding to the TE_{111} mode is given by:

$$P_{Sim.}^{(0)}=\frac{1}{2}R_s(\varphi_1,r_0)\tilde{I}_n^2 \quad (8)$$

The value of $P_{Sim.}^{(0)}/Q\tilde{I}_n^2$ is plotted in Figs. 2-3 and compared with the analytical and measurement results. From the previous plot it is possible to verify that it is possible to write the eq. (8) in the form:

$$P_{Sim.}^{(0)}\cong\frac{1}{2}\frac{R}{Q}Q_0\cos(\varphi_1)^2 r_0^2\tilde{I}_n^2 \quad (9)$$

The values of ω_r, Q_0 and R/Q obtained by the simulations are reported in Table 2 (second column).

If the cavity is coupled through a small probe to an external load, then the average dissipated power in the system is still given by eq. (5) or (9) but with Q_0 replaced by the loaded Q_L. The average power dissipated in the load ($P_{Ext}^{(0)}$) is related to the power dissipated in the cavity by:

$$P_{Ext}^{(0)}=P_{cav}^{(0)}\beta/(1+\beta) \quad (10)$$

where β is the coupling coefficients between the probe and the cavity mode TE_{111} and it can be obtained from reflection measurement at the probe port.

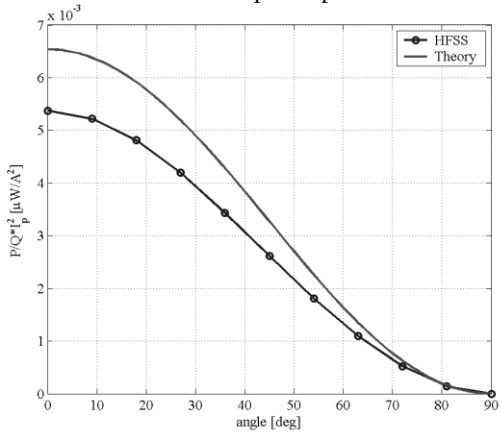

Figure 3: $\underline{P}^{(0)}/Q\tilde{I}_p^2$ as a function of φ_1 for r_0=0.6 mm.

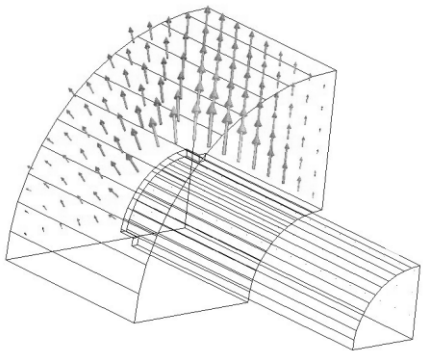

Figure 4: HFSS model with E field lines.

4 PROTOTYPE MEASUREMENTS

Wire measurements have been performed on the aluminum prototype shown on Fig. 5. An antenna probes the signal in the cavity.

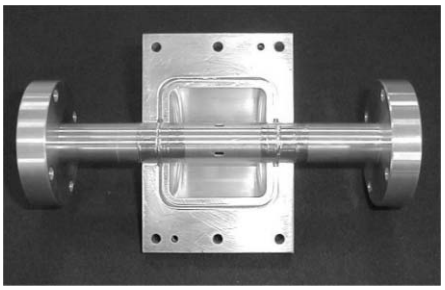

Figure 5: beam position monitor prototype.

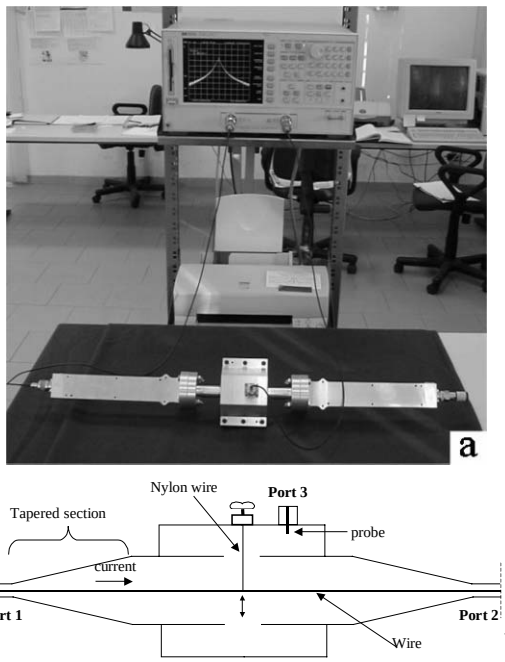

Figure 6: measurement setup

The measurements setup is shown Fig. 6a and schematically represented in Fig 6b. The wire has a radius of 1.5 mm. In order to minimize reflections at the ports 1 and 2 we have inserted two tapered sections that match the 50 Ω impedance of the Network Analyzer with the ~114 Ω impedance of the wire in the beam pipe. To excite the dipolar mode TE_{111} the wire inside the beam pipe has been properly displaced from the axis of the beam pipe. To this purpose, a thin nylon wire has been connected to the wire in order to displace it from the beam pipe axis in a controlled way and to excite the polarity φ_0. The measured transmission coefficient S_{21} and S_{31} are shown in Fig. 7 for a displacement of the wire of ~1.5 mm.

The average dissipated power in the cavity is given by:

$$P_{cav}^{(0)} = P_{Ext.}^{(0)} \frac{(1+\beta)}{\beta} \cong \frac{1}{2} Z_c \frac{|S_{31}(\omega_r)|^2}{|S_{21}(\omega_r)|} \frac{(1+\beta)}{\beta} \tilde{I}_n^2 \qquad (11)$$

The plot of $P_{cav}^{(0)} / Q\tilde{I}_p^2$ as a function of r_0 is reported in Fig. 2. It is clear that $P_{cav}^{(0)}$ can be written in the form (5) or (9) and the equivalent R/Q is reported in Table 2. The Q factor of the resonant mode is lower than the theoretical one because of RF losses in the mechanical contacts. Similar considerations than those developed in [6] can be done from the point of view of the induced errors in the measurement setup.

By the system of equations (4) it is possible to calculate the position of the bunches in the beam pipe when the b.p.m is inserted in the accelerator, by the formulae:

$$\begin{cases} r_0 = \dfrac{\sqrt{P_{Ext.}^{(\pi/2)} / \underline{P} + P_{Ext}^{(0)} / \underline{P}}}{\tilde{I}_n} \\ \varphi_1 = \pm \arctan\left(\sqrt{\dfrac{P_{Ext.}^{(\pi/2)}}{P_{Ext}^{(0)}}} \right) \pm \pi \end{cases} \qquad (12)$$

where the calibration coefficient $\underline{P}$ is given by:

$$\underline{P} = \frac{1}{2} Z_c \frac{|S_{31}(\omega_r)|^2}{|S_{21}(\omega_r)|} \frac{1}{r_0^2} \qquad (13)$$

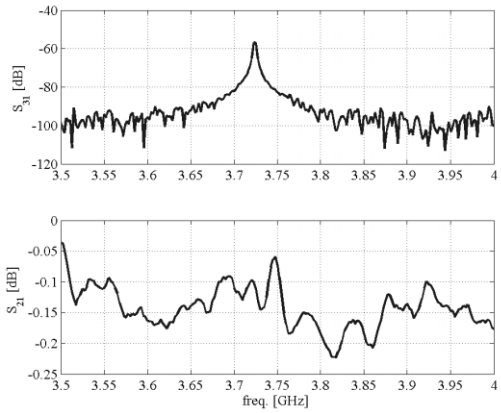

Figure 7: measured transmission coefficients (S_{12}, S_{31}).

5 CONCLUSIONS

A novel bunch position monitor has been described. Measurements on an aluminium prototype have been compared to the theoretical and numerical expectations of the power dissipated by the first dipolar mode in the cavity. The compare shows a good agreement between theory and simulations expecially considering the mechanical differencies between the prototype and the ideal structure. These results confirm the potential application of this device as a beam position monitor. The very low coupling impedance of the device and the possibility of calibration by simple wire measurements make the device hopefully usable in the accelerator machines.

6 REFERENCES

[1] S. De Santis and L. Palumbo, Phy. Rev. E, vol 55, pp. 2052-2055, 1997.

[2] C. D'Alessio, Tesi di Laurea, Univ. "La Sapienza", 2002.

[3] http://www.ansoft.com

[4] F. Caspers, in Handbook of Accelerator physics and engineering, pp. 570-574, World Scientific, 1999.

[5] A. Hofmann, "Beam Instabilities", CERN 95-06, Geneva, 1995.

[6] D. Alesini et al., Proc. of EPAC 2002, pp. 1834-1836, Paris

BUNCH-TO-BUNCH ENERGY STABILITY TEST OF THE NB PROTOTYPES OF THE TESLA SUPERSTRUCTURE

V. Ayvazyan, P. Castro, R. Kammering, H. Schlarb*, S. Schreiber, J. Sekutowicz,
S. Simrock, M. Wendt, (DESY), M. Hüning (FNAL), M. Ferrario (INFN)

Abstract

Two 2x7-cell Nb superstructures have been tested with beam during the last TESLA Test Facility (TTF) linac run in summer 2002. The structures have been operated at 2 K in the standard TTF cryomodule and have been installed in the linac after the injector. We report on the bunch-to-bunch energy stability test which showed that energy stored in the superstructure could be refilled in the time between two passing bunches. The goal to keep the bunch-to-bunch energy stability below $5 \cdot 10^{-4}$ has been achieved.

INTRODUCTION

An alternative layout of the TESLA linear collider [1, 2, 3], is based on weakly coupled multi-cell superconducting structures, called the superstructures (SST). The weak coupling of 0.04% between the multi-cell structures, the subunits, is achieved by connecting the cavities with $\lambda/2$ tubes. This has two advantages: it reduces significantly the investment cost due to a simplification the RF system and secondly increases the filling factor of the main accelerator. The fundamental power coupler (FPC) supplying the entire chain of subunits with 1.3 GHz RF is mounted at one end of the SST. The energy flow through the superstructure is controlled by means of cold tuners allowing to balance the stored energy and thus the accelerating gradient in each subunit. Unlike a standard multi-cell cavity, the accelerating mode in a SST is the π-0 mode – π cell-to-cell phase advance and 0 subunit-to-subunit phase advance – which is below cut-off in the interconnecting tubes. This allows to attach higher order mode (HOM) couplers at the interconnection, in the middle of the multi-cell structure. In this way, good damping of parasitic modes can be maintained, avoiding extensive heating of the HOM couplers.

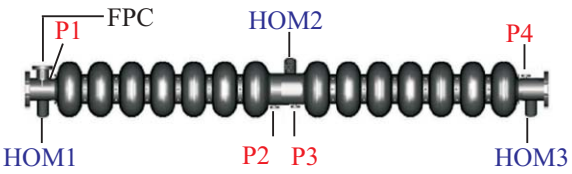

Figure 1: Scheme of a 2x7-cell Nb superstructures.

After several RF test on warm copper models of the superstructure [3] the next step was to study the performance of niobium SST's at 2 K with beam. In summer 2002, two 2x7-cell superstructures, sketched in Fig. 1, have been installed in the TESLA Test Facility linac to address the following questions:

- balancing the acceleration field in subunits,
- damping of the higher order modes,
- achievable energy stability of the electron beam.

In this paper, we adress the third item the refilling process in cavities with high beam loading. A detailed description of the mechanical layout, the cavity tuning, and the HOM damping in a superstructure can be found elsewhere [4, 5]. Numerical simulations of the transient state and the bunch-to-bunch energy spread predict that there is enough time to refill the cells energy before the next bunch arrives. The computed bunch-to-bunch energy deviation for a 2×7-cell and a 2×9-cell (preferred design in TESLA TDR) are shown in Fig. 2. For all bunches in the train the computed

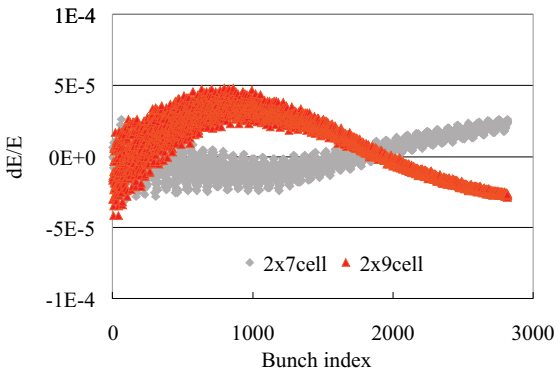

Figure 2: Computed energy deviation for the TESLA beam:2820 bunches, 3.2 nC/bunch, spacing 337 ns.

variation for both versions of the SST was very small, less than $\pm 5 \cdot 10^{-5}$. The difference in shape of the two curves is due to the different mode beating.

EXPERIMENTAL SETUP

The TTF photo injector is based on a normal conducting laser driven L-band RF gun and a single superconducting 9-cell cavity boosting the beam energy to 15.3 MeV. The beam is then accelerated by two acceleration modules. High resolution energy spectrometer are situated at the injector and the end of the linac (see Fig. 3). For this experiment, two 2×7-cell superstructures (SST-1 and SST-2) have been installed after the photo-injector. They have an active length of 3.26 m. Unfortunately, the second accleration module with eight standard 9-cell super-

* schlarb@desy.de

conducting cavities has been installed after the superstructures but before the spectrometer. For the energy stability measurements, the SST's have been operated at a gradient of 14.3 MV/m, while the cavities in the second cryomodule were detuned to reduce the their influence. This results in a total energy E_{tot} of 62 MeV at end of the linac. The bunch spacing was 1 μs to meet the highest possible data aquisition rate of the front-end electronics allowing to sample parameters for each bunch in a pulse train. Bunch charges of typically 4 nC (nominal 8 nC) and beam durations between 530 μs and 760 μs (nominal 800 μs) at 1 Hz repetition rate have been chosen to achieve the required operation stability for this experiment.

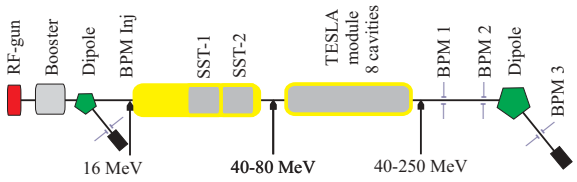

Figure 3: Scheme of TTF linac for the SST test.

MEASUREMENT OF FIELD PROBES

A flat energy distribution of the bunches in a macro-pulse train does not necessarily proof a proper refilling of the weakly coupled subunit. A reduced gradient in one subunit may have been compensated by overfilling the other. This would have been possible, since the low level RF system (LLRF) controlles the phase and amplitude of the vectors sum of all cavities and not of each cavity individually. Using the signals of all four field probe (P1-P4 in Fig. 1) the gradients can be monitored at the entrance and the exit celss of both cavities. An example recorded with 4 mA beam current and 530 μs pulse duration is shown in Fig. 4. Without the energy refilling the beam would take almost 70% of the energy stored in cells and the voltage would drop by 45%. No such phenomenon was observed. All probes show noise fluctuations mainly caused by the down-converters of

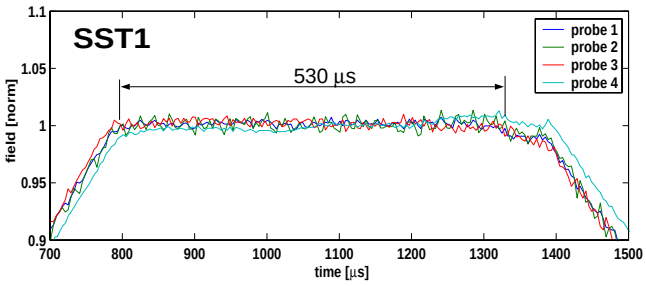

Figure 4: Signals from field probes P1-P4 measured during acceleration of 530 bunches (I = 4 mA, g =14.3 MV/m).

the LLRF-system (250 kHz oscillations).

BEAM ENERGY STABILITY

The TTF linac layout does not provide the possibility to measure the beam energy spread before and behind the SST simultanously. Therefore the energy stability of the beam exiting the injector had to be carefully studied. The goal was to measure bunch to bunch energy variations with a resolution well below 0.01%. It was also necessary to examine effects of the second acceleration module even through their cavities have been detuned.

Energy jitter from the photo-injector

Because the energy gain in the SST is set to be 47 MeV only, phase and amplitude jitter of the laser, the RF gun or the booster cavitiy might seriously spoil the energy measurement for the SST. After tuning the injector parameters properly, a beam energy spread of 0.09% during a time period of 30 min has been achieved. The bunch to bunch energy variation for 100 macro-pulses are plotted in Fig. 5. The energy $E_{i,m}$ of the i^{th} bunch in the m^{th} train can be

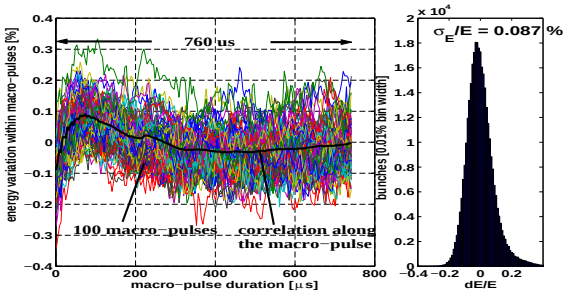

Figure 5: Left: Injector bunch-to-bunch energy variation of 100 macro-pulses (color curved). Right: Energy spread of for all bunches (E = 15.3 MeV).

decomposed as

$$E_{i,m} = E_{inj} + \Delta E_m + \Delta E_{corr,i} + \delta E_{i,m} \quad (1)$$

with E_{inj} the average energy of all bunches, ΔE_m the energy deviation of the m^{th} macro-pulse train, $\Delta E_{corr,i}$ the energy time correlation common in all macro-pulses (black curve in Fig. 5) and $\delta E_{i,m}$ a residual fast bunch-to-bunch energy jitter. Only the later contribution is critical for our purpose. The rms widths of $\delta E_{i,m}$ amounts to 6.7 keV (see Tab.1) and sets the lower limit on the σ_E/E_{tot} measurement at the end of the linac to $1.1 \cdot 10^{-4}$.

Accuracy of the energy measurement

The energy variation of the bunches is calculated by means of two strip-line BPMs upstream the spectrometer dipole to correct for the incoming orbit jitter (see Fig.3) and BPM3 located in the spectrometer line with large dispersion ($\eta_x = -1.48$ m). All BPMs have been calibrated by steering the transverse position of the beam in the BPMs with well known dipole corrector. The control software

calculates online the energy of all bunches in the entire bunch train and compensates for the non-linear response of the BPMs for large beam offsets [8]. The accuracy of the BPMs has been determined to be 60 μm rms [9] resulting in a relative energy resolution of $\sigma_{E,res}/E_{tot} = 1.2 \cdot 10^{-4}$.

Influence of the second accleration module

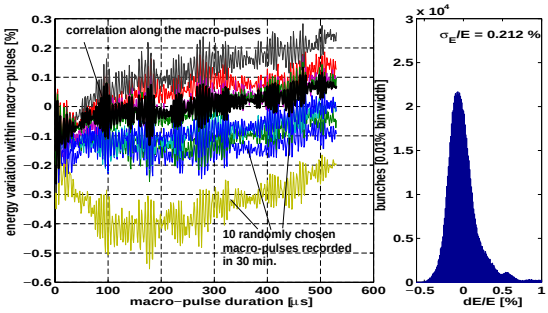

Figure 6: Energy deviation along a pulse train measured in the spectrometer ($I = 3.8$mA, $t = 530\mu$s).

Fig. 6 shows typical energy distributions of pulse trains recorded in 30 minutes. The overall energy spread of the beam amounts to 0.2%. The contributions split according to Eq. 1 are listed in Tab. 1. The dominating contribution of the energy spread comes from the macro-pulse to macro-pulse energy jitter. Unlike the smooth energy distribution observed in the injector, very fast oscillations are superimposed to slow low frequency drifts across the pulse trains. A careful analysis of the energy spectrum obtained by fourier, shown in Fig. 7, states that the largest part of the fast oscillations are induced by the eight detuned cavity. The resonance at 250 kHz is identified as an uncompleted removal of the down-converter noise perturbing the LLRF-regulation. A couple of other smaller resonances are related to the feedback gain of the LLRF feedback loop. Some of the resonances are strongly enhanced if high gains between 50 and 100 are adjusted. This increases the energy spread within the macro-pulse but reduce the energy jitter from pulse train to pulse train. The presented data are taken at a loop gain of 30 (small). If the influence of 2^{nd} acc. module is removed by using an approximation depicted by the dashed lines in Fig. 7, a relative rms energy spread within the 1800 macro-pulses of $4.2{\cdot}10^{-4}$ is calculated. If only 100 macro-pulses with the smallest drifts are taken into account one finds $2.2{\cdot}10^{-4}$ as the lowest achieved value for the intra macro-pulse energy deviation of the bunches.

Table 1: Contributions of energy spread at the injector (E_{inj} =15.3 MeV) and at the end of the linac (E_{tot} =61.5 MeV)

	$\sigma(\Delta E_m)$	$\sigma(\Delta E_{corr,i})$	$\sigma(\delta E_{m,i})$	σ_E
inj	10.1 keV	5.5 keV	6.7 keV	13.4 keV
tot	122.9 keV	32.9 keV	25.4 keV	130 keV

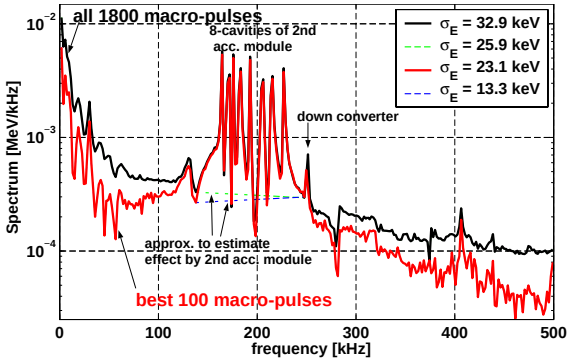

Figure 7: Spectrum of the energy modulation.

SUMMARY

In this experiment with 2×7-cell superstructures we achieved a bunch-to-bunch energy stability in macro-pulses of 0.064% for more than 30 minutes. Significant influences of the second acceleration module and the LLRF on the measurement have been found, while investigation on the incoming energy jitter from the injector states that these influences can be neglected. The upper limit for the bunch-to-bunch energy deviation caused by the cavities of the superstructures only has been estimated to be $\sigma_E/E = 2.2 \cdot 10^{-4}$, well below the TESLA specification of 0.05%.

REFERENCES

[1] "TESLA Technical Design Report, Part II: The Accelerator" , DESY 2001-011, Hamburg; March 2001.

[2] J. Sekutowicz et.al.,"Superconducting Superstructure" , Proc. of LC97, Zvenigorod, Sep. 29-Oct. 3, 1997.

[3] J. Sekutowicz et.al., "Superconducting superstructure for the TESLA collider; A concept", PR-ST A.B, 1999.

[4] J. Sekutowicz et.al., "Active HOMs Excitation in the First Prototype of Superstructure" , Proc. of PAC03, Portland, May 12- 16, 2003.

[5] P. Castro et.al., "Analysis of the HOM damping with Modulated Beam in the First Prototype Superstructure" , Proc. of PAC03, Portland, May 12-16, 2003.

[6] J. Sekutowicz et.al., "A Superstructure for High Current FEL Application" , Proc. of PAC03, Portland, May 12- 16, 2003.

[7] M. Ferrario et.al., "Multi-Bunch Energy Spread Induced by Beam Loading in a Standing Wave Structure" , Par. Accel., Vol. 52, 1996.

[8] N. Sturm,"Energie-Stabilisierung für den Freien Elektronlaser an der TESLA-Test-Anlage" Dipoma Thesis, DESY 2002, Hamburg.

[9] H. Schlarb,"Collimation System for a VUV Free-Eelectron Laser at the TESLA Test Facility", DESY-THESIS-2001-055.

CTF3 PROTOTYPES: DESIGN, TESTS AND MEASUREMENTS

A. Ghigo, D. Alesini, C. Biscari, R. Boni, A. Clozza, G. Delle Monache, A. Drago, A. Gallo, F. Marcellini, C. Milardi, C. Sanelli, M. Serio, F. Sgamma A. Stecchi, A. Stella, M. Zobov, INFN-LNF, Frascati, Italy.
R. Corsini, L. Rinolfi, CERN, Geneva, Switzerland.

Abstract

The high efficiency in the 30 GHz power production is maintained if the beam quality is preserved along the rings and the transfer lines of the CLIC Test Facility (CTF3) compressor system [1,2]. The energy loss and energy spread, caused by vacuum chamber components coupling impedance and by coherent synchrotron radiation (CSR) emission, must be minimized.

The magnetic layouts of the first ring of the compressor system, called Delay Loop (DL) and of the transfer line between the Linac and DL are presented. Tests and measurements on several vacuum chamber components prototypes are reported. The 3 GHz RF deflectors, that will provide the injection in the Combiner Ring, have been studied, realized, tested, installed and successfully used in the first interlaced bunch trains injection in the CTF3 preliminary phase. A standing wave 1.5 GHz RF deflector for injection into the Delay Loop is proposed.

INTRODUCTION

The 30 GHz RF power production, needed in the CLIC project, depends on the drive beam structure; after the recombination system very short bunches with regular spacing are required. To preserve the beam quality in the CTF3 compressor system the ring lattices are isochronous and the R_{56} of the transfer lines is kept very small.

The study of rings and transfer lines optics has been reported in the CTF3 Design Report [1] and in several articles [2,3]. The coherent synchrotron radiation effect for short bunches as well as the vacuum chamber coupling impedance become important issues, leading to an energy loss and to an increase in energy spread. In fact, the energy losses give rise to relative phase errors between bunches through non perfect isochronicity, which results in deterioration of the timing between individual bunches and merging trains; the energy spread leads to bunch lengthening and phase space distortion.

The INFN Frascati laboratories will provide the first of the two rings of the compressor system called Delay Loop (DL). At the exit of this ring the frequency of the bunches coming from the Linac (1.5GHz) will be doubled with an increment of the current by a factor two. A magnetic bunch stretcher chicane is part of the transfer line that join the Linac with the DL; it is used to increase the bunch length in order to reduce CSR and impedance effects.

Therefore the magnetic stretcher/compressor chicane was designed with an R_{56} tunable in the range of +50, -30 cm that allows to vary the bunch length in a very wide range.

Systematic experimental studies of the CSR effect in the compressor are also foreseen with an energy analyser and an emittance measurement system at the chicane exit. In this paper the study and the prototype realization of several components of the vacuum chamber are described. The tests of the RF deflectors realized by LNF, and successfully used in the CTF3 preliminary phase [5], are also reported.

MAGNETIC LAYOUT

The optics of Delay Loop and Transfer lines have been well studied including multiparticle tracking [3]. The magnetic layout of the Delay Loop and transfer lines has been completed using existing dipole and quadrupole magnets of the EPA complex in CERN together with the injection extraction septa magnet. In Fig. 1 the layout of the magnetic elements is shown.

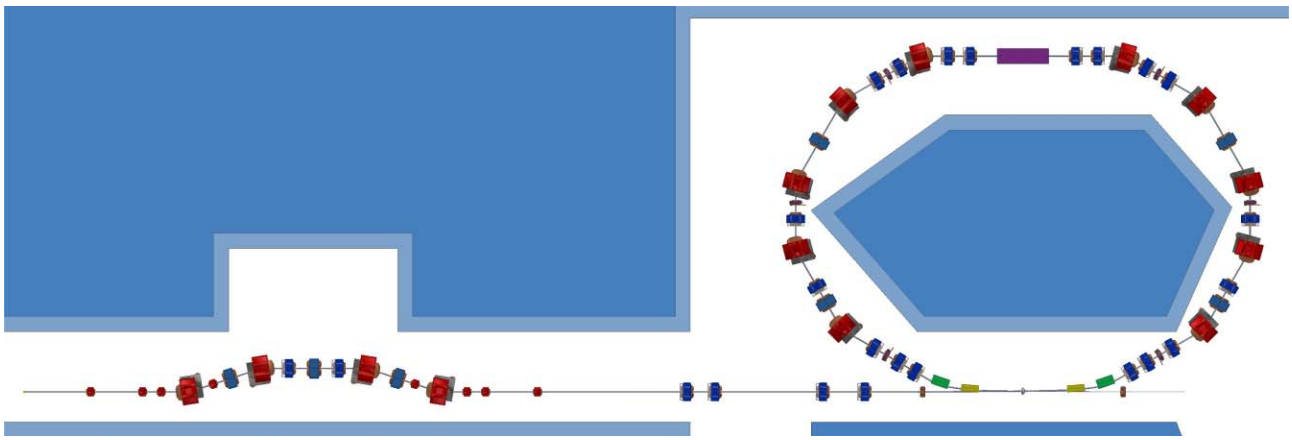

Figure 1: Layout of the Delay Loop and Transfer Line magnetic elements.

PROTOTYPES

The first prototypes vacuum chamber components studied and realized are the pump ports, shielded bellows and beam position monitors. The longitudinal impedance measurements of these devices have been done because their large number along the rings and transfer lines can contribute in significant way to the impedance. The Combiner Ring RF deflectors have been also tested and installed in the CTF3 preliminary phase [5]. The Delay Loop RF deflector has been studied.

Vacuum pump port

In the design of vacuum pump ports RF screen the hidden slots idea, applied successfully for PEP II, has been adopted. This allows to reduce by some orders of magnitude the coupling impedance and to prevent radiation into the pump chamber. The realized RF screen consists of 38 grooves 72 mm long, 2 mm wide and 2 mm deep in the rectangular vacuum chamber pipe with 4 mm thickness; these grooves are used to decrease the coupling impedance. Along each groove 25 circular holes of 1 mm (smaller than the bunch longitudinal size) are drilled for pumping purpose; these holes prevent penetration of the RF fields outside of the beam pipe. To decrease further the impedance in the rectangular geometry of the beam pipe, the grooves are placed closer to the chamber corners and there are no grooves on the lower and upper desks of the chamber near the symmetry axis.

The impedance of the prototype section, 8 cm long, that provides a vacuum conductance of 60 l/s, has been measured with the wire methods with resistive matching. The measurements, extended up to 4.5 GHz (maximum allowable range with resistive matching), have shown that the impedance values are too small to be detected by the measurement apparatus. The calculated impedance of these pumping screen is Z/n=j $4.3*10^{-6}$ Ω. No resonant mode seems to appear.

Shielded Bellows

A prototype of the shielded bellows that provides the vacuum chamber flexibility has been developed. The RF shielding is a sliding finger structure, similar to that used in the KEKB rings, with the same inner shape of the rectangular vacuum chamber. The number and the shape of the sliding contact have been chosen in order to reduce the coupling of the bunch field to the bellows structure; the thickness and position of the spring finger have been chosen to maximize the electrical contact. The bellows impedance, predominantly inductive, has been evaluated to be about 10^{-6} Ω.

Beam Position Monitor

The CTF3 BPM works in principle as a transformer excited by the beam. The beam image current is diverted to four metallic strips placed outside the vacuum chamber ceramic gap and short-circuited to the two ends of the metallic vacuum chamber. Small ferrite core transformers, placed at the end of each strip, provide signals whose amplitude depends on the beam position [1].

The striplines are surrounded by ferrite tiles to improve the low frequency response. Such ferrites, at high frequency, have high RF losses and damp unwanted resonances of the external metallic shield.

Measurements based on the coaxial wire method have been performed to estimate the transfer impedance of the device and showed a low frequency cut-off at 400kHz [3].

To investigate position sensitivities of the device, a series of measurements with a movable wire has been performed at the calibration bench shown in Fig.2.

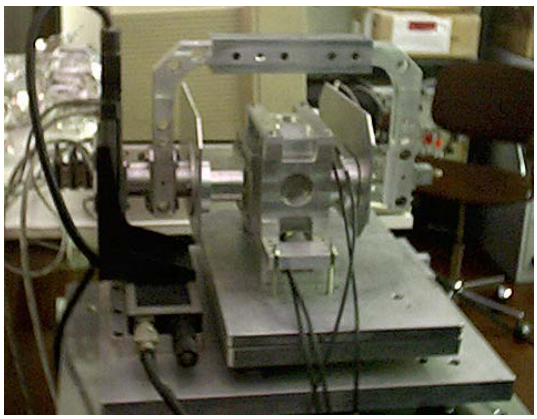

Figure 2: BPM calibration bench

Beam position is derived from the ratios U,V (pseudo-positions) between the peak intensities v_i of the signals from the windings by using a non linear fit:

$$x = k_x \cdot U + f(U,V) \quad y = k_y \cdot V + g(U,V)$$

where k_x and k_y are the inverse sensitivities to beam displacement and $f(U,V)$ and $g(U,V)$ are polynomial functions.

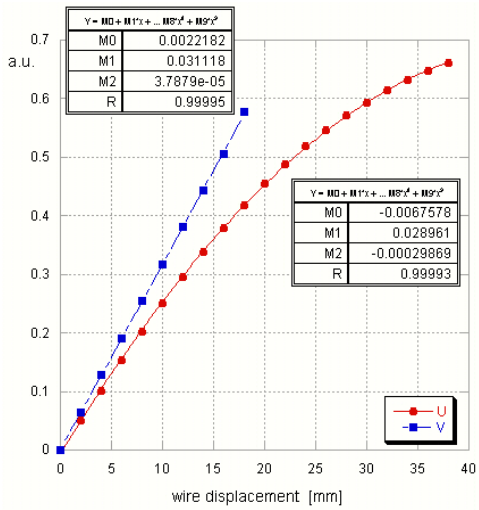

Figures 3: Position sensitivities along the horizontal and vertical axis

The outputs v_i at a fixed frequency from each secondary winding have been acquired for several transverse wire positions to derive coefficients of the polynomial functions (f and g) used to correct non linearities of the BPM for large beam offsets (see Fig. 3).

Data from these measurements showed 20dB maximum amplitude excursion between the four signals Vi for a beam offset by 70% of the vacuum chamber dimensions.

In order to reduce the beam coupling impedance, the internal wall of the ceramic gap will be coated with a conductive film whit thickness that allows only lower frequency components of beam fields to propagate outside to be picked up by the secondary windings.

RF DEFLECTORS

Combiner Ring RF Deflectors

The bunch trains interlacing scheme of CTF3 is based on the use of RF deflectors as injection kickers. The Combiner Ring RF deflector design has been based on an already optimized TW deflecting structure. The interaction between the beam and the deflector operating mode (beam loading) has been studied to evaluate the impact on the quality of the extracted beam. We came to the conclusion that the beam loading in a pair of 10-cells TW deflectors does not produce a significant degradation of the beam quality, provided that the betatron phase advance between the two devices is properly chosen [1]. Following these results, two deflectors used in CTF3 preliminary and nominal phases have been built in collaboration with the Soltan Institute for Nuclear Studies (Swierk, Poland).

The INFN-LNF CTF3 group collaborated in the CTF3 preliminary phase (which started in autumn 2001 and has been completed during year 2002) having a goal to demonstrate the "funnelling" injection scheme and bunch train compression in an isochronous lattice. The main difference between these preliminary experiments and the nominal CTF3 is the limited beam current available from CERN LEP Injector Linac.

In CTF3 preliminary phase the concept of bunch train combination by means of RF deflectors has been demonstrated experimentally [5].

Delay Loop RF Deflector

The Linac bunch train, 1.4 μs long, is composed by sequence of 140 ns bunch trains, with 1.5 GHz repetition rate, phase shifted by one 3 GHz RF cycle. The odd trains are injected into the Delay Loop and recombined at the extraction after one turn with the pair incoming trains. This scheme is used to double the current in the 140 ns train increasing to 3 GHz the bunch repetition rate. An RF deflector, working at 1.5 GHz RF frequency, placed at the conjunction point of transfer line and Delay Loop, provides the injection/extraction in/from the Delay Loop.

The pulsed RF source is a 1.5 GHz Klystron, custom developed for this purpose, with maximum RF delivered power of 20 MW with 5 μs pulse length. The requested deflection angle is 15 mrad at the maximum energy of 300 MeV (nominal energy of the full current beam is 150 MeV).

Different design solutions for this device have been investigated. A standing wave cavity, that has more compact design with respect to the multicell travelling wave structure and provides better kick efficiency, has been chosen. In Table 1 the characteristics of two different standing wave single-cell deflectors with different Q value are presented. Because of the filling time and finite RF pulselength, there are different deflection angles from head to tail of the bunch train coming from the Linac. The cavity with lower Q is less efficient but minimizes these kick differences that produce a transverse emittance growth.

Table 1. Different Q value cavities comparison

Q	**4200**	**5800**
P (15mrad@300MeV)	18 MW	14 MW
ΔV start to end	1.5 %	4.0 %

Figure 4 shows the HFSS model of the developed single cell standing wave deflecting cavity. The cavity is fed by two waveguide placed on opposite sides in the horizontal plane.

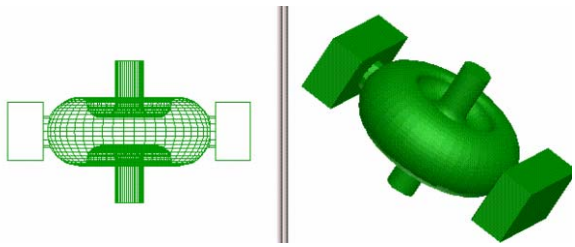

Figure 4: 1.5 GHz RF deflector model

ACKNOWLEDGMENTS

The authors wish to thank G. Fontana, V. Lollo, and A. Zolla for the machine layout and the mechanical project of the presented prototypes; S. Pella for the technical support during measurements; the CTF3 CERN technical staff for the RF deflectors installation and power test.

REFERENCES

[1] G. Geschonke, A. Ghigo et al., “CTF3 Design Report” CERN/PS 2002-008 (RF), LNF-02/008 (IR)

[2] C. Biscari et al., “CTF3: Design of Driving Beam Combiner Ring”, EPAC’2000, Vienna, p.450.

[3] D. Alesini et al., “CTF3 Compressor System”, Proceedings of EPAC 2002, Paris, France, p.416.

[4] D. Alesini et al., “RF Beam Deflector for CTF3 Combiner Ring”, Proceedings of EPAC 2002, Paris, p.2115.

[5] F. Tecker et al. “Bunch Frequency Multiplication in the CLIC Test Facility CTF3” PAC 2003, these proceedings.

A RECIPE FOR LINEAR COLLIDER FINAL FOCUS SYSTEM DESIGN

Andrei Seryi, Mark Woodley SLAC, USA*
Pantaleo Raimondi INFN, Italy

Abstract

The design of Final Focus systems for linear colliders is challenging because of the large demagnifications needed to produce nanometer-sized beams at the interaction point. Simple first- and second-order matrix matching have proven insufficient for this task, and minimization of third- and higher-order aberrations is essential. An appropriate strategy is required for the latter to be successful. A recipe for Final Focus design, and a set of computational tools used to implement this approach, are described herein. An example of the use of this procedure is given.

INTRODUCTION

The new compact final focus system [1], based on local chromaticity correction in the final doublet, is now being adopted for all of the linear collider designs because of its superior performance over the traditional final focus design. At the same time, we are receiving an increasing number of requests for a more detailed recipe for the optical design of such a system. A brief, spontaneously written recipe was discussed at the recent Nanobeam workshop [2]. A more detailed treatment is given here.

Some traditional FF systems have been designed using the FFADA (Final Focus Automatic Design and Analysis) program [3]. Although FFADA automates the generation of different solutions for the final telescope, the most tedious part of the design process, minimization of the third-order U3466 aberration (the notation of TRANSPORT [4] is used here and below) still required a trick - one needed to use FFADA to generate a system with certain demagnifications Mx and My, check U3466, change Mx and/or My, recheck U3466, and iterate until the aberration vanished.

This process can be expressed as a recipe: while preserving the desired linear and second-order properties of the system under consideration, scan possible solutions along particular degrees of freedom (Mx or My in this case), find the optimum, scan along other degrees of freedom, and continue iterating until a proper solution is found. Sometimes no satisfactory solution can be found, either because you are stuck in a local minimum or because the requested performance cannot be achieved. In these cases you must use your intuition to know when you need to go back and change something.

A similar approach can be used for designing a compact FF system. In this case, there are many more free parameters that can be changed, but the basic procedure is the same.

* Work supported in part by US DOE, Contract DE-AC03-76SF00515.

A TUNING RECIPE

The following steps were used to design a compact FF system, which will be presented in the next section. The procedure has been implemented as a semi-automatic design tool based on Matlab. As with any recipe, this one should be considered a guide more than a detailed map. It may be necessary to change the strategy or add more steps, depending on the situation (e.g. how far you are from a solution) or depending on the tools being used. The FF system presented in [1] was designed entirely using TRANSPORT. In the following, it is assumed that the basic matching is done with MAD [5]. The element names correspond to those shown in Figure 1. Only those steps of the design which involve variables ($knobs$) important for aberration tuning are highlighted.

0) Design the betatron and energy collimation systems.

1) Work backwards from the IP starting with design values for β^*, η'^*, and L^*. Choose reasonable lengths for the Final Doublet (FD) quadrupoles QD0 and QF1 and the separation between them. At a later stage the quadrupole lengths and their separation can be varied to trade synchrotron radiation in the FD against FD vibration tolerances. Make a linear match, varying the strengths of QD0 and QF1, to obtain certain values for α_x and α_y at the exit of QF1 (going away from the IP). These values will later be used to optimize 3rd order aberrations (such as U3246, U1226, etc.).

2) Make a linear match, varying the strength of QD2A, QF3, QD2B, QD4, QF5, QD6, and QF7, to obtain the following conditions: a) "pseudo -I" transform between SD0 and SD4 (all Rii=-1, R12=V_1, and R34=V_2); b) "pseudo +I" transform between SF1 and SF6 (all Rii=1, R12=V_3, and R34=V_4); c) horizontal and vertical waists ($\alpha_{x,y} = 0$) at the center of QF7. These V_i are knobs to be used for further aberration tuning (usually for geometric terms such as U1222, U3224, U3444, etc.).

3) Make a linear match, varying the bending angles of B1, B2, and B5, to obtain zero dispersion ($\eta = 0$ and $\eta' = 0$) at the end of the system, with a certain nonzero value of dispersion at SF5. This dispersion value becomes another tuning knob (affects geometric and chromo-geometric terms).

4) Make a linear match, varying the strengths of six beta-matching quadrupoles (labelled "QM" in Figure 1) to obtain a telescopic transformer (diagonal) matrix for the system with certain demagnifications Mx and My.

5) Reverse the system and start from the FF entrance. Make a second-order match, varying the strengths of all sextupoles, to zero the T126, T122, T166, T346, and T324 aberrations. At a later stage, when one is close to a solution, SF5 or SF6 can be excluded from the match and left for

later hand/automated tuning.

Further minimization of higher-order aberrations involves both computation of the higher-order transfer matrices for the system and manipulation of beam properties determined by tracking. Implementation will depend on the available tools. In our example, we use the complementary programs TRANSPORT and TURTLE [6] to minimize higher-order aberrations. TRANSPORT calculates matrices up to third-order, while TURTLE is a six-dimensional particle tracking code. Note that it is important to do the tracking and higher-order matrix calculation with codes that are consistent with one another. Using DIMAD [7] for the tracking is also a good choice.

6) Convert the matched optics from MAD to a TRANSPORT/TURTLE deck (using a conversion program developed at SLAC). For convenience of further evaluation of aberrations, calculate the inverse of the total first-order matrix of the FF system and insert this matrix at the beginning of the beamline, so that the overall first-order matrix becomes the identity matrix.

7) Run TRANSPORT to calculate the second- and third-order matrices, as well as the beam matrix with energy offset $+\Delta$ and $-\Delta$. The higher-order chromatic aberrations can be determined from the off-energy matrices.

8) Using the same TRANSPORT beamline, track the beam to the IP using TURTLE. Either the aberrations or the tracked beam sizes could be used as criteria for automatic minimization. In addition the bandwidth of the system, or the variation of the tracked IP beam sizes with energy, is an important quantity to optimize.

Remember this state, then return to the beginning and change the value of some knob. In essence you are computing numerical derivatives of the important aberrations and beam properties with respect to each knob and with respect to energy. Do this for all the knobs. Some knobs affect several aberrations, but differently, eventually allowing all of the major aberrations to be minimized (if in principle a solution exists for the requested parameters). In general all lengths, especially the lengths of the bends B1 and B2 and the drifts surrounding them, are additional knobs (in particular for U3466). Select the best set of knob values, keeping in mind that iteration of this process will be required due to the nonlinearity of the response of the aberrations to knob changes.

Repeat until an acceptable solution is found. Use knobs appropriate to the situation. Most of the steps in this procedure can be performed automatically. For example, Matlab-based scripts are used in our example to generate the TRANSPORT/TURTLE files, run these programs, read, analyze, and present the results, and then to search for an optimal solution using Matlab's optimization routines.

When a solution is close to optimum, and most of aberrations are small, use octupoles OC10 and OC1 near QD10 and the FD, respectively, for fine tuning of U3246 and U3244.

Typically the third-order aberrations can be made small and the bandwidth of the system is limited by fourth order terms, in particular V32246 (observed in the way that U3224 changes with energy). Use decapoles DEC6 and DEC4 (see Figure 1) with equal strengths to cancel this aberration. For better cancellation of V32446, use a sum of aberrations as a minimization criterion, constraining U3244$_{+\Delta E}$ and U3244$_{-\Delta E}$ to be asymmetric (as in Figure 4). In our case, since TRANSPORT and TURTLE do not handle decapoles, it was necessary to use DIMAD tracking to optimize the strength of these elements.

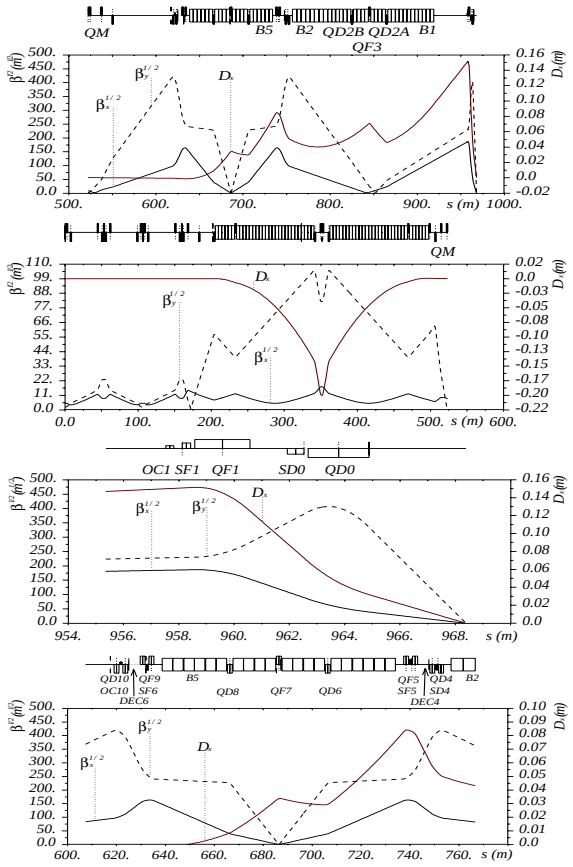

Figure 1: Preliminary optics for the NLC low energy BDS, $L^* = 3.51$ m, $\eta'^* = 0.009$. Final focus proper, collimation section, final doublet region, aberration correction region.

The authors wish to note here that we do not know of a single optics code that can do all that we need, e.g. TURTLE/TRANSPORT do not handle decapoles or synchrotron radiation, while MAD does not calculate or allow matching of higher-order aberrations. Clearly, there is a need for a more complete beam optics design code.

BDS FOR THE SECOND IR OF NLC

The methods and tools described above have been used to design a Beam Delivery System (BDS) for a second, low energy, Interaction Region (IR) for NLC. This BDS must be somewhat shorter than the primary, high energy, IR BDS (which is 1.4 km long), to allow space for the transport lines that provide the necessary separation between the two IRs (see [8] for more discussion of this configuration). The optics for this preliminary design are shown in Fig-

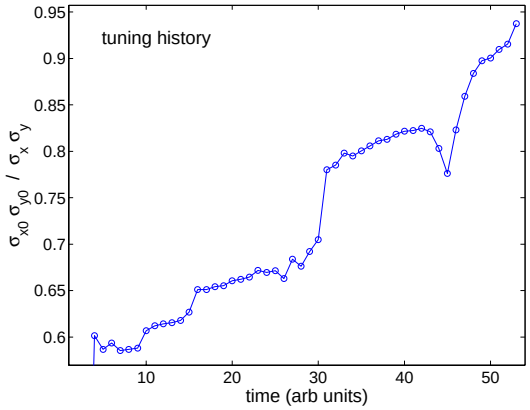

Figure 2: Tuning history for the low energy NLC BDS design. σ_{x0} and σ_{y0} are the nominal linear IP spot sizes.

ure 1. The nominal input beam parameters are: energy E = 250 GeV/beam, emittances $\gamma\varepsilon_{x,y} = (3.6, 0.04)\ 10^{-6}$m, energy spread $\sigma_E = 0.25\%$, bunch length $\sigma_z = 0.11$ mm. At the IP $\beta^*_{x,y} = (8, 0.11)$ mm and $\sigma^*_{x,y} = (243, 3)$ nm.

The optics shown is optimized for 250 GeV/beam. For the 500 GeV/beam case (and for 650 GeV/beam, available with reduced beam current), the final doublet will be replaced with a longer version in order to reduce synchrotron radiation in the FD ("long doublet" version), and the angle of the B1, B2, and B5 bends will be reduced by approximately a factor of two (with simultaneous adjustment of the bends in the energy collimation section to keep the IP location fixed) to reduce synchrotron radiation in the bends.

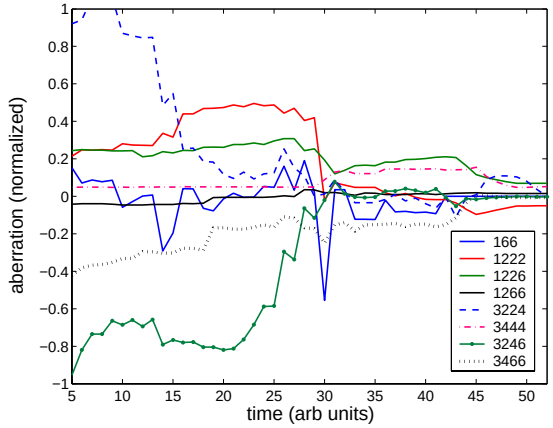

Figure 3: Predominant second and third order aberrations during tuning (normalized to the nominal beam sizes).

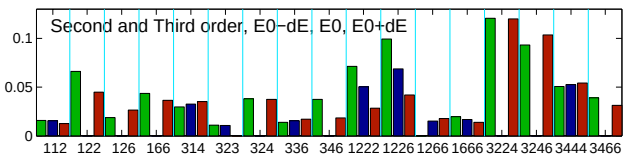

Figure 4: Predominant second and third order aberrations (for the on-energy beam and for $+\Delta E$ and $-\Delta E$) at the final stage of tuning (absolute values, normalized to the nominal beam sizes). Note the symmetry of U3244$_{+\Delta E}$ and U3244$_{-\Delta E}$ terms.

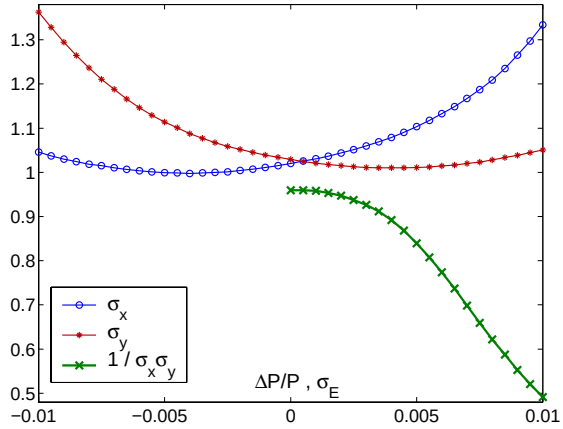

Figure 5: DIMAD tracking results for the final system. Luminosity equivalent IP beam sizes versus energy offset, and $1/\sigma_x\sigma_y$ (normalized) versus energy spread. Hour-glass, beam-beam effects, and synchrotron radiation are not included.

Figures 2 and 3 show the history of the tuning process. The quantity plotted in Figure 2 is equivalent to fractional luminosity. Note that not all intermediate steps are shown. Both hand tuning and automatic optimization with Matlab were used during this process.

Figure 4 shows the predominant second- and third-order aberrations remaining after tuning (absolute values, normalized to the nominal IP beam parameters) for both the on-energy beam and for beams with $\pm 0.2\%$ energy offset. Observation of these aberrations can aid in the creation of additional tuning knobs. Matrix elements for the off-energy beams and their asymmetry give information about fourth- and fifth-order chromatic aberrations. Figure 5 shows the resulting bandwidth of the system, obtained by tracking.

Finally, we note that in spite of the seeming tediousness of this approach to FF design, this method is almost directly applicable for tuning a real final focus during commissioning and operation.

CONCLUSION

A recipe for the optical design of a compact final focus system is presented and illustrated with an example of a preliminary design for the low energy NLC beam delivery system.

REFERENCES

[1] P. Raimondi and A. Seryi, Phys. Rev. Lett. **86**, 3779 (2001).
[2] A. Seryi, SLAC-PUB-9648, 2003.
[3] O. Napoly, B. Dunham, CEA-DAPNIA-SEA-94-12.
[4] D. Carey, K. Brown, F. Rothacker, SLAC-R-530, 1998.
[5] H. Grote, F. C. Iselin, Nucl. Instr. Meth. A **293**, 464 (1990).
[6] D. Carey, K. Brown, F. C. Iselin, SLAC-R-544, 1999.
[7] R. Servranckx, et al., SLAC-0285, 1990.
[8] T. Markiewicz, et al., in these proceedings.

DEVELOPMENTS IN LINEAR AND NON-LINEAR DAΦNE LATTICE

C. Milardi, G. Benedetti, M. E. Biagini, C. Biscari, M. Boscolo, S. Guiducci, M. Preger,
P. Raimondi, C. Vaccarezza, M. Zobov, INFN-LNF, Frascati, Italy

Abstract

The agreement between the DAΦNE model and the measured machine parameters (betas, dispersion etc) has further improved in the 2002 runs. A better dispersion function control has been obtained by modifying the closed orbit correction algorithm, which now includes corrector strength minimization.

The model has been integrated in the accelerator control system, providing a faster and reliable tool for fine and on-line machine optics tuning.

New measurements, such as the machine second order dispersion, have proved to be very effective in studying the second order terms in the rings.

Measurements of second order chromaticity and tune shift on amplitude have extended our knowledge about the lattice up to the third order.

INTRODUCTION

DAΦNE [1], the Frascati electron-positron collider working at the energy of the Φ resonance, has run in year 2002 mainly for providing luminosity to the physics experiments. Nevertheless, 10% of its uptime has been used for machine optics studies aimed at improving the machine model understanding as well as the machine performances.

DAΦNE has two Interaction Regions (IRs), each housing an experiment: KLOE studies CP violation in kaon decays and DEAR investigates exotic atoms. The two experiments cannot run at the same time and have different collision optics, due to the strong differences in their IRs magnetic structures and in their experimental setups.

LINEAR MODEL

As a matter of fact, the model of an operating accelerator evolves continuously. At DAΦNE during the past year the lattice model experienced a remarkable evolution due to a deeper understanding of the machine behaviour.

The model is based on the MAD design program [2]. The machine element description has been completely reorganized in order to make file sharing and evolution easier. The agreement between measured and simulated Twiss parameters (betas, dispersion, tunes) has been improved. The same model describes now, using the same set of model parameters, the two collider rings. These parameters have been moved back to their nominal values, with the exception of those few, describing situations really different from the nominal one. It's worth recalling that DAΦNE is a very compact machine (97.98 m long), with no periodicity at all, running with the KLOE strong detector solenoid always on ($\int Bds$ = 2.4 Tm, to be compared with a magnetic rigidity $B\rho$ = 1.7 Tm). As a consequence the model parameters are far from being independent.

The description of the machine quadrupoles has been improved and their focusing strength related directly to the magnet power supply readout. The same has been done for the splitter magnets.

Procedures have been written, using the MAD formalism, to easily change scalar quantities such as tunes, momentum compaction and energy at constant optical functions. The same has been done for optical variables such as betatron functions, horizontal and vertical dispersion and phase advances. Special care has been dedicated to the beta functions at the IPs to investigate their impact on luminosity and beam-beam behaviour and at the position of sextupoles to optimize their efficiency and therefore the dynamic aperture. All these procedures can start from any operating point of the ring, calculate the required variations, returning the results in terms of current changes to be set on the magnetic elements specified.

The upgraded model has been ported on the Control System [3] and almost completely integrated in the Control System Software. A first version of model interface has been developed allowing comparison among different simulated optics and between simulated and measured optical functions, see Fig. 1.

The on-line model has demonstrated to be a flexible tool not only in computing, but also in exploring efficiently different machine configurations, even during experiment data taking.

DEAR Optics

ONE of the most relevant modifications to the DAΦNE optics concerns the DEAR IR [4].

The original design of the DEAR IR is based on quadrupole triplets (FDF) placed at both sides of the Interaction Point (IP) and providing a low vertical beta. In this configuration at the end of 2001, the optical functions at the IP were β^*_x = 4.4 m and β^*_y = .04 m.

By switching off the inner focusing quadrupole and by retuning the other two (FD), it has been possible to reach β^*_x = 1.7 m and β^*_y = .038 m (see Fig. 1) thus reducing the DEAR IR contribution to the chromaticity. The optics of the two rings has been kept almost unchanged outside the DEAR IR, avoiding a time consuming optimization due to different phase advances between sextupoles, between injection kickers and different beta values at the feedback pick-ups.

Last but not least, the new configuration has provided 50% reduction of β_x at the first parasitic crossing (occurring .405 m from the IP), making collisions with

100 bunches out of 120 buckets possible [5] (20 empty buckets are necessary to neutralize ion trapping effects).

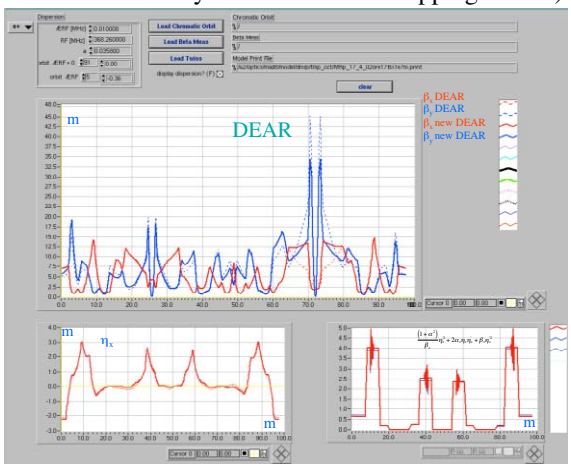

Figure 1: DEAR optics evolution presented by the Control System model interface.

Before such modifications DAΦNE was operated with interleaved bunches (one full and one empty bucket), with a maximum number of 50 bunches in collision. Further modifications in the DEAR IR optics have included an increase of the crossing angle, (from 25 to 29 mrad), and 10% reduction in the beam horizontal emittance.

In a four months run the collider has provided an integrated luminosity $L_{\int 2002}$ = 68 pb^{-1}(to be compared with $L_{\int 2001}$ = 3 pb^{-1}), enough for the DEAR experiment to go through its preliminary phase with the observation of kaonic Nitrogen, and to to make the first experimental test of the hydrogen target.

KLOE Optics

The extension of the β^*_x reduction adopted for the DEAR optics to the KLOE one has not been straightforward since low-β at the KLOE IP is realized with a couple of permanent quadrupole triplets embedded in the field of the experimental solenoid, whose field is compensated by two superconducting solenoids, one at each side of the IP. In this context it is not possible to locally modify the IR optics.

The KLOE horizontal beta has been modified by changing the currents of the quadrupoles closest to the IR, going, in successive steps, from β^*_x = 5.7 m to β^*_x = 2.7 m, the minimum compatible with the β_x limitation imposed, at the splitter magnets by stay-clear requirements. β^*_y has been only slightly changed, from .03 to .026 m, the minimum value compatible with the hour-glass effect. The horizontal emittance has been reduced by 10% in both rings also for the KLOE optics.

The reduction in β^*_x has been remarkable (~ 50%), but not enough to avoide parasitic crossing, in fact during 100 bunches operations problems such as bunch pattern degradation, beam blow-up and peak luminosity limitation have been still observed. Nevertheless the modified KLOE optics has given a relevant contribution to the luminosity improvement summarized in Table 1. The peak luminosity has reached L_{peak} = .8·10^{32} cm^{-2}s^{-1}, the best integrated luminosity over a day $L_{\int day}$ = 4.8 pb^{-1} and the luminosity lifetime τ_L = .6 hours.

Table 1: DAΦNE luminosity

	2001	**2002**
KLOE L_{peak} cm^{-2} s^{-1}	.5·10^{32}	.8·10^{32} n_b=49
KLOE $L_{\int day}$ pb^{-1}	3.2	4.8 n_b=49
DEAR L_{peak} cm^{-2} s^{-1}	.1·10^{32}	.7·10^{32} n_b=100
DEAR $L_{\int day}$ pb^{-1}	.24	2.2 n_b=100

CLOSED ORBIT CORRECTION

The closed orbit correction application has been upgraded and now includes explicitly a steering strength minimization procedure [6]. The steering strength minimization is beneficial in avoiding stray dispersion bumps as well as local orbit deviations due to the presence of couples of strong nearby perturbations; at DAΦNE it has proved to be powerful in minimizing parasitic dispersion and as well as in limiting the background rate seen from the experimental detectors.

NON LINEAR MODEL

Non-linearities at DAΦNE have been observed and studied from the beginning of machine operation; they essentially come from higher order components in the field of the wigglers [7]. Their negative influence affects machine dynamic aperture and beam lifetime and therefore the integrated luminosity. Moreover, non-linearities influence beam-beam behaviour inducing beam blow-up, thus reducing the achievable peak luminosity.

In 2002 three ocupole magnets have been installed in each ring in order to provide non-linearities tuning [8].

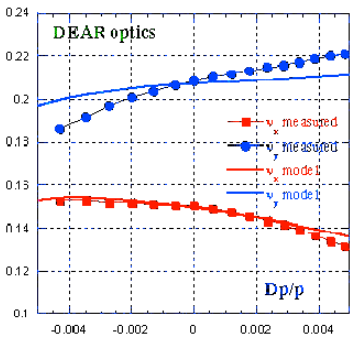

Figure 2: Tune shift versus energy for the DEAR optics.

The non-linear model has been upgraded to include the new elements and sextupole terms detected during the wiggler magnetic measurements have been included in the wiggler model.

The agreement between measured and computed chromaticity has been improved both at the first and second order, as shown in Fig. 2 for the DEAR optics and in Fig. 3 for the KLOE one. Still there is some discrepancy in the vertical plane, but it is small when

compared to the machine chromaticity without sextupoles. The tune shift on amplitude predicted from the model is very close to the measured one [9], see Table 2.

Table 2: Strength of the cubic non-linearity

	$C_{11}^{measured}$ m^{-1}	C_{11}^{model} m^{-1}
Sextupole on	-175.	-187.5
Sextupole off	-73.11	-98.5

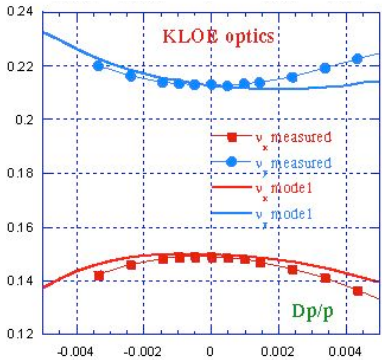

Figure 3: Tune shift versus energy for the KLOE optics

The second order dispersion η_{1x} has been measured as orbit shift versus energy and it is quite similar, for the KLOE optics (see Fig. 4), to the one predicted by the model.

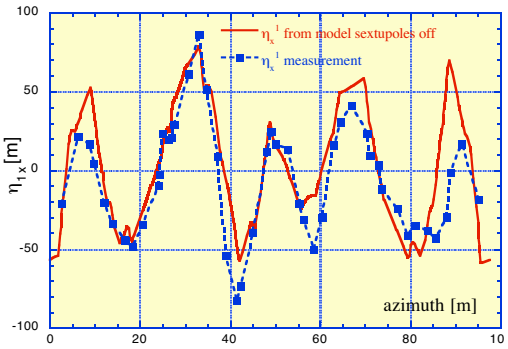

Figure 4: η_{1x} (sextupole off).

Even the computed sextupole contribution to η_x^1 agrees with the measured one (Fig. 5) confirming once more that the betatron functions predicted by the model at the sextupoles are the same as the real ones in the machine.

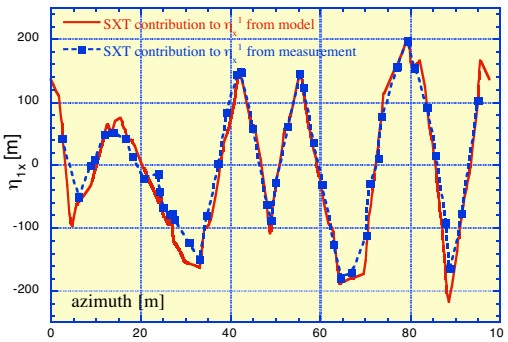

Figure 5:Sextupole contribution to η_{1x}.

Collider operation has shown that the reduction of η_{1x} is beneficial for dynamical aperture and beam-beam behaviour, since the best luminosity results have been obtained after cancelling, almost completely η_{1x} in the KLOE IR (IP at 25.72 m), see Fig. 6.

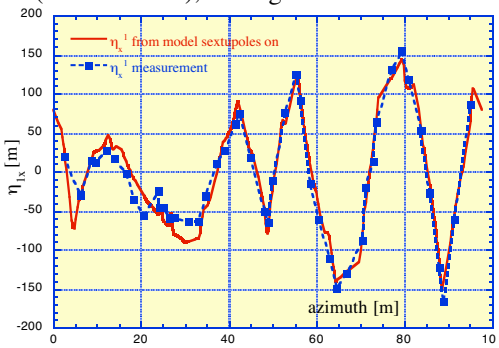

Figure 6: η_{1x} (sextupole on).

CONCLUSIONS

The linear and non-linear model has been extensively used to optimize DAΦNE optics, contributing to a gain of 60% in the peak luminosity and 50% in the daily integrated luminosity, with respect to the year 2001.

The improvements obtained in decreasing β^*_x at DEAR have suggested a new design in which the two IRs are rebuilt substituting quadrupole triplets with doublet ones. With this new configuration it will be possible to reach β^*_x as low as 1.5 m and collide with 100 bunches at both IPs, which could allow, assuming a current per bunch I_b = 20 mA, a total current per beam I_t = 2 A.

In this context it seems quite reasonable to expect further luminosity increases.

REFERENCES

[1] G. Vignola and DAΦNE Project Team, “DAΦNE the Frascati Φ Factory”, PAC 93, Washington, May 1993.

[2] H. Grote and F. C. Iselin “The MAD program”.

[3] G. Di Pirro et al., “DANTE Control System for DAΦNE based on Macintosh and LabView”, PCaPAC 2002, Frascati, Italy.

[4] C. Biscari et al., “Half β^*_x at DEAR”, DAΦNE Technical Note, BM-9, April 2002.

[5] A. Drago et al. “100 Bunches Operations at DAΦNE”, this conference.

[6] P. Raimondi et al., “Emittance Optimization with Dispersion Free Steering at LEP”, CERN-SL-2000-YY OP, DAΦNE May 2000.

[7] C. Milardi, “ Effects of non-linear terms in the wiggler magnets at DAΦNE”, PAC 01, Chicago, June 2001.

[8] C. Vaccarezza et al., “Preliminary results on DAΦNE operation with octupoles”, EPAC 02, Paris, June ‘01.

[9] A. Drago et al., “The dynamic tracking acquisition system for e^+ e^- collider”, DIPAC 01, Grenoble, France.

AN OVER-DAMPED CAVITY LONGITUDINAL KICKER FOR THE PEP-II LER*

P. McIntosh, R. Akre, D. Anderson, S. DeBarger, M. Dormiani, J. Fox, K. Jobe, H. Schwarz, D. Teytelman, U. Wienands, A. Young, SLAC, Stanford, CA 94025, USA. F. Marcellini, INFN-Frascati, Italy. M. Tobiyama, KEK, Japan

Abstract

Both rings of PEP-II use drift tube kickers in the longitudinal bunch-by-bunch feedback system. Efforts are now underway to increase the stored beam currents and luminosity of PEP-II, and beam-induced heating of these structures, particularly in the Low Energy Ring (LER) is of concern. An alternative kicker design based on the over-damped cavity kicker, first developed by INFN-Frascati is being built for PEP-II. This low loaded Q (or wide bandwidth) structure is fed by a network of ridged waveguides coupled to a simple pill-box cavity. Beam induced RF power is also coupled out of the cavity to external loads, so that the higher order modes (HOMs) excited in the structure are well-damped. This paper details the kicker design for PEP-II and discusses some of the design trade-offs between shunt impedance and bandwidth, as well as the influence of the feedthroughs on the kicker parameters. Estimates of the expected power deposition in the cavity are also provided.

INTRODUCTION

The longitudinal bunch-by-bunch feedback systems at PEP-II use wide-band drift-tube kickers [1] that have performed very well at beam currents up to 1.9 A and 6.3 ns bunch spacing and roughly 1000 bunches in the LER. However, with plans to substantially increase the beam currents, with bunch currents much higher than originally anticipated, the thermal stresses in these kickers will become quite high. The drift tube kickers are difficult to cool since the drift-tubes are supported only by rather thin electrodes. In order to prevent these kickers from becoming a beam current limit we are building new feedback kickers based on the successful design of an over-damped cavity developed at INFN-Frascati [2] and used elsewhere [3][4] to replace the existing feedback kickers in the LER. The new structure is easily cooled from the outside and expected to more than double the current capability of the LER kickers.

THE NEW LFB CAVITY KICKER DESIGN

The bandwidth requirement for the new kicker derives from the spectrum of modes in the beam. At PEP-II, every 2nd RF bucket can be filled, the bandwidth required to perform efficient damping is then equal to $f_{RF}/4$, or 119 MHz. A bandwidth of ~ $f_{RF}/2$ or 238 MHz has been chosen to provide more linearity over its operating band. The cavity fundamental TM_{010} mode therefore has to be very broadband with a low loaded Q, which is contrary to traditional RF cavity design requirements. A simple pill-box cavity is employed, strongly coupled to which are four large waveguides (see Figure 1) which are terminated externally to 50 Ω, reducing the Q to give a $Q_L \sim 5$.

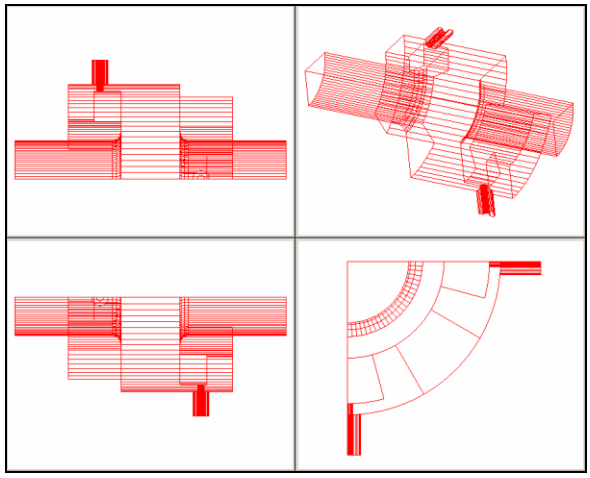

Figure 1 HFSS Longitudinal Feedback Kicker Geometry

The frequency chosen for the new kicker is 9/4 f_{RF} or 1.071 GHz as this gives the highest shunt impedance solution of the options available (13/4 and 9/4 f_{RF}) [5]. The existing longitudinal feedback system also operates at 1.071 GHz and has enough power to drive the new kickers, so infrastructure modifications are minimal. The HOM spectrum of the kicker is shown in Table 1 and the fundamental mode shunt impedance is ~ 1.5 times as much as the drift-tube kicker so that some voltage kick increase is expected from the same amplifier power. The TM_{01} mode cut-off frequency of the 89 mm beam pipe is 2.6 GHz and modes above that are highly damped as confirmed by MAFIA simulations.

Table 1 Kicker Fundamental and HOM Characteristics

Mode	Freq (GHz)	Q_L	BW (MHz)	R_s (Ω)
TM_{010}	1.071	4.8	224	626
TM_{110}	1.5151	22	69	16.7 k
TE_{111}	1.7114	210	8	19.2 k
TM_{011}	2.0507	13	157	65
TM_{020}	2.4117	116	21	76

The new kicker cavity has been developed using the Ansoft finite element, electro-magnetic solver – HFSS [6]. A bandwidth response of 224 MHz, centered at 1.071 GHz (see Figure 2), has been achieved by optimization of the waveguide profile and coupling transitions.

* Work supported by Department of Energy contract DE--AC03--76SF00515

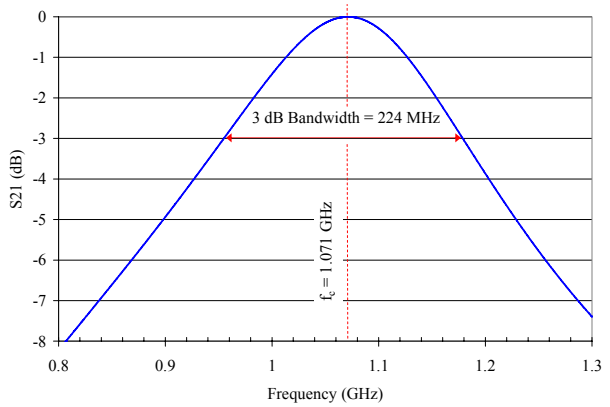

Figure 2 Transmission Frequency Response of Kicker

The kicker structure (see Figure 3) is being fabricated from OFHC copper for efficient cooling and to avoid multipactor problems that can arise in aluminium structures without Titanium Nitride coating.

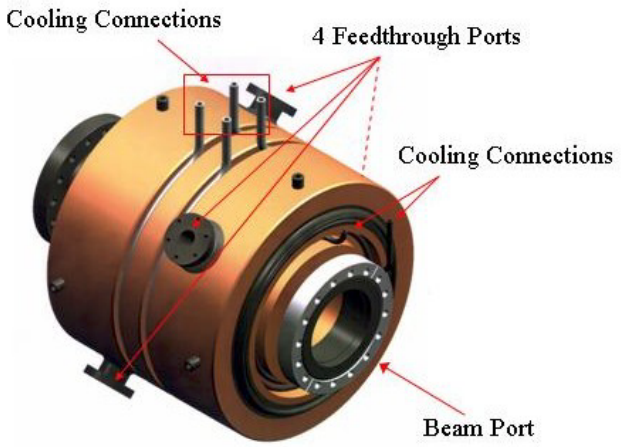

Figure 3 New Kicker Mechanical Assembly

KICKER BEAM INDUCED POWER

Both the existing drift-tube and cavity kickers present impedances that absorb power from the circulating beam. The center frequencies of both designs are selected to minimize the impedance at multiples of the RF frequency for which there are very strong harmonic content in the circulating current. However, due to gaps in the filling patterns and unequal charges in the stored buckets, there is significant power deposited by the beam in both structures. As seen in figures 4 and 5, the 3A nominal fill in the LER would deposit roughly 14 kW in the cavity kicker and 12 kW in the drift-tube kicker.

One important difference between the structures is seen in the periodic impedance of the drift tube, which absorbs power from the beam at high frequencies as well as in the operating band. The drift-tube structure has a finite directivity in the 1 - 2 GHz band, so that the bulk of the power in this band is coupled out of only two load ports. Therefore the power to the drift tube load ports is higher, by almost a factor of 2, than in each of the 4 symmetric ports on the cavity kicker.

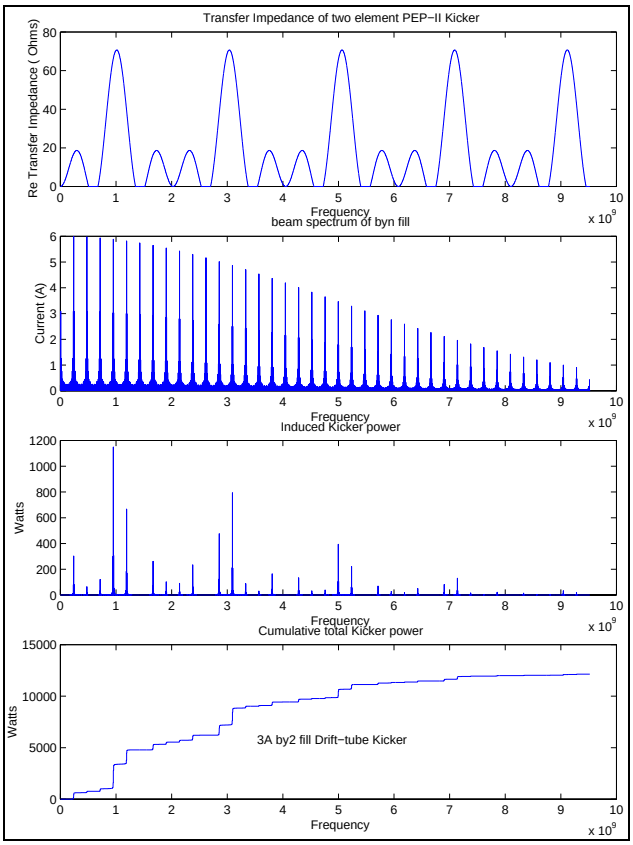

Figure 4 Beam Induced Power for Existing Drift-tube Kicker

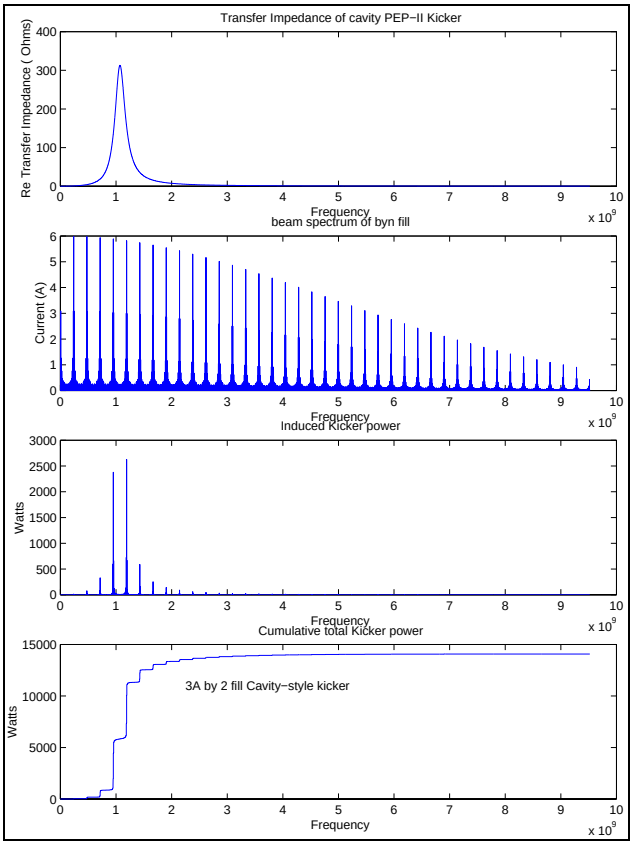

Figure 5 Beam Induced Power for New Cavity Kicker

On the other hand, the cavity kicker requires the installation of high power circulators between power amplifier and kicker. The most important advantage of the cavity kicker is thermal management, as it has no internal structure, and the cavity itself can be water-cooled on surfaces outside the vacuum chamber.

A NEW RF FEEDTHROUGH

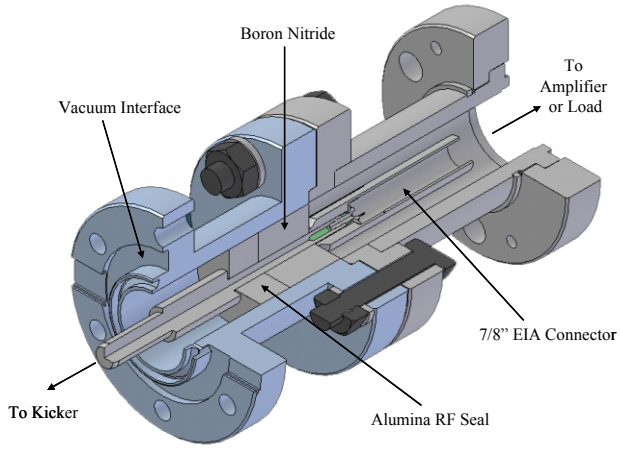

Figure 6 The New High Power RF Feedthrough Design

Each feedthrough has to be able to handle at least ¼ of the total beam induced power (plus ~¼ of the amplifier power). To have some safety margin in the power handling capability and allow beam current increases to 4.5 A in the future, a new high power RF feedthrough has been developed at SLAC. The design may also be an attractive solution for other high power feedthrough applications. The feedthrough is being built by industry (see Figure 6) and is specified to handle 10 kW at 1 GHz, although we expect some leakage of frequencies up to 8 GHz due to excitation of HOMs.

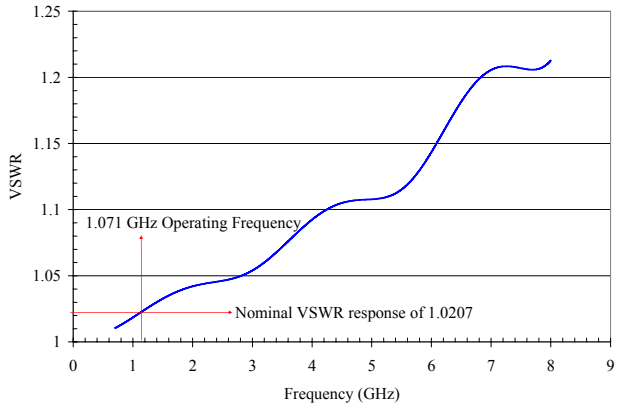

Figure 7 HFSS RF Feedthrough Frequency Response

HFSS has again been utilized to optimize the feedthrough to have a good VSWR response over a wide bandwidth, extending up to 8 GHz (see Figure 7). The new feedthrough comprises a 7/8" EIA interface and incorporates an alumina ceramic vacuum seal; it also has a boron nitride ceramic which is used to dissipate some of the thermal energy generated in the inner coax. There are optimized impedance transformations at either side of the ceramics which control the VSWR response up to this high frequency. The output coax then has a smooth 50 Ω impedance transition to the cavity kicker.

Attaching the feedthroughs to the cavity kicker has the effect of perturbing the fundamental mode bandwidth. The magnitude of the perturbation is intrinsically related to the mismatch the feedthrough presents. Experience at both DAΦNE and KEK, who also use this type of cavity kicker and feedthrough configuration, albeit with different operating characteristics, has shown that the operational bandwidth perturbation can be as much as 20% [7][8]. With this in mind, by having a low VSWR at its fundamental operating frequency, HFSS simulations predict that when attached to the new kicker, the induced perturbation from this new feedthrough is only ~5% (see Table 2).

Table 2 TM_{010} Mode Perturbation Due to Feedthroughs

TM_{010}	Freq (GHz)	Q_L	BW (MHz)	R_s (Ω)
w/o f/thru	1.071	4.8	224	626
with f/thru	1.071	4.6	235	620

CONCLUSIONS

This collaboration has developed a new 4-port longitudinal feedback kicker which should not limit the LER operation on PEP-II up to 4.5 A. The increased shunt impedance of the structure enables a larger voltage kick to be applied to the bunch than with the present drift-tube kicker, for the same amplifier power. Operation of the LER at 4.5 A will generate more beam-induced power which is extracted from the structure through the RF feedthroughs. A new high-power feedthrough design will be able to fulfill this requirement. Two kicker cavities are currently being manufactured at SLAC and the associated feedthroughs manufactured by industry, for installation on the PEP-II LER this summer.

REFERENCES

[1] J. N. Corlett et al, "Longitudinal and Transverse Feedback Kickers for the ALS", Proc. EPAC'94, London, June 1994.
[2] R. Boni et al, "A waveguide Overloaded Cavity as a Longitudinal Kicker for the DAΦNE Bunch-by-Bunch Feedack System", Particle Accelerators, 1996, Vol. 52, pp 95 – 113.
[3] M. Tobiyama et al, "Bunch-by-Bunch Feedback System for KEKB Rings", Proc. APAC'98, Tsukuba, March 1998, pp 540 – 542.
[4] T. Knuth et al, "Longitudinal and Transverse Feedback Kickers for the BESSY II Storage Ring", Proc. PAC'99, New York, March 1999, pp 1147 - 1149
[5] F. Marcellini et al, "Study and Design of a New Over-Damped Cavity Kicker for the PEP-II Longitudinal Feedback System", BIW'02, Brookhaven, May 2002.
[6] HFSS is licensed to Ansoft Corporation, Pittsburgh, USA.
[7] Private communication M. Tobiyama, KEK.
[8] Private communication F. Marcellini, INFN Frascati.

THE SPARC PROJECT: A HIGH BRIGHTNESS ELECTRON BEAM SOURCE AT LNF TO DRIVE A SASE-FEL EXPERIMENT

D.Alesini, S.Bertolucci, M.E.Biagini, C.Biscari, R.Boni, M.Boscolo, M.Castellano, A.Clozza, G.Di Pirro, A.Drago, A.Esposito, M.Ferrario, V.Fusco, A.Gallo, A.Ghigo, S.Guiducci, M.Incurvati, C.Ligi, F.Marcellini, M.Migliorati, C.Milardi, L.Palumbo, L.Pellegrino, M.Preger, P.Raimondi, R.Ricci, C.Sanelli, M.Serio, F.Sgamma, B.Spataro, A.Stecchi, A.Stella, F.Tazzioli, C.Vaccarezza, M.Vescovi, C.Vicario, M.Zobov, *INFN-Frascati*

F.Alessandria, A.Bacci, I.Boscolo, F.Broggi, S.Cialdi, C.DeMartinis, D.Giove, C.Maroli, V.Petrillo, M.Romè, L.Serafini, *INFN-Milano*

D.Levi, M.Mattioli, G.Medici, *INFN-Roma1*

L.Catani, E.Chiadroni, S.Tazzari, *INFN-Roma2*

R.Bartolini, F.Ciocci, G.Dattoli, A.Doria, F.Flora, G.P.Gallerano, L.Giannessi, E.Giovenale, G.Messina, L.Mezi, P.L.Ottaviani, L.Picardi, M.Quattromini, A.Renieri, C.Ronsivalle, *ENEA-Frascati*

A.Cianchi, A.D'Angelo, R.Di Salvo, A.Fantini, D.Moricciani, C.Schaerf, *Universita' Roma Tor Vergata*

J.B. Rosenzweig, *UCLA - Dept. of Physics and Astronomy*

Abstract

The Project SPARC (Sorgente Pulsata e Amplificata di Radiazione Coerente), proposed by a collaboration among ENEA-INFN-CNR-Universita` di Roma Tor Vergata-INFM-ST, was recently funded by the Italian Government. The aim of the project is to promote an R&D activity oriented to the development of a coherent ultra-brilliant X-ray source in Italy (SPARX proposal [1]). The SPARC collaboration identified a program based on two main issues: the generation of ultra-high peak brightness electron beams and experimental study of SASE-FEL process with generation of resonant higher harmonics. The SPARC project is being designed in order to encompass the construction of an advanced photo-injector producing a 150-200 MeV beam to drive a SASE-FEL in the optical range. The machine will be built at LNF, inside an underground bunker: it is comprised of an rf gun driven by a Ti:Sa laser, injecting into three SLAC accelerating sections. We foresee conducting investigations on the emittance correction[2] and on the rf compression techniques[3], which are expected to increase the peak current achievable at the injector exit up to kA level, with proper preservation of the transverse emittance. Although the system is expected to drive a FEL experiment, it can be used also to investigate beam physics issues like surface-roughness-induced wake fields, bunch-length measurements in the sub-ps range, emittance degradation in magnetic compressors due to CSR, and Compton backscattering production of sub-ps X-ray pulses.

PROJECT OVERVIEW

The overall SPARC Project consists of 4 main lines of activity:

1) *150 MeV Advanced Photo-Injector*: the performances of X-ray SASE-FEL's are critically dependent on the peak brightness of the electron beam delivered at the undulator entrance. Two main issues to investigate: generation of the electron beam and compression via magnetic and/or velocity bunching.
2) *SASE-FEL Visible-VUV Experiment*: this is aimed to investigate the problems related to the beam matching into an undulator and the alignment with the radiation beam, as well as the generation of non-linear coherent higher harmonics. The SASE FEL experiment will be performed with the 150 MeV beam, using a segmented undulator with additional strong focusing to observe FEL radiation at 500 nm and below.
3) *X-ray Optics/Monochromators*: the X-ray FEL radiation will provide unique radiation beams in terms of peak brightness and pulse time duration (100 fs). This project will pursue a vigorous R&D activity on the analysis of radiation-matter interactions in the spectral range of SASE X-ray FEL's (from 0.1 to 10 nm), and on the design of new optics and monochromators.
4) *Soft X-ray table-top Source:* to test these optics and start the R&D on applications the project will undertake the upgrade of the presently operated table-top source of X-rays at INFM - Politecnico Milano, delivering 10^7 soft X-ray photons in 10-20 fs pulses by means of high harmonic generation in a gas.

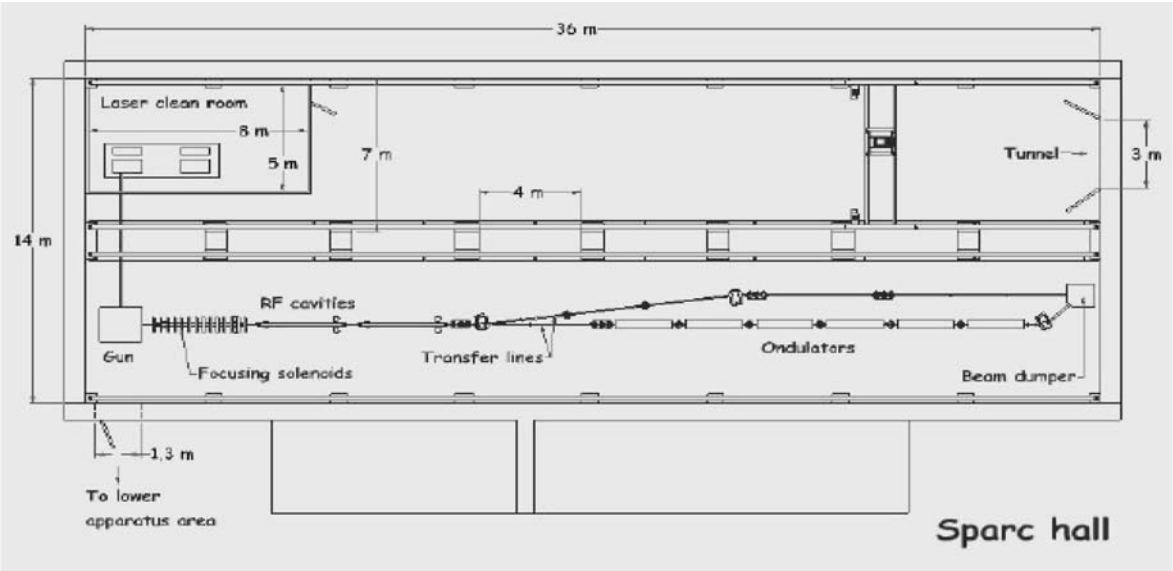

Figure 1 : Lay-out of SPARC Advanced Photo-Injector and SASE-FEL Experiment

In the following we present an overview of the design for the system under construction at the Frascati National Laboratories of INFN, by a collaboration between two national research institutions, INFN and ENEA namely, aiming at reaching the scientific and technological goals indicated in the first two topics listed above, *i.e.* the production of a high brightness electron beam and the operation at saturation of a SASE-FEL experiment driven by such an electron beam.

ADVANCED PHOTO-INJECTOR

The main goals of this activity are the acquisition of expertise in the construction, commissioning and characterization of an advanced photo-injector system and the experimental investigation of two new ideas that have been recently conceived and presented by the study group: the optimum working point for high brightness RF photo-injectors and RF bunch compression technique.

The 150 MeV injector will be built inside an available bunker of the Frascati INFN National Laboratories: the general layout of the system is shown in Fig. 1. The system consists of a 1.6 cell RF gun operated at S-band (2.856 GHz, of the BNL/UCLA/SLAC type) and high peak field on the cathode (120 MeV/m) with incorporated metallic photo-cathode (Cu or Mg), generating a 6 MeV beam[4]. The beam is then focused and matched into 3 accelerating sections of the SLAC type (S-band TW) which accelerates the bunch up to 150-200 MeV. For the Laser system it is planned to use the third harmonic of the radiation from a Ti:Sa laser with the oscillator pulse train locked to the RF . To obtain the time pulse shape we are going to test the manipulation of frequency lines in the large bandwidth of Ti:Sa, in order to produce the 10 ps flat top shape. We can use a liquid crystal mask in the Fourier plane for nondispersive optic arrangement or a collinear acusto-optic modulator for line frequency manipulation. The goal of these tests is to obtain a pulse rise time shorter than 1 ps with intensity ripples along the 10 ps pulse smaller than 30% (peak to peak): under such a condition the beam emittance achievable at the end of the photo-injector is foreseen to be smaller than 1 μm.

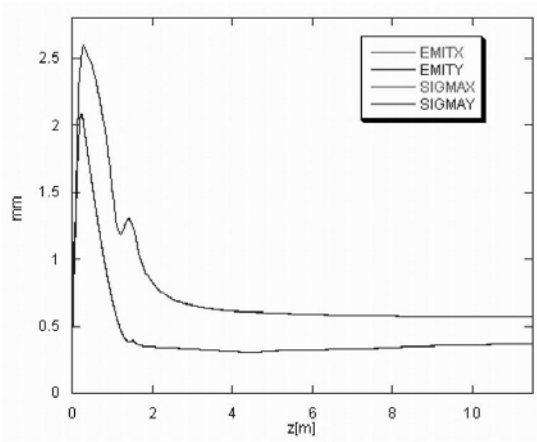

Figure 2: Parmela simulation of emittance and envelope evolution along the SPARC photo-injector (only two accelerating sections taken into account)

The first experiment is planned to verify the beam emittance compensation process. The key point is the measurement, at different bunch charges, of the emittance oscillation in the drift after the gun where a double minima behavior is expected. The optimum beam matching to the booster is predicted on the relative maximum, see Fig. 2. A dedicated movable emittance measurement station has been designed, as shown in Fig. 3. Our simulations using PARMELA indicate that we can generate in this way a beam as required by the FEL experiment at 150 MeV. The rms correlated energy

spread is 0.2% with a rms norm. emittance lower than 2 μm (at 1 nC bunch charge, 85 peak current). The slice energy spread and the slice norm. emittance, calculated over a 300 μm slice length, are below 0.05% and 1 μm respectively, all over the bunch. A complete investigation over the parameter range of the system is in progress, in particular tolerances and sensitivities are being considered in the beam dynamics simulations [5].

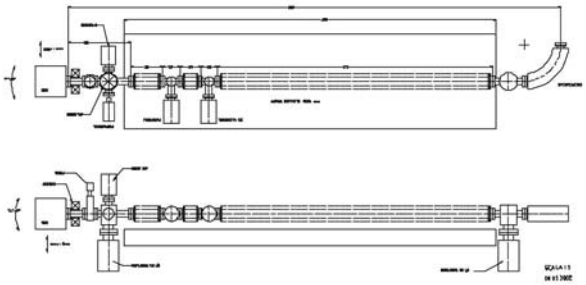

Figure 3: movable emittance measurement station. A pepperpot and a screen are connected with three bellows in order to scan the emittance along 1m long drift

SASE FEL EXPERIMENT

The FEL SASE experiment will be conducted using a permanent magnet undulator made of 6 sections, each 2.13 m long, separated by 0.36 m gaps hosting single quadrupoles which focus in the horizontal plane. The undulator period is set at 3.0 cm, with an undulator parameter k_w = 1.4. A simulation performed with GENESIS is reported in Fig. 4, showing the exponential growth of the radiation power along the undulator. Almost 108 Watts can be reached after 14 m of total undulator length. Preliminary evaluations of the radiation power generated into the non-linear coherent odd higher harmonics show that 10^7 and $7x10^5$ W can be reached on the third and fifth harmonics, respectively.

FURTHER EXPERIMENTS

Two main upgrades will be implemented in a second phase of the project. A dedicated accelerating section will be inserted downstream the RF gun in order to exploit the full potentialities of the velocity bunching technique. Furthermore, in the parallel beam line a magnetic chicane will be installed to allow the experimental investigation of CSR induced effects on emittance degradation and surface roughness wake-field effects. Its design and construction will proceed in parallel to the commissioning of the SPARC injector system (RF gun + 3 standard SLAC-type 3 m sections). These tests are of great relevance in our R&D program in view of the development of a coherent X-ray source according to the SPARX proposal[1], the general layout of which foresees a mixed compression scheme: RF compression in the photo-injector and one single stage magnetic compression at 1 GeV up to the final peak current of 2.5 kA.

Applying velocity bunching in the SPARC photo-injector with low charge bunches (about 15 pC) will allow the production of ultra-short electron bunches, in the range of a few μm rms bunch length, fully synchronized to the Ti:Sa laser pulses. A further upgrade of the laser system to produce multi-TW pulses, by means of a third stage of amplification and an under vacuum pulse compressor, will allow to conduct laser wake-field plasma acceleration experiments with external injection of high quality ultra-short bunches into the plasma wave, for ultra-high gradient acceleration of electron beams.

This naturally projects SPARC as a more general test facility to conduct advanced beam physics and new acceleration technique experiments at LNF in the near future.

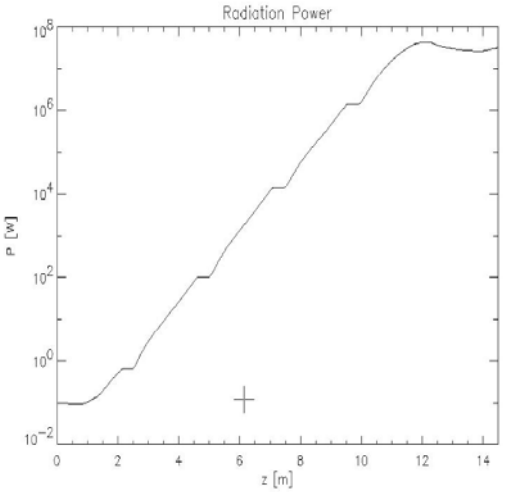

Figure 4: FEL radiation power growth along the undulator

REFERENCES

[1] D. Alesini *et al*., *Conceptual design of a High Brightness Linac for Soft X-Ray SASE-FEL Source* , Proceedings of the FEL-2002 Int. Conference

[2] M. Ferrario *et al*., *Recent Advances and Novel Ideas for High Brightness Electron Beam Production based on Photo-Injectors*, INFN Rep. LNF-03/06 (P), May 2003

[3] L. Serafini and M. Ferrario, *Velocity Bunching in Photo-Injecto*rs, *AIP CP* **581** (2001) 87

[4] D.T. Palmer, PhD. Thesis, Stanford University

[5] M. Biagini *et al*., *Beam Dynamics Studies for the SPARC Project,* this conference

CODE COMPARISON FOR SIMULATIONS OF PHOTO-INJECTORS

C.Limborg[*], Y.Batygin[*], M.Boscolo[•], JP.Carneiro[♣], M.Ferrario[•], K.Floetmann[♣],

V. Fusco[•], L.Giannessi[♦],C.Ronsivalle[•], M.Quattromini[♦]

([*]) MS 69 SLAC 2275 Sand Hill Road, Menlo Park , 94025 CA, USA

([♣])DESY, Notkestrasse 85, 22603 Hamburg, Germany

([•])INFN-LNF, Via E. Fermi 40. I-00044, Frascati (Roma), Italy

([♦])ENEA Research Center Via Enrico Fermi 45, 00044 Frascati (Roma), Italy

Abstract

RF photo-cathode injectors constitute one of the key components of many future single pass FEL based synchrotron radiation sources. The possibility of reaching very high brightness beams had been anticipated by using various simulations tools. Several experiments have proven that the 1mm.mrad normalized projected emittance for 1 nC, 10 ps pulses is within reach. For optimizing these photo-injectors, a first search of parameters is efficiently performed with HOMDYN. Further refinement in the tuning is usually obtained using a multi-particle tracking code such as ASTRA, PARMELA or BEAMPATH. In this paper, we compare results from HOMDYN, ASTRA, PARMELA, and BEAMPATH for the cases of an S-Band photo-injector. Limitations in their accuracy and differences between the codes are discussed.

1- MOTIVATION

Many codes are available for studying the dynamics of intense electron bunches at low energy in the space charge dominated regime. Newcomers in the field often ask which code to use to start studying a system based on a photo-cathode RF gun. In this paper, we compare codes which use five very different algorithms to compute the space charge: a code which solves the envelope equation HOMDYN [1], a Cloud-In-Cell (CIC) code BEAMPATH [2], a ring based algorithm PARMELA[3] and ASTRA[4], a fast Particle-In-Cell (PIC) algorithm for PARMELA spch3d and and a Lienard-Wiechert potentials approach for TREDI [5]. The test problem studied consists in an S-Band RF gun, a compensation solenoid and a drift. Quantities of interest such as rms beam size, emittance bunch length could be matched for all those codes when optimal running conditions.

2- DESCRIPTION OF CODES

HOMDYN

HOMDYN relies on a multi-envelope model based on the time dependent evolution of a uniform bunch[1]. The basic approximation, in the description of the beam dynamics, lies in the assumption that each bunch is represented by a uniformly charged cylinder whose length and radius vary, assuming a uniform charge distribution inside the bunch. The HOMDYN algorithm is very efficient and despite some strong simplifying assumptions it allows the quick relaxation of the large number of parameters involved in parameter studies, to quickly find a reasonably optimized configuration.

BEAMPATH

BEAMPATH is used for 2D and 3D simulation of axial-symmetric, quadrupole-symmetric and z-uniform beams in a channel containing RF gaps, radio-frequency quadrupoles, multipole lenses, solenoids, bending magnets, and user-defined elements. The space charge potential of the beam is calculated from the direct solution of Poisson's equation by cloud-in-cell method in a moving system of coordinates with Dirichlet boundary conditions at the aperture and periodic conditions in z-direction. Simulation of the beam with large energy spread is performed utilizing Green function method for interaction of particles with individual energies. To simulate particle emission in RF photoinjector, the code was updated by an additional space charge routine which solves Poisson's equation inside a cylindrical iron box. This approach automatically takes into account image charges arising both from injection plane and from surrounding aperture.

PARMELA / ASTRA

PARMELA and ASTRA compute the space charge force by Lorentz-transforming the particles positions and field maps into the average rest frame of the beam. It then applies static forces to the various rings of the cylindrical map assuming a constant charge density inside a ring. This algorithm requires to have at least 5 particles in each of the cell of the cylindrical grid.

PARMELA /SPCH3D

The SPCH3D algorithm of PARMELA-LANL is based on a fast Fourier Transform set on a 3D grid over which the electric field is solved to verify Poisson’s equation [6].

It is quite time consuming as it requires running at least 100k particles and small aspect ratios of the cell dimensions. This algorithm is nevertheless necessary to be used when the aspect ratio horizontal to vertical of the beam is more than 2 and when the transverse profile does not have a cylindrical symmetry. The automated remeshing is included when using this algorithm.

TREDI

TREDI is a fully three dimensional Monte Carlo code devoted to the simulation of beam dynamics. Space charge fields can be evaluated in a point to point or point to mesh & interpolation mode, calculating the fields according to the Lienard Wiechert formalism and taking into account the effects due to the finite propagation velocity of signals. This is accomplished by storing the histories of macro-particles, and by tracking back in time the source coordinates until a retarded condition is fulfilled. Short bunch injector simulations (as the test case) can be run also in a faster "Static" mode, where instantaneous signal propagation is assumed. The "Retarded" mode allows the simulation of a wider class of problems such as CSR effects in bendings.

3- PROBLEM DESCRIPTION

The test problem consisted of simulating a S-Band gun with an emittance compensation solenoid and a drift for a 10ps square pulse, 1 mm uniform transverse laser pulse producing a 1 nC charge. No thermal emittance was included. The solenoid was set to 2.541 kG.

The first difficulty in performing such comparisons consists in implementing exactly the same maps of fields (electromagnetic for the gun field and magnetostatic for the solenoid). All of the five codes studied can translate outputs from SuperFish and Poisson. So identical maps were used. The second difficulty consists in using the same starting conditions. Each of the codes has its own launching conditions. To check that starting parameters were in agreement for all codes, we compared energy and beam sizes output for cases run without space charge. A very good overlap was obtained with the 5 codes. We could then study the single impact of the different space charge algorithms.

4- RESULTS OF COMPARISONS

Good agreement inside gun

The rms quantities beam size, emittance, bunch length and energy spread could be matched exactly for all the 5 codes inside the gun. The rms beam size obtained at the gun exit was slightly smaller with HOMDYN, see figure 1. The differences become larger in the drift which follows.

Some disagreement in drift

The local maximum in emittance around 1.5 m shows at 1.2 m in HOMDYN but around 1.5 for all the other codes, See figure 2. The first local emittance minimum is nearly identical for the multiparticle codes and the agreement is not as good for the second minimum. The energy spread from HOMDYN is closer to that of the other codes if only the core slices are taken into account for the comparison.

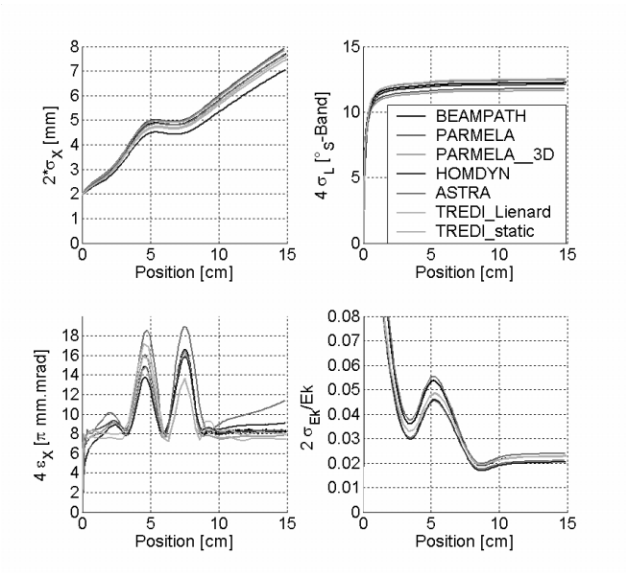

Figure 1.Comparison of evolution of rms beam size, bunch length, emittance and energy spread inside gun for the 5 codes

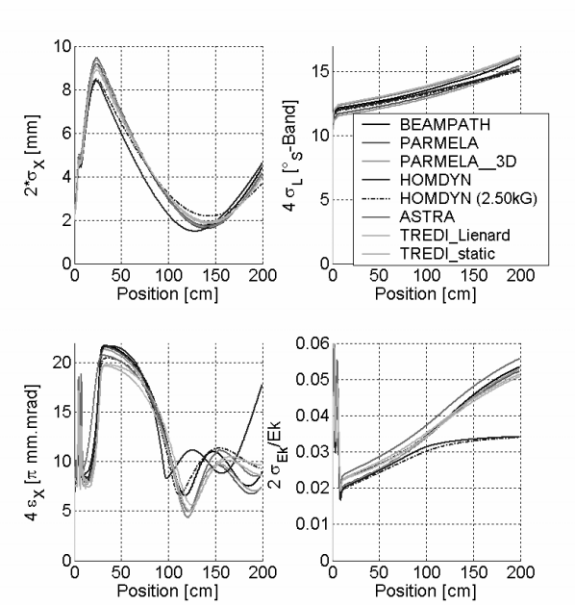

Figure 2.Comparison of evolution of rms beam size, bunch length, emittance and energy spread up to 200 cm for the 5 codes; second HOMDYN case run with solenoid reduced from 2.541kG down to 2.5 kG

5- MESHING IN TIME AND SPACE

Results depend strongly on the meshing used for the CIC code and for the SCHEFF algorithm. As a rule of thumb, each mesh should contain about 5 particles.

Table 1 – Comparison CPU time

Code	Platform	CPU	Num. particles	Mesh points N_r x N_z	Mesh size h_r x h_z	Integration step	CPU time (s)
HOMDYN	PC Win		75 slices			0.13 ^{o}	45
BEAMPATH	PC Win	1 GHz	10^4	256 x 2048	50x50μm^2	0.1^o , 1^o	8000
PARMELA	"	1 GHz	2.5 10^4	25 x 75	"	"	9846
" spch3d	"	1 GHz	10.10^4	32 x 32 x 1024	Automatic	"	1.4.10^4
ASTRA	"	1.8 Ghz	1.5 10^4	20 x 60	Automatic	Adaptative	420
Tredi Stat.	16 nodes	1.8 GHz	5.0 10^4	20 x 30	Automatic	Adaptative	7.5 10^3
Tredi Lien.	PC Win	1.8 GHz	5.0 10^4	20 x 30	Automatic	Adaptative	7.4 10^4

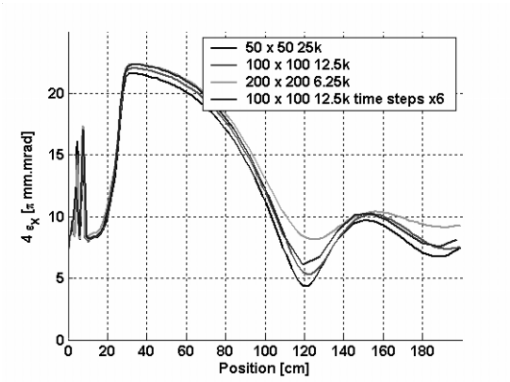

Figure 3. PARMELA results for the different meshes described in Table 2; Only the emittance varied for those 4 different cases, other parameters stayed constant

Table 2: PARMELA CPU Time on 1GHz PC

time	**SPACE Mesh.**	**TIME Mesh.**	**Particles**
9846 s	50 x 50 μm^2	1100, 0.1° then 1°	25 k
1286 s	100 x 100 μm^2	1100, 0.1° then 1°	12.5 k
445 s	200 x 200 μm^2	1100, 0.1° then 1°	6.25 k
345 s	100 x 100 μm^2	505, 0.2° then 1°	12.5 k

6- PHYSICS REPRESENTED

INITIAL ACCELERATION

A comparison of the dynamics between PARMELA and PIC codes [7], has shown that:

1- the image charge model is good enough to represent the boundary conditions at the origin
2- the computation of space charge forces, performed in the frame of the center of mass of the bunch in PARMELA type codes, when the Lorentz factor is small give good enough results compared with PIC or Lienard-Wiechert codes
3- neglecting the radial force generated from the beam self-induced azimuthal magnetic field does not affect the results

It was confirmed with BEAMPATH and TREDI that the approximation described in the second is correct. In TREDI the approximation is simply not used and BEAMPATH can perform computations using a Poisson solver for which individual energies are taken into account. The use of this solver for the first few mm is very time consuming but did not change the results at the end of the gun.

THERMAL EMITTANCE

In each of these codes the initial distribution can be given such that a thermal emittance is included. None of the codes include the physics involved in the generation of that thermal emittance. This is one of the key issues of the RF-Cathode gun to be tackled.

SHOTTKY EFFECT

ASTRA is the only code which includes this effect.

LONGITUDINAL PROFILE

Each of the codes can include the rise and fall time of the initial pulse but HOMDYN.

TRANSVERSE NON-UNIFORMITY

When the transverse profile does not have cylindrical symmetry, only 3D space charge algorithm should be used as in TREDI or PARMELA in the spch3d mode. ASTRA is being upgraded to offer a similar possibility.

PARMELA-UCLA and PARMELA-LANL include the possibility of using 3D maps of fields. It was checked [7] that the quadrupole moment present in the S-Band gun to be used for LCLS has negligible effects in the dynamics of the beam.

*limborg@slac.stanford.edu

SLAC is operated by Stanford University fot the Department of Energy under contract number DE-AC03-76SF00515

REFERENCES

[1] M.Ferrario, HOMDYN code : http://www.slac.stanford.edu/pubs/slacpubs/8000/slac-pub-8400.html
[2] Y.Batygin, "Particle-in-cell code BEAMPATH for beam dynamics simulations with space charge", ISSN 1344-3877, RIKEN-AF-AC-17 (2000), 81 p.
[3] L.Young, J.Billen , PARMELA, LANL Codes, laacg1.lanl.gov/laacg/services/parmela.html
[4] K.Floetmann,ASTRA, http://www.desy.de/~mpyflo/Astra_dokumentation/
[5] F. Ciocci, L. Giannessi, A. Marranca, L. Mezi, M. Quattromini, Nucl. Instr. & Meth. A 393, 434 (1997)., Web site: http://www.tredi.enea.it
[6] R.Ryne et al., Proc. 1998 Linac Conf., Chicago,IL
[7] E.Colby, et al."Simulation Issues for RF Photoinjectors" 7th Computational Accelerator Physics Conference, Michigan State U. Oct15-18-2000